Material Science and Technology Division

Heavy Vehicle Propulsion Materials Program
Quarterly Progress Report for
January through March 2006

D. R. Johnson
Technical Project Manager

Prepared for
U.S. Department of Energy
Assistant Secretary for Energy Efficiency and Renewable Energy
Office of FreedomCAR and Vehicle Technologies Program
VT 05 01 020

Prepared by the
OAK RIDGE NATIONAL LABORATORY
Oak Ridge, Tennessee 37831-6066
Managed by
UT-Battelle, LLC
for the Department of Energy
Under contract DE-AC05-00OR22725

CONTENTS

Materials for Advanced Fuel Systems

Mechanical Reliability of Piezo Stack Actuators (ORNL)

Materials for Exhaust Aftertreatment

Materials for Exhaust Aftertreatment (Caterpillar Inc.)

Development of NO_x Sensors for Heavy Vehicle Applications (ORNL and Ford Motor Company)

Development of Materials Analysis Tools for Studying NO_x Adsorber Catalysts (ORNL and Cummins Engine Company)

Catalysis via First Principles (ORNL)

Materials for Air Handling and Thermal Management

Advanced Cast Austenitic Stainless Steels for High Temperature Components (ORNL and Caterpillar Inc.)

Friction and Wear Reduction in Diesel Engine Valve Trains (ORNL)

Materials for Structural Components

Advanced Machining and Sensor Concepts (University of Michigan)

Synergistic Process-Enhanced Grinding of Advanced Engine Materials (ORNL)

Materials for Hot Section Components

NDE Development for Ceramic Valves for Diesel Engines (Argonne National Laboratory)

Life Prediction of Diesel Engine Components (ORNL and Caterpillar)

Lightweight Valve Train Materials (Caterpillar Inc.)

An Integrated Surface Modification of Engineering Materials for Heavy Vehicle Applications (NIST)

Characterization of Physical and Mechanical Properties

Mechanical Property Test Development (NIST)

Coating Evaluation and Performance (ORNL)

Mechanical Reliability of Thermoelectrics (ORNL)

Emerging Technologies

Processing and Characterization of Structural and Functional Materials for Heavy Vehicle Applications (North Carolina A&T State University)

Powder Processing of Nanostructured Alloys Produced by Machining (Purdue University)

Next Generation Ceramics for Heavy Vehicle Propulsion Applications (ORNL)

Mechanical Reliability of PZT Piezo-Stack Actuators for Fuel Injectors

A. A. Wereszczak and H. Wang
Ceramic Science and Technology (CerSAT)
Oak Ridge National Laboratory

Objective/Scope

The use of piezoelectric stack actuators as diesel fuel injectors has the potential to reduce injector response time, provide greater precision and control of the fuel injection event, and lessen energy consumption (e.g., for use in homogeneous charge compression ignition, HCCI, engines). Though piezoelectric function is the obvious primary function of lead zirconate titanate (PZT) ceramic stacks for fuel injectors, their mechanical reliability can be a performance and life limiter because PZT is both brittle, lacks high strength, and may exhibit fatigue (i.e., slow crack growth) susceptibility. That brittleness and relatively low strength can be overcome with proper design though. This project combines in-situ micromechanical testing, microstructural-scale finite element analysis, probabilistic design sensitivity, and structural ceramic probabilistic life prediction methods to systematically characterize and optimally design PZT piezoelectric stack actuators that will enable maximized performance and operational lifetime.

Technical Highlights

A fuel injection system can employ a piezoelectric actuator where the actuator exhibits a proportional relation between an applied voltage and linear displacement (i.e., contraction and expansion). An injector needle (connected to the piezoelectric actuator through a hydraulic transfer) is therefore moved up and down so as to open and close an injector nozzle [1]. Compared to conventional solenoid materials, the piezoelectric materials have at least one order-of-magnitude reduction of response time: that enables more precise control of the start, rate shape, and duration of the injection event, more precise timing, and potentially multiple injections in one engine cycle [2]. The latter is extremely attractive because precisely controlled multiple injections can substantially increase fuel economy and lessen emissions. Innovative design of the modern diesel fuel injection system utilizes a direct-actuated injector where the piezoelectric actuator operates the needle valve of injector and eliminates the servo-hydraulic circuit. Consequently, it takes less than 100 microseconds to open and close the needle valve of the injector and to spray the high-pressure diesel fuel into the engine, thusly allowing five (or more) injections per engine cycle. Such a system can deliver 10% higher power and 30% less particulate matter and NOx emission. This direct acting common rail system therefore depends on the actuation and reliability of the (brittle) PZT and the comingled architecture of it and the electrodes.

Efforts have been made to consider the application of PZT actuators in diesel fuel injection systems. Delphi implemented a PZT actuator in the common rail fuel injection system and was planning to commercialize a system in 2007. In other DOE programs [2, 3], improvements in PZT stack manufacturing were sought and the feasibility of PZT actuator fuel injection was examined. The work was limited within the laboratory however and not extended to the application or the stack design. Other findings from the literature -

1. Due to the multilayer architecture of a piezoactuator, significant stress and electric field concentrations occur at the electrode ends and the interface between the activated and un-activated regions. The material in these regions therefore is subjected to multi-axial electro-mechanical loading [4]. The concentrated electric field can exceed the coercive field of the PZT even though the PZT is designed to function below it. The poled PZT may undergo domain-switching resulting in non-linear material response.
2. The PZT ceramic generally exhibits dielectric and butterfly hysteresis under electrical cyclic loading when the load level is significant. In the PZT actuator, the high load may result from the concentration of electrical and mechanical fields. The degradation of PZT ceramics initiates from micro-defects, including grain boundary, domain wall, lead and oxygen vacancies, as well as cracks and pores. This degradation manifests itself macroscopically as decreases of remnant polarization and remnant strain, and the increase of coercive electrical field [4].
3. Phenomenological modeling takes into account the characteristics of dielectric and butterfly hysteresis and has been generalized into 3-D and implemented in finite element codes such as PSU [5].
4. Fracture toughness of unpoled and poled PZT has been extensively investigated with respect to electric field. Experimental results typically exhibit significant scatter, and can even be contradictory because reported observations usually are from different test configurations and electrical-mechanical load levels [6]. Linear piezoelectric fracture mechanics has been used to explain the effect of electrical field and domain switching has been used to interpret a toughening mechanism (when it exists).
5. A few studies were conducted with regard to the crack initiation and growth in PZT under electrical cyclic loading but the results were not systematic [7]. Therefore, the growth of crack as related to the load levels of both the electrical and the mechanical has not been well defined.

Professor Osama Jadaan (University of Wisconsin-Platteville) will fulfill a sabbatical at ORNL during parts of Q3 and Q4 and will assist in the literature survey, FEA analysis, and preliminary life prediction exams.

Status of FY 2006 Milestones

Create and develop a general finite element model that predicts operational stresses in a PZT piezo stack actuator and that enables probabilistic life prediction estimation. [09/06]
On schedule.

Communications/Visits/Travel

Wereszczak visited Caterpillar's M. Long and J. Sun on 02 March 2006 at the Caterpillar Technical Center, Peoria, IL.

Publications

None.

References

[1] Rueger, J. -J., Mrosik, M., Pitzal, V., and Schulz, U., "Methods and Apparatus for Regulating Voltage and Voltage Gradients for Driving Piezoelectric Elements," U.S. Patent 6,619,268, Sept. 16, 2003.

[2] Joshi, U., Kalish, Y., Savonen, C., Venugopal, V., Henein, N., "Smart Materials for Diesel Fuel Injector," FY 2003 Progress Report, DOE program on Heavy Vehicle Propulsion Materials.

[3] Kiggans, J. O., Montgomery, F. C., Tiegs, T. N., and Maxey, L. C., "Cost-Effective Smart Materials for Diesel Engine Application," FY 2003 Progress Report, DOE program on Heavy Vehicle Propulsion Materials.

[4] Lupascu, D. C. and Rodel, J. "Fatigue in Bulk Lead Zirconate Titanate Actuator Materials," *Adv. Eng. Mater.*, **7** 882-898 (2005).

[5] Kamlah, M., "Ferroelectric and Ferroelastic Piezoceramics – Modeling of Electromechanical Hystereses Phenomena," *Continuum Mech. Thermodyn*. **13** 219-268 (2001).

[6] Chen, Y-H and Hasebe, N., "Current Understanding on Fracture Behaviors of Ferroelectric/Piezoelectric Materials," *J. Intel. Mater. Syst. Struc.*, **16** 673-687 (2005).

[7] Zhu, T and Yang, W., "Fatigue Crack Growth in Ferroelectrics Driven by Cyclic Electric Loading," *J. Mech. Phys. Solids*, **47** 81-98 (1999).

Materials for Exhaust Aftertreatment

Corey Shannon, Herbert DaCosta, Matt Stefanick, Ron Silver and Craig Habeger
Advanced Materials Technology, Caterpillar Inc.

Objective/Scope

The objective of the effort is to develop and evaluate materials that will be utilized in aftertreatment systems for diesel engine applications. These materials include catalysts for CO and hydrocarbon oxidation, NOx reduction, and filtration media to improve particulate abatement capabilities in the exhaust system. The project is a part of the Caterpillar strategy to meet EPA requirements for regulated diesel emissions in 2007 and beyond.

This year's focus is to assess the durability of various catalyst technologies in terms of phosphorous, sulfur and thermal degradation, and to identify diesel particulate trapping materials that have high durability and filtration efficiency to comply with future emission regulations for heavy-duty diesel engines.

Technical Highlights

Diesel Particulate Filter (DPF).

A catalyzed diesel particulate filter (DPF) obtained from a supplier was loaded with particulate matter on the diesel fuel-burner bench and regenerated. This process was repeated after 100 hours of thermal aging (equivalent to 24x25-minute regenerations), and again after 200 total hours of thermal aging. In all cases, the filtration efficiency either stayed about the same or increased slightly. One trend found in this study was that the backpressure during the test decreased on catalyzed samples of the alternative DPF substrate, but increased on un-catalyzed samples. However, the backpressure stayed about the same when testing both catalyzed and un-catalyzed cordierite samples. Additional backpressure data was taken as a function of increasing flow rate, before and after loading the DPF with particulate matter. The data shows that the trend of backpressure vs. flow rate decreases after thermal aging with both catalyzed cordierite and the alternative DPF. However, the trend increased when the test was performed on un-catalyzed samples, as seen in Figures 1 and 2.

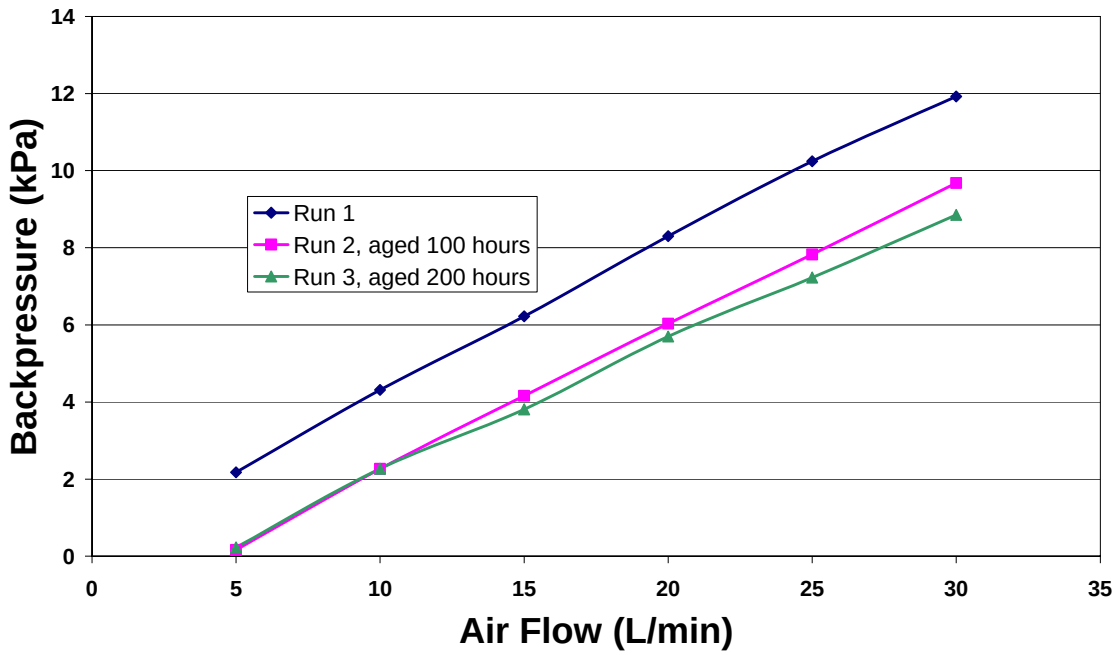

Figure 1. Backpressure versus flow rate for catalyzed cordierite before and after aging at 100 h and 200 h.

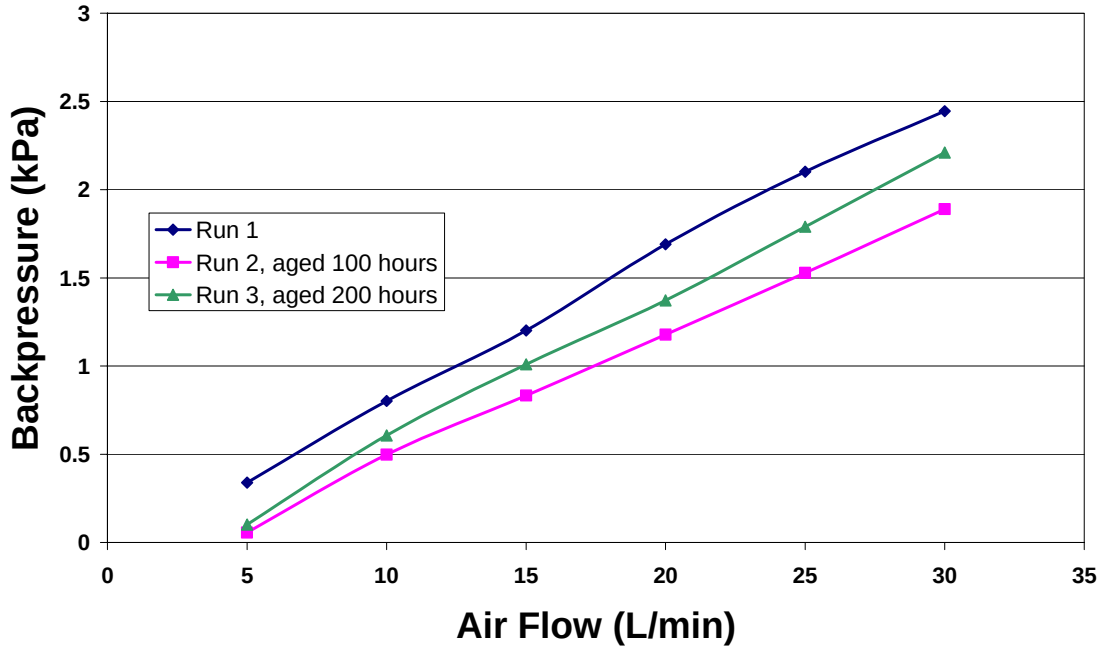

Figure 2. Backpressure versus flow rate for catalyzed alternative DPF, before and after aging at 100 h and 200 h.

Catalyst Durability.

Urea- SCR:

A zeolite based urea SCR catalyst was previously mildly aged with phosphorus alone. Using a diesel fuel burner, additional core samples were taken from this catalyst and exposed to phosphorus plus significant levels of SO_2, such that the resulting sulfur weight exposure was equal to the phosphorus exposure. The activity of these aged samples was characterized by doing a temperature sweep, an NH_3/NO_x ratio sweep, and a NO_2/NO_x ratio sweep over the aged catalyst. Initial results indicate the addition of sulfur into the aging mix accelerates the degradation of zeolite SCR performance.

Results in Figure 3 show the effect of phosphorus (P) and sulfur (S) on the NO_x and NH_3 conversions, calculated by dividing the aged catalyst activity by its previously tested fresh performance under the same conditions. The relative performance of the sample aged using only P is also plotted in this figure. Results from mild aging with P showed little or no loss of NH_3 and NO_x conversion activity. The addition of S to the aging mix drops the relative performance by about 10 % for both the NO_x and the NH_3. The relative NO_x conversions from both agings appear to be slightly lower at low temperatures, and then increase with temperature. This seems to indicate that active sites for low temperature NO_x reaction are more strongly impacted by P and S. An analysis of NO and NO_2 conversions from these agings indicates that NO conversion is lost at low temperature. The decline in activity is due to a decrease in NO oxidation to NO_2. In contrast, the activity loss for NH_3 conversion due to exposure to P, or P and S, seems to be constant with increasing temperature.

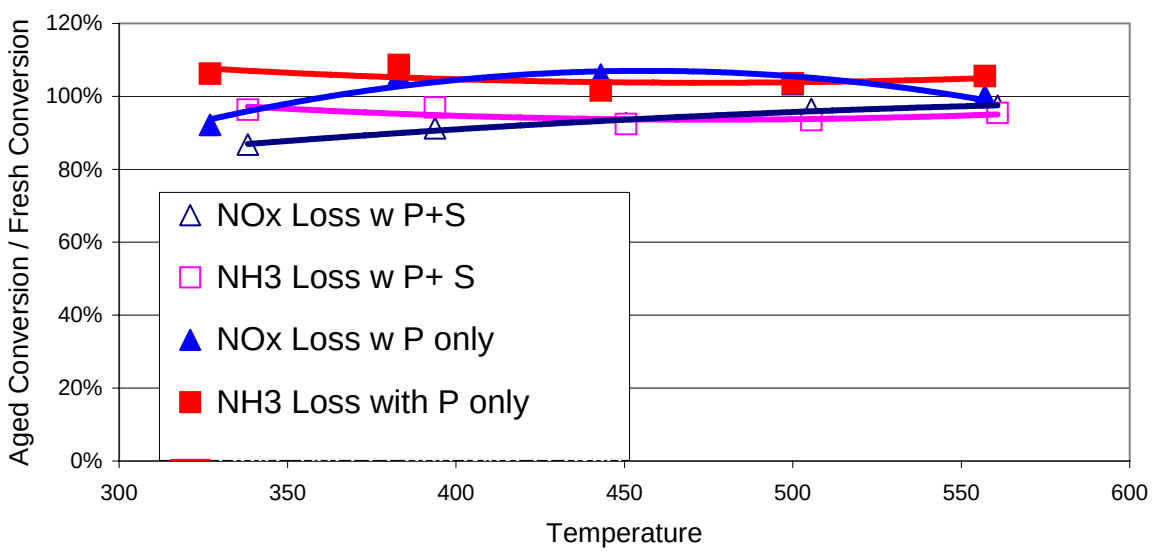

Figure 3. Relative performance of SCR catalysts after exposure to phosphorus plus sulfur or phosphorus only.

The effect of core size was also investigated. A 1-inch diameter by 3-inch long core from a zeolite SCR catalyst was exposed to the same level of S and P as a 1 inch by 6-inch long core. The results are shown in Figure 4 and indicate the longer core has better low temperature NOx conversion, both fresh and after aging. In fact, the aged 6-inch core has a NO_x lightoff temperature similar to the fresh 3-inch core. At high temperature, the activity of the 6-inch core drops below the performance of the 3-inch core. This may be due to the longer residence time of NH_3 in the 6-inch core, which allows NH_3 oxidation to occur earlier.

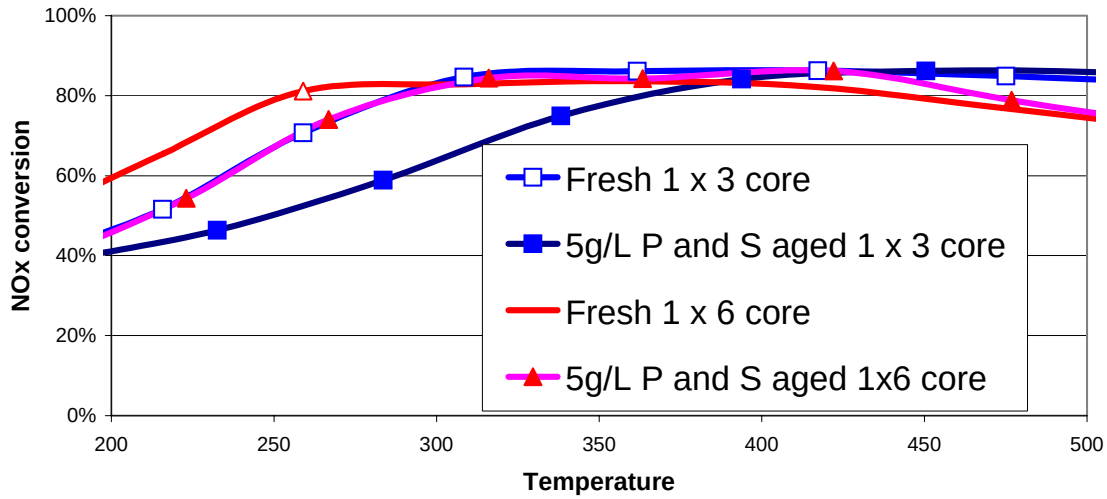

Figure 4. Comparison of NO_x conversion in 1-in. x 3-in. cores versus 1-in. x 6-in. cores, before and after aging in phosphorus plus sulfur.

Future Plans

1. Additional exposure of zeolite SCR catalyst to the phosphorus plus sulfur combination to determine the impact as a function of exposure level, followed by thermal aging.
2. Continue searching for and testing of new substrate materials for DPF filters.
3. Test the thermal durability of the DPFs to see how lightoff temperature is affected on both catalyzed and un-catalyzed samples.
4. Load samples of catalyzed DPFs with varying levels of P to see how lightoff temperature is affected on both catalyzed and un-catalyzed samples.

Travel

None this quarter.

Presentations/Publications

None this quarter.

Status of FY 2006 Milestones

1. Tested 1-in. x 3-in. core samples un-catalyzed and catalyzed DPF for soot regeneration.
2. Urea-SCR catalyst has been initially aged with P and S, additional exposure is scheduled.

Development of NO_x Sensors for Heavy Vehicle Applications

Timothy R. Armstrong, David L. West, Fred C. Montgomery
Oak Ridge National Laboratory

CRADA No. ORNL 01-0627
with Ford Motor Company

Objective

This project seeks to develop technologies and materials that will facilitate the development of NO_x and ammonia sensors. The development of low-cost, simple NO_x sensors will facilitate the development of ultra-low NO_x emission engines, directly supporting the OHVT goals.

Technical Highlights

There were two main technical highlights for the 2nd quarter of FY 2006:

1. Pursuant to a request from the CRADA partner (Ford) the effect of a proprietary substrate chemical etchant on sensing performance was examined. This etchant had been used by Ford in the past on other zirconia-based sensors. Some representative data from the testing done is shown in Fig. 1. The data in Fig. 1 indicate that the etchant has no effect on the sensing performance.

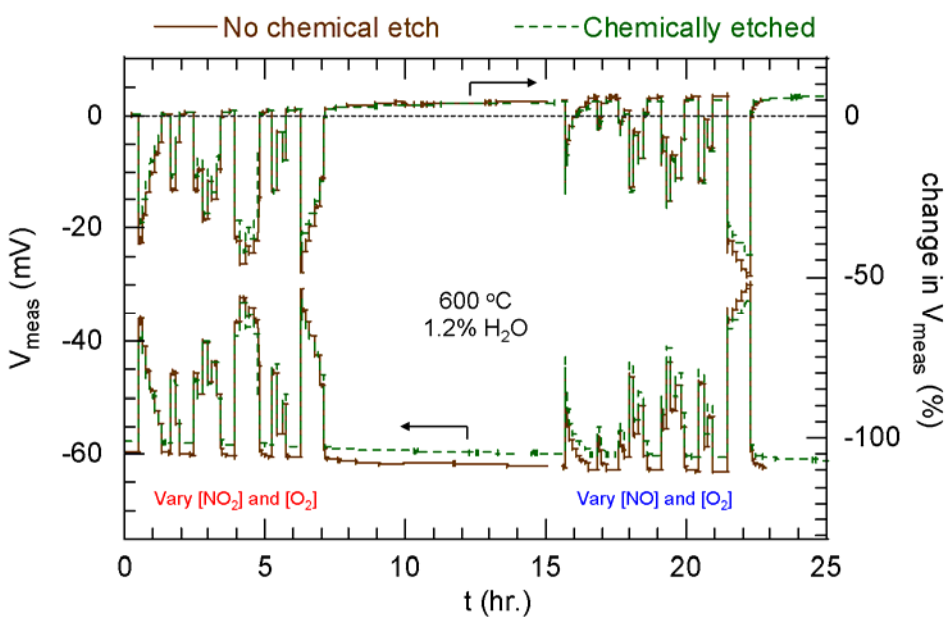

Figure 1: Response to NO_x of sensing elements made with untreated and chemically etched substrates. The etchant does not appear to affect the sensing behavior.

2. The cross-sensitivity of the elements mentioned above to expected interferents (e.g., the representative hydrocarbon C_3H_6) was characterized. Figure 2 shows some typical results from this testing. In Fig. 2, we have plotted the changes in element resistance (R)

as functions of normalized concentration for the potential interferents C_3H_6 and NH_3. (NH_3 might be present due to the projected use of urea SCR for NO_x remediation.) The effects of varying O_2 and H_2O were also characterized as these will vary in diesel exhausts. Figure 2 indicates that the most troublesome interferents are expected to be NH_3 and oxygen and stream. In the end-use application [O_2] will be known from the engine operating condition and limited testing by the CRADA partner has indicated that the [H_2O] sensitivity may not be an issue in the [H_2O] ranges that are more typical of diesel exhausts (~1.4–7 vol %[1], for the data in Fig. 2 [H_2O] was varied between 0.3 and 1.5%). Thus the cross-sensitivity to NH_3 is would appear to be the most troublesome. However our current view is that since in O_2-containing atmospheres at high temperatures NH_3 will tend to oxidize to NO virtually all high-T NO_x sensors will suffer from "cross-sensitivity" to NH_3. Therefore, an NH_3 sensor may be required for the successful implementation of urea SCR irrespective of the NO_x sensor used for control and/or diagnostics.

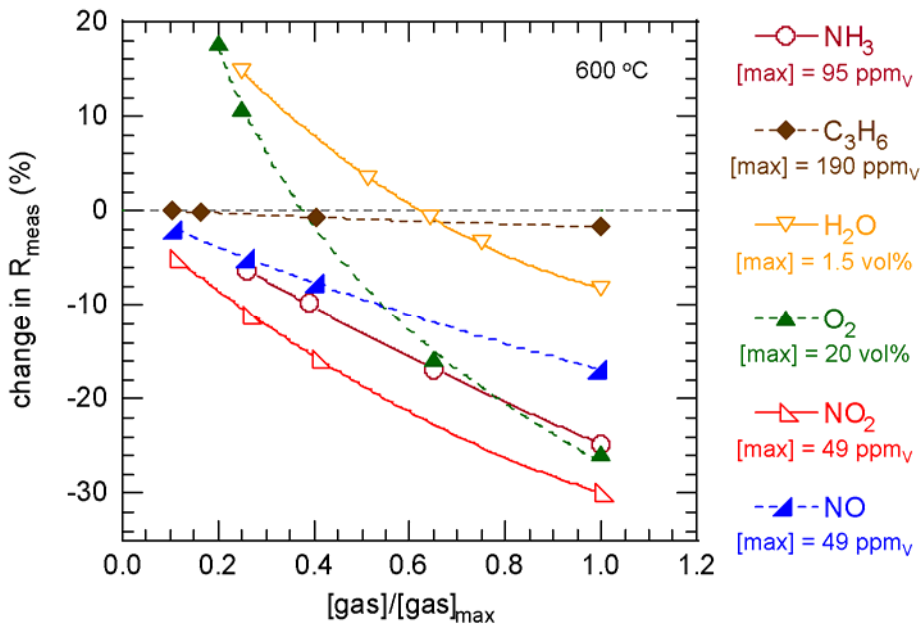

Figure 2: Element response to NH_3, C_3H_6,varying [O_2] and [H_2O], and NO_x. The concentration of each individual species has been normalized to the maximum concentrations given in the legend (95 and 190 ppm_V for NH_3 and C_3H_6, 1.5 and 20 vol % for H_2O and O_2, and 49 ppm_V for NO_x).

Future Plans

- At the request of the CRADA partner (Ford), attempts are underway to increase electrode electrical impedance and adhesion/durability, primarily through electrode formulation.
- Samples designed for this are being fabricated and will be characterized in-house to gauge the impact of the formulation changes on the sensing performance.
- Following internal characterization, prototype elements will be furnished to Ford for dyno testing.

Status of FY2006 milestones

(1) Detailed understanding of sensing mechanism **(09/06)**
Collaborations had been established with two different universities in order to pursue this milestone. One agreement was established with Georgia Tech to study surface reactions with IR and an agreement was made with Northwestern University to characterize electrode reactions with AC impedance spectroscopy. Results of preliminary experiments at Georgia Tech were not promising; however the collaboration with Northwestern is beginning to produce results.

On track.

(2) Evaluate cross-sensitivities, including H_2O from 1 to 10 vol %. **(06/06)**.
Relevant cross-sensitivities have been evaluated, save that for the higher H_2O concentrations. Testing at higher [H_2O] will require capital outlays that may be inconsistent with current budgetary levels, and higher [H_2O] can be obtained in testing at Ford.

Partially completed / on hold.

(3) Evaluate stability in real exhausts. **(06/06)**.
The CRADA partner is setting up for dyno testing, and prototype elements are currently being fabricated and screened in-house.

On track.

(4) Investigate use of time-varying electrical stimulus (e.g. square wave variation) (**06/06**).
Preliminary results did not indicate that signal stability was enhanced with this technique.

On hold.

Communications/Visits/Travel

- A meeting was held March 8–9 at ORNL with representatives from Lawrence Livermore National Laboratory (LLNL) and Ford. The way forward agreed to at this meeting consisted of the items in "Future Plans" above.
- Biweekly teleconferences were held with LLNL and Ford during the quarter.

Problems Encountered

None

Publications

D. L. West, F. C. Montgomery, and T. R. Armstrong, "Total NO_x sensing elements with compositionally identical oxide electrodes," *Journal of the Electrochemical Society*, **153**[2], H23–8, 2006.

Intellectual Property Filed

None

References

[1] J. Kašpar, P. Fornasiero, and N. Hickey, "Automotive catalytic converters: Current status and some perspectives," *Catalysis Today*, **77**, 419–449, 2003.

Development of Materials Analysis Tools for Studying NOx Adsorber Catalysts

Thomas Watkins, Larry Allard, Doug Blom, Michael Lance, Harry Meyer, Larry Walker and Chaitanya Narula
Oak Ridge National Laboratory

Cheryl Klepser, Tom Yonushonis, Howard Fang and Roger England
Cummins Inc.

Objective

The objective of this effort is to produce a quantitative understanding of the processing and in-service effects on NO_x adsorber catalyst technology leading to an exhaust aftertreatment system with improved catalyst performance capable of meeting the 2007 Environmental Protection Agency (EPA) emission requirements in the United States.

Samples and Approach

A Cummins catalyst supplier provided new catalyst materials, which are being examined with diagnostic tools developed under the CRADA. Investigations of these candidate-production materials are being implemented on both the bench and engine research scale. These investigations include the examination of unused, reactor and engine-aged catalyst samples. Investigative tools included transmission electron microscopy (TEM), X-ray diffraction (XRD), X-ray photoelectron spectroscopy (XPS), Raman Spectroscopy and infrared spectroscopy (IR).

Technical Highlight

A diesel oxidation catalyst (DOC) is a flow through device composed of a porous honeycomb structure within which a high surface area ceramic washcoat is situated. Small amounts of precious metal are dispersed within the washcoat and provide the catalytic activity necessary to oxidize carbon monoxide, gaseous hydrocarbons and liquid hydrocarbon particles (unburned fuel and oil).[i] Regulated emissions are thus controlled.

A new DOC (see Figure 1) that has not seen service was examined with XRD, XPS, Raman spectroscopy and the electron microprobe. A typical XPS survey spectrum for this sample and resulting composition is shown in Figure 2. The absence of magnesium indicates that the signal originates from the washcoat, which is likely some sort of alumino-silicate, based on the majority elements. In Figure 3A, XRD indicates that the substrate is cordierite ($2MgO{\bullet}5SiO_2{\bullet}2Al_2O_3$) and that the wash coat contains γ-alumina. The broad peak at low angle at ~20° 2Θ may be due to both γ-alumina and amorphous SiO_2. Raman spectroscopy confirmed the presence of γ-alumina in the washcoat (see Figure 4). There is some XRD (1 peak at 15.4° 2Θ) and Raman evidence to suggest a small a mount of θ-alumina *may* also be present. In Figures 5A and B, XPS data shows the variation of the major and minor elements, respectively, along the length of a trough in the cordierite honeycomb. Except for the minority element of F, the percentages were effectively constant along the sample length.

Electron microprobe was employed to obtain x-ray (elemental) maps of a typical cross-section. In Figure 6, a portion of the cordierite honeycomb is seen in upper right of the image. The

washcoat was deposited in two stages with interface marked with an arrow. In Figure 7, X-ray maps of Pt, Si, Al and O are from the same area as in Figure 6. The distribution of Pt is uniform Pt distribution and there appears to be some silicon bearing material within the washcoat in addition to the γ-alumina. No Pt was detected with XRD. In Figure 3B, scans at various angles of incidence were employed in an unsuccessful attempt to observe Pt. The markers for Pt are shown indicate that Pt cannot be discerned due to peak overlap with the γ-alumina. Quantitative X-ray line scans were conducted with the electron microprobe, starting at the washcoat/cordierite interface (see Figure 8). A 10 micron diameter electron beam was stepped every 10 microns through the washcoat. The Pt content slowly varies between 0.5 and 0.8 weight %. The Al_2O_3/SiO_2 ratio is essentially constant through the thickness of the washcoat.

Figure 1- The parent DOC sample from which ~1" diameter cores were taken for characterization.

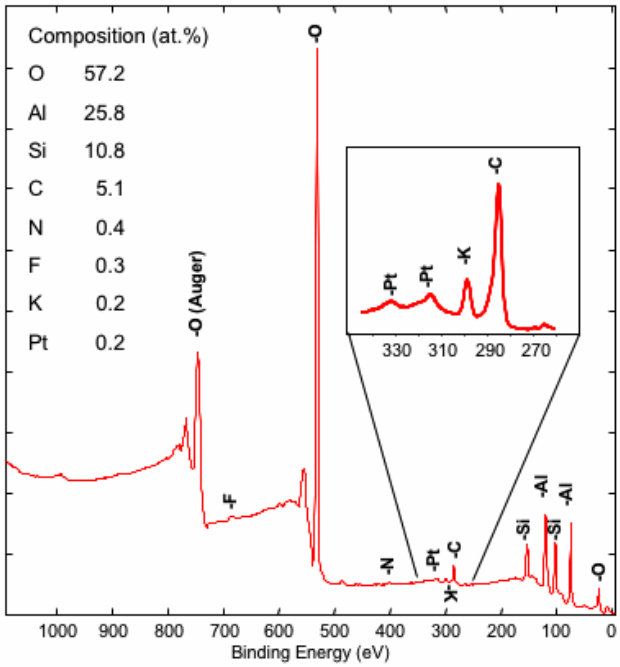

Figure 2- Typical XPS results for the DOC sample.

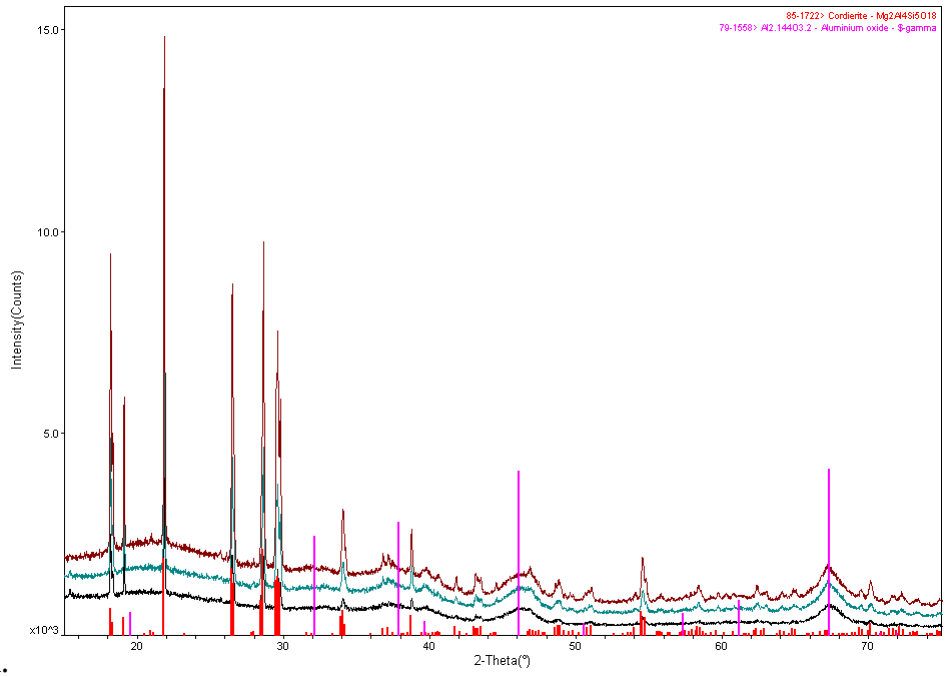

A.

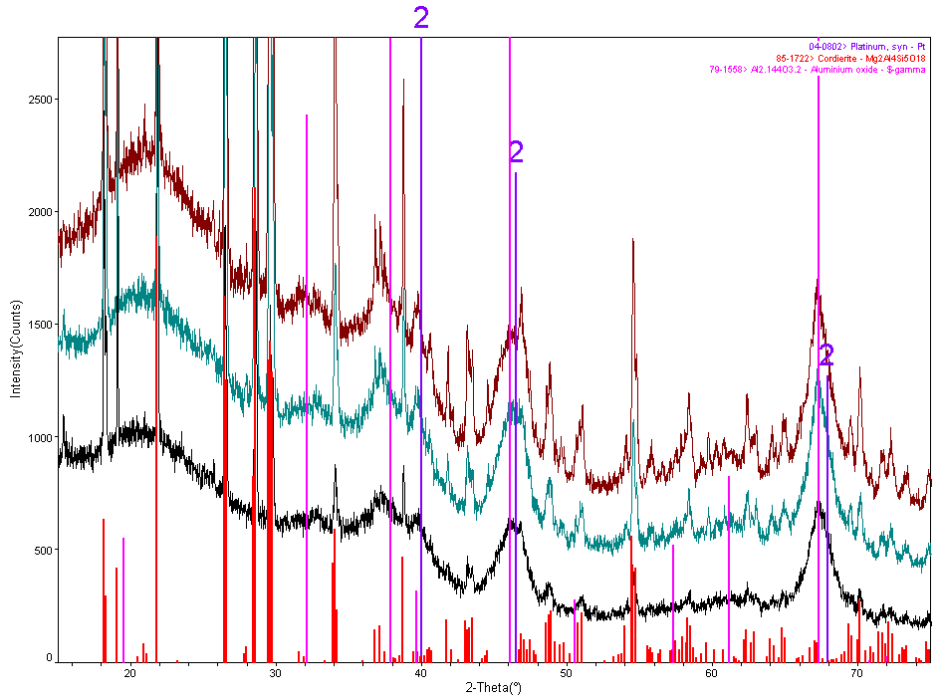

B.

Figure 3- XRD patterns of the sample taken a various angles of incidence: A. full scale and B. expanded scale: angles of incidence: 1, 4, 10° for lower, middle and upper curves.

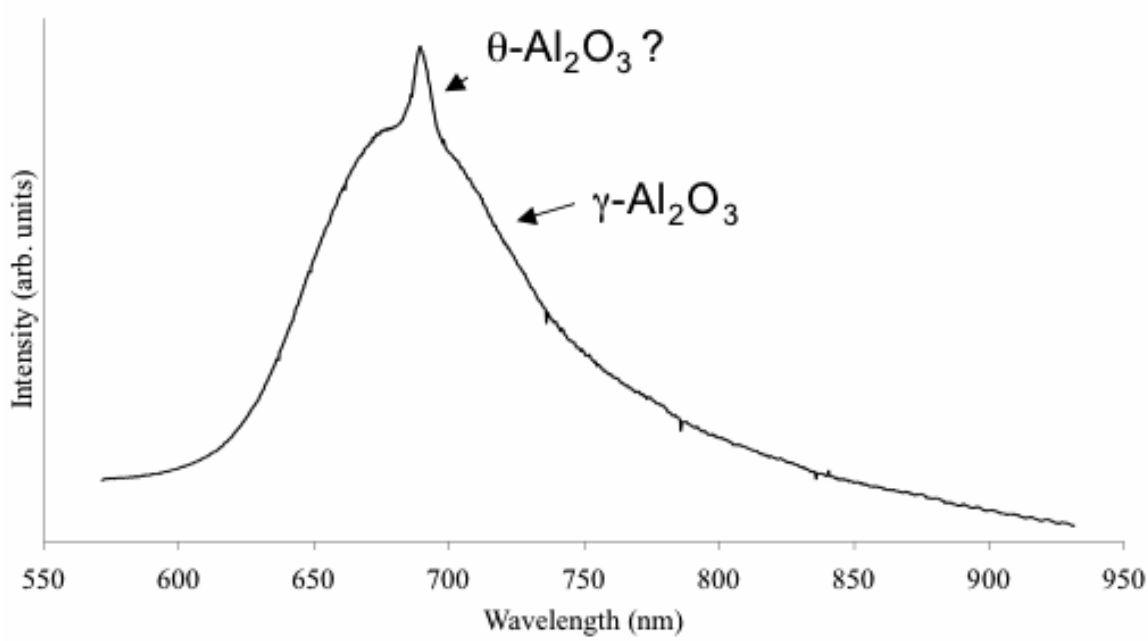

Figure 4- Raman spectrum of the DOC washcoat.

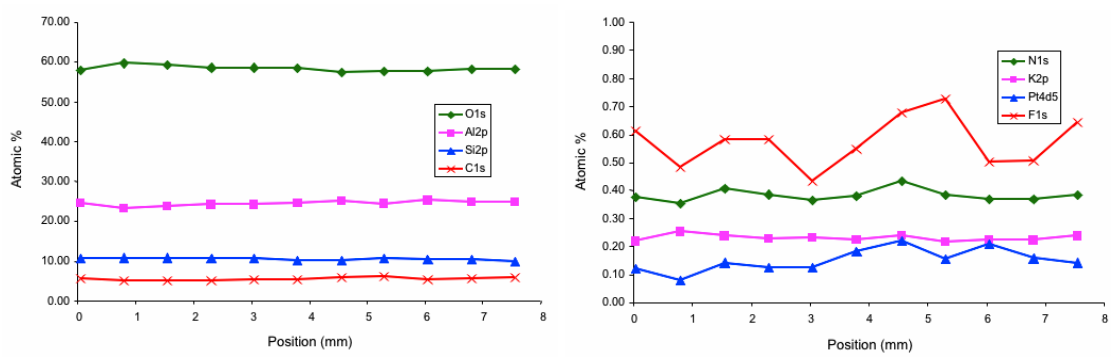

A. B.

Figure 5- The variation of the A. major and B. minor elements along the length of a trough in the cordierite honeycomb.

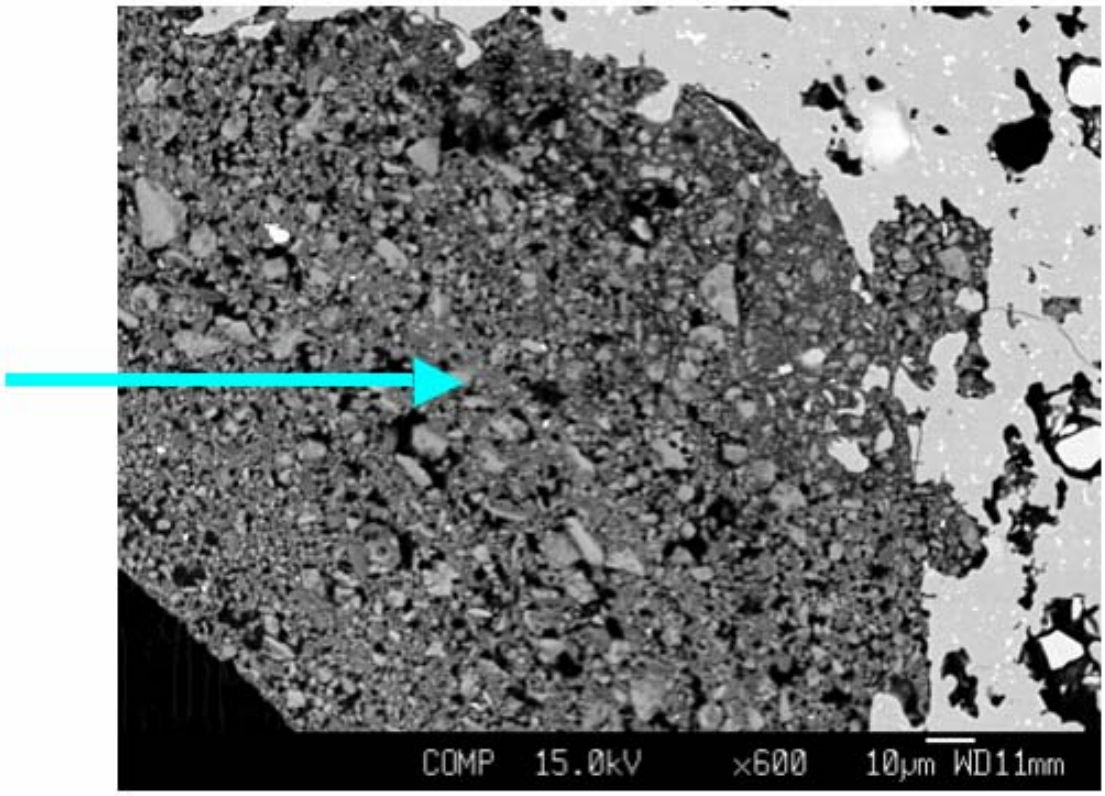

Figure 6- Backscattered electron image of catalyst core from DOC catalyst. The arrow indicates the interface between two different layers/applications of washcoat.

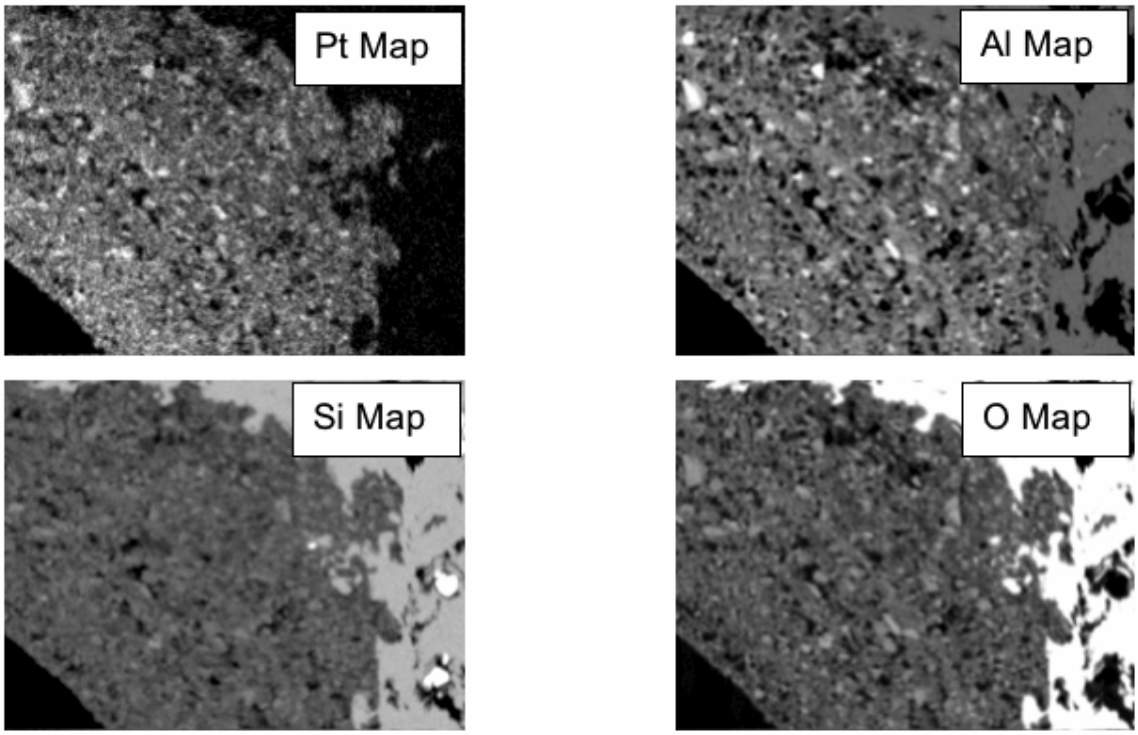

Figure 7- X-ray maps from the same area shown in Figure 6.

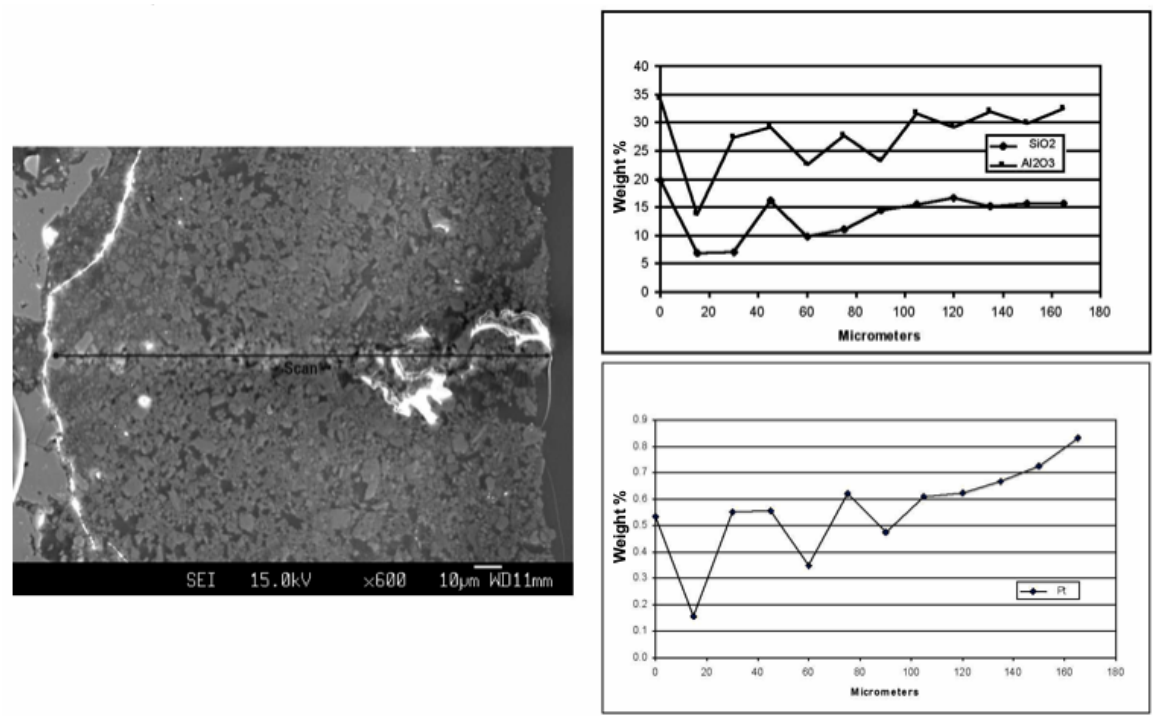

Figure 8- A secondary electron image of the region showing the location of the quantitative x-ray line scans. These started at the washcoat/cordierite interface.

References

[i] Washington State University Extension Energy Program, Diesel Oxidation Catalyst, http://www.energy.wsu.edu/pubs/.

Catalysis By First Principles - Can Theoretical Modeling and Experiments Play A Complimentary Role in Catalysis?

C. Narula, W. Shelton, Y. Xu, M. Moses and L. Allard
Oak Ridge National Laboratory

Objective/Scope

This research focuses on an integrated approach between computational modeling and experimental development, design and testing of new catalyst materials, that we believe will rapidly identify the key physiochemical parameters necessary for improving the catalytic efficiency of these materials. The results will have direct impact on the optimal design, performance, and durability of supported catalysts employed in emission treatment e.g. lean NO_x catalyst, three-way catalysts, oxidation catalysts, and lean NO_x traps etc.

The typical solid catalyst consists of nano-particles on porous supports. The development of new catalytic materials is still dominated by trial and error methods, even though the experimental and theoretical bases for their characterization have improved dramatically in recent years. Although it has been successful, the empirical development of catalytic materials is time consuming and expensive and brings no guarantees of success. Part of the difficulty is that most catalytic materials are highly non-uniform and complex, and most characterization methods provide only average structural data. Now, with improved capabilities for synthesis of nearly uniform catalysts, which offer the prospects of high selectivity as well as susceptibility to incisive characterization combined with state-of-the science characterization methods, including those that allow imaging of individual catalytic sites, we have compelling opportunity to markedly accelerate the advancement of the science and technology of catalysis.

Computational approaches, on the other hand, have been limited to examining processes and phenomena using models that had been much simplified in comparison to real materials. This limitation was mainly a consequence of limitations in computer hardware and in the development of sophisticated algorithms that are computationally efficient. In particular, experimental catalysis has not benefited from the recent advances in high performance computing that enables more realistic simulations (empirical and first-principles) of large ensemble atoms including the local environment of a catalyst site in heterogeneous catalysis. These types of simulations, when combined with incisive microscopic and spectroscopic characterization of catalysts, can lead to a much deeper understanding of the reaction chemistry that is difficult to decipher from experimental work alone.

Thus, a protocol to systematically find the optimum catalyst can be developed that combines the power of theory and experiment for atomistic design of catalytically active sites and can translate the fundamental insights gained directly to a complete catalyst system that can be technically deployed.

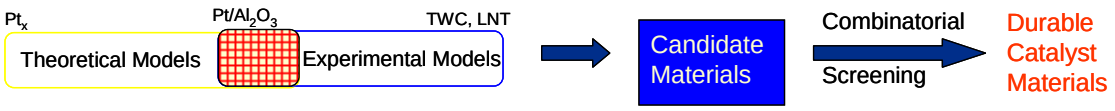

Although it is beyond doubt computationally challenging, the study of surface, nanometer-sized, metal clusters may be accomplished by merging state-of-the-art, density-functional-based, electronic-structure techniques and molecular-dynamic techniques. These techniques provide accurate energetics, force, and electronic information. Theoretical work must be based electronic-structure methods, as opposed to more empirical-based techniques, so as to provide realistic energetics and direct electronic information.

A computationally complex system, in principle, will be a model of a simple catalyst that can be synthesized and evaluated in the laboratory. It is important to point out that such a system for experimentalist will be an idealized simple model catalyst system that will probably model a "real-world" catalyst. Thus it is conceivable that "computationally complex but experimentally simple" system can be examined by both theoretical models and experimental work to forecast improvements in catalyst systems.

Our goals are as follows:

- Our theoretical goal is to carry out the calculation and simulation of realistic Pt nanoparticle systems (i.e., those equivalent to experiment), in particular by addressing the issues of complex cluster geometries on local bonding effects that determine reactivity. As such, we expect in combination with experiment to identify relevant clusters, and to determine the electronic properties of these clusters.
- Our experimental goal is to prepare and characterize metal carbonyl clusters, decarbonylated metal clusters, sub-nanometer metal particles, and metallic particles (~5 nm) on alumina (commercial high surface area, sol-gel processed, and mesoporous molecular sieve). The characterization of such catalyst is now possible with the availability of ACEM at ORNL. We will then evaluate these systems for CO conversion efficiencies to determine the species that participates in CO oxidation catalysis.
- This approach will allow us to identify the catalyst sites that are responsible for CO, NOx, and HC oxidation. We will then address support-cluster interaction and design of new durable catalysts systems that can withstand the prolonged operations.

Technical Highlights

Our results on theoretical and experimental work on Platinum-Alumina Systems are summarized in following paragraphs.

Experimental Studies: As reported previously, we synthesized 2% Pt/γ–alumina by impregnation of γ–alumina with $H_2PtCl_6 \bullet 6H_2O$ followed by calcinations in air at 450ºC. Images of the platinum particles obtained by scanning transmission electron microscope indicate 1.1 nm diameters (avg) and typically range from 0.6-1.4 nm. The absence of the high angle diffraction peaks for Pt in the X-ray diffraction patterns support the presence of only the small platinum diameters seen by electron microscopy see Figure 1a.

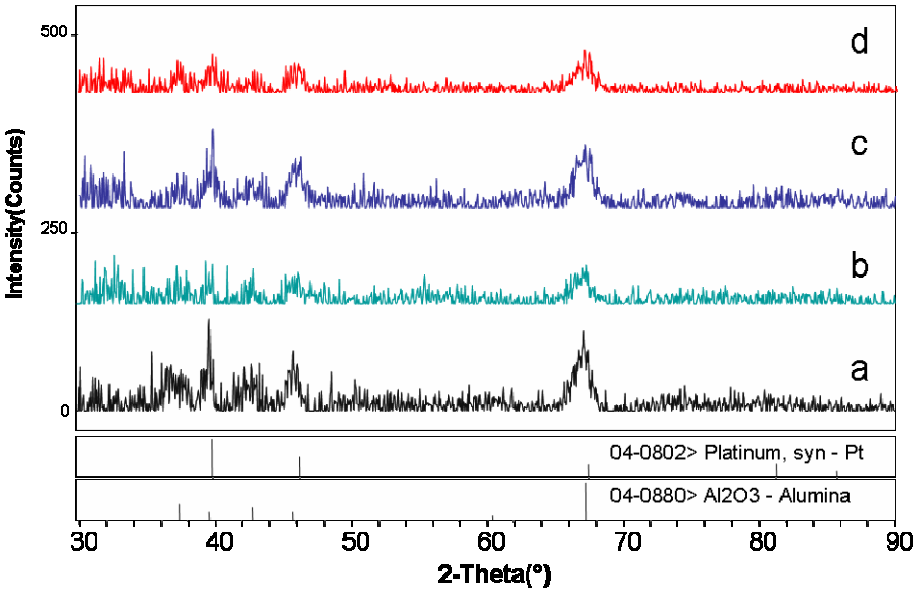

Figure 1: X-ray diffraction pattern of fresh 2% Pt/γ-A_2O_3 (a) fresh and after CO oxidation tests: (b) CO oxidation initiation (c) 50% CO light-off (d) 3 cycles of 100% CO conversion.

A second catalyst was prepared from the 2% Pt/γ-Al_2O_3 catalyst by annealing at 650°C/5h in air. Larger platinum particles are present compared to the fresh catalyst tested in the previously mentioned CO oxidation experiments according XRD, see Figure 5. Profile fitting of the high angle Pt peaks (ca. 81.4° and 85.8°) suggests that the platinum particles are 11-18.5 nm in diameter. The overlap of the lower angle Pt and alumina peaks make it more appropriate to use the high angle peaks for particle size calculation.

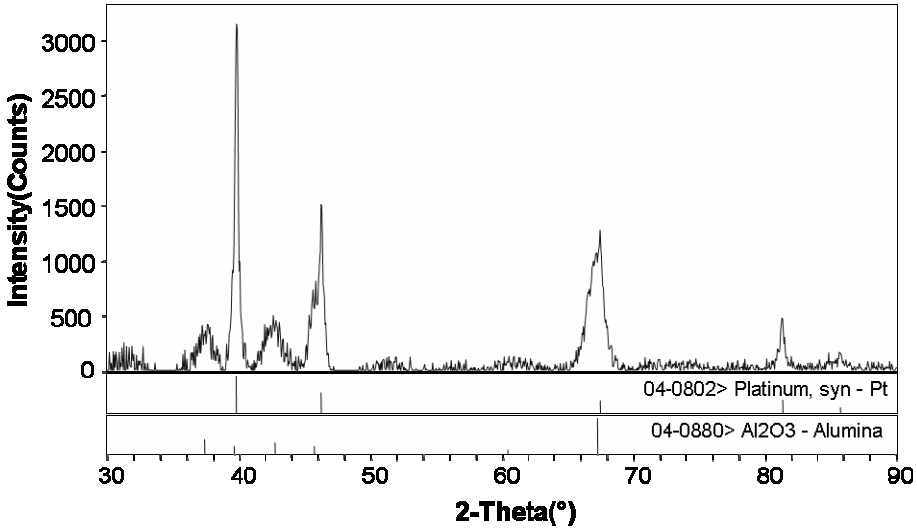

Figure 2: X-ray diffraction pattern of the fresh 2% Pt/γ-Al_2O_3 catalyst that was annealed at 650°C/5h. JCPDF patterns indicate the presence of Pt and alumina.

A third catalyst, 2% Pt/ θ-Al_2O_3, was prepared by annealing sol-gel derived γ-Al_2O_3 at 900°C/34h. Platinum was deposited on the θ-Al_2O_3 by impregnation method from $H_2PtCl_6 \bullet 6H_2O$ followed by calcinations in air at 450ºC. STEM images of the fresh catalyst indicate that the Pt particle size ranges from 0.6-1.3 nm and have an average diameter of 1.1 nm, see Figure 5.

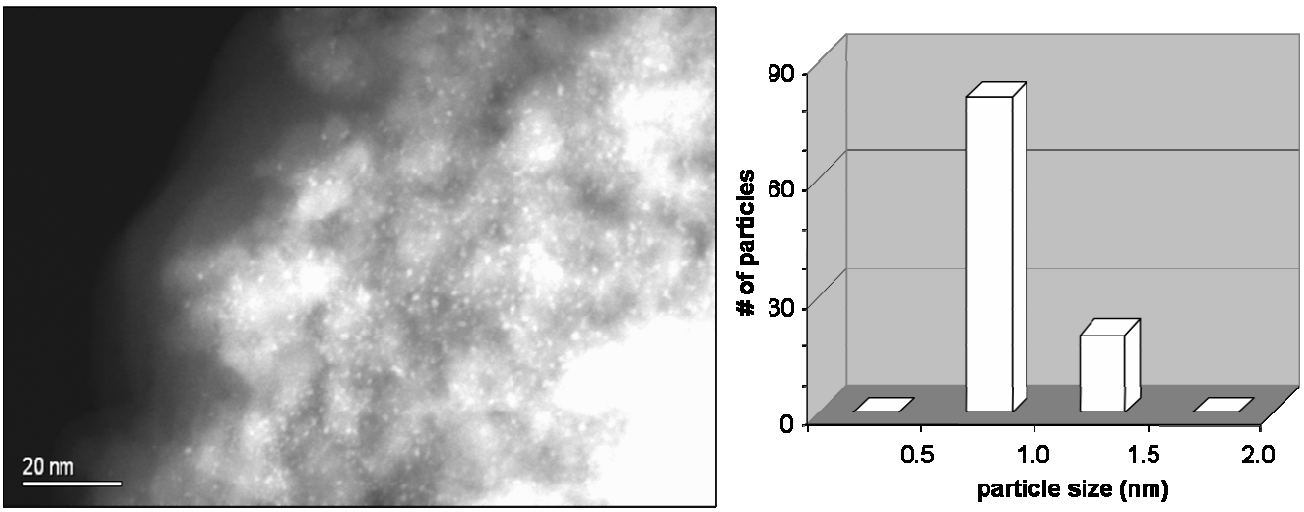

Figure 3: STEM image of fresh 2% Pt/θ-Al_2O_3 and Pt particle size distribution.

We evaluated the catalyst in a 5 mL reactor employing a gas flow of 100 cc/min comprised of 5% CO, 5% O_2, and 90% N_2. Multiple tests were run under these conditions to evaluate the effect that the CO oxidation reaction has on the platinum particle size:

a. The first test was designed to study the initial effect of CO oxidation. The temperature of the reactor was heated to 150°C then gradually increased in 20°C increments till the CO oxidation became noticeable (light-off condition).

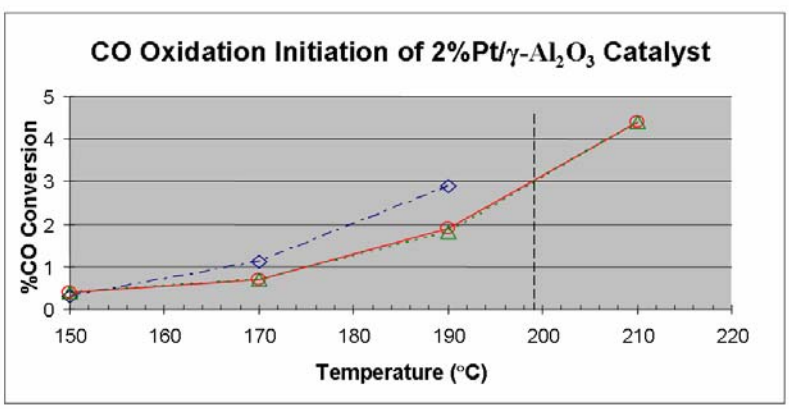

Figure 4: Initiation of catalyst conversion as a function of temperature.

The reaction was immediately stopped and catalyst sample was collected. This test was repeated 3 times to show the homogeneity of the catalysts. The CO conversion as a function of temperature is shown in Figure 1. CO oxidation initiates between 150-175ºC and is about 3% at 200°C. The X-ray diffraction pattern of the tested material, Figure 1b, indicates no significant growth of the Pt particles.

b. The second test was carried out on the 2% Pt/γ-Al_2O_3 catalyst to evaluate the effect of 50% CO conversion on the catalysts microstructure. The test was done under conditions similar to the initiation (3%). After the reactor was heated to 150°C the temperature was increased in 10°C increments. After reaching 290°C/15 minutes, the catalyst reaction approaches 50% CO conversion to CO_2, see Figure 3. No particles growth is observable by X-ray diffraction, see Figure 1c.

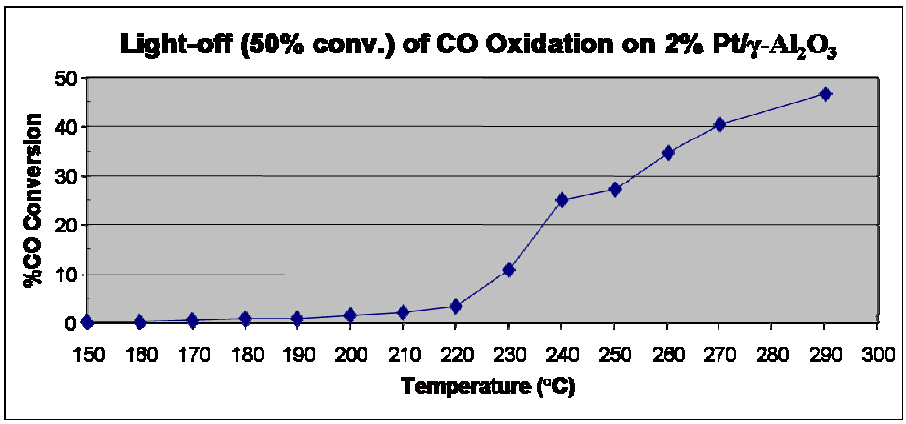

Figure 5: Catalyst light-off for CO oxidation as a function of temperature.

c. The third test was done on the 2%Pt/γ-Al_2O_3 catalyst to test for complete CO oxidation under similar conditions used for the initiation (3%) tests. However, after the reactor was heated to 150°C, the temperature was increased in 30°C increments instead of the 20°C increments used in the initiation tests. The same sample was cycled through these conditions 3 times to obtain a "degreened" catalyst. All three cycles approach 100% CO conversion at 450°C, see Figure 4. An X-ray diffraction pattern of the tested catalyst show no growth of the Pt particles, see Figure 1d.

d. In order to evaluate whether the 2% Pt/γ-Al_2O_3 catalyst active for CO conversion is based on temperature or involves a CO mediated mechanism, a fourth test was performed. A sample of the catalyst was heated to 210°C by the same method used in our CO oxidation initiation test in which we heated it to 150°C then increased the temperature in 20°C increments holding at each temperature for approximately 15 minutes. Carbon monoxides involvement was assessed by only flowing nitrogen and oxygen gas over the catalyst until 210°C was reached. At 210°C, the CO gas was introduced into the system along with the N_2 and O_2 gases allowed to flow through the reactor. When the additional flow made it to the GC, a sample was taken to analyze on the GC and the gases where

quickly turned off and the reactor system was cooled. The GC analysis indicates no CO or CO_2 was present in the 100 mL/min gas flow; however, an increase in O_2 was observed.

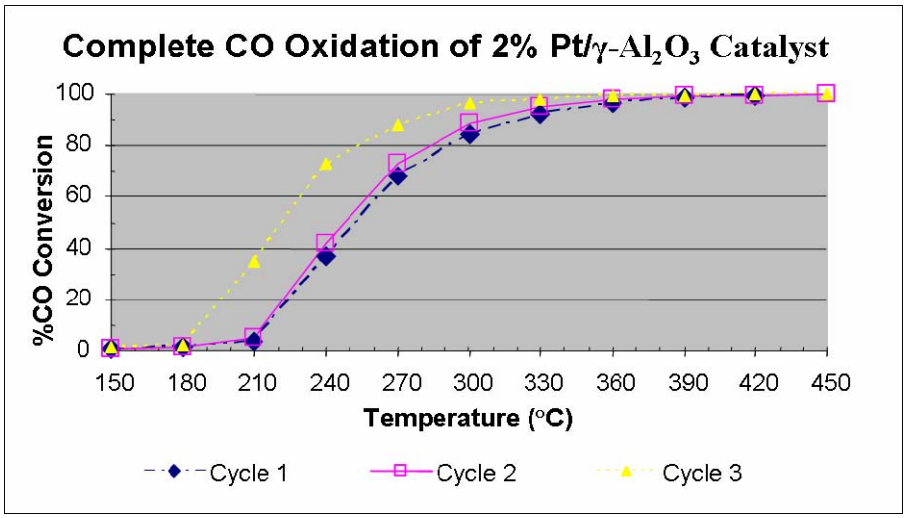

Figure 6: Complete catalyst conversion of CO to CO_2 as a function of temperature.

These results suggest the following:

- The Pt particle size change during CO oxidation is undetectable by X-ray powder diffraction data. Further examination of samples by TEM will provide information on changes in particles as a result of CO oxidation.
- The residence time and temperature are essential parameters for the conversion of CO to CO_2 over a 2% Pt/γ-Al_2O_3 catalyst.

Theoretical Studies: We have been using Density Functional Theory (DFT) based methods to investigate the oxidation of CO and NO on Pt nanoclusters. The results obtained so far indicate that the reaction energetics is strongly dependent on the size of the clusters as well as the extent of oxidation of the clusters.

We first look at the adsorption of the relevant atomic and molecular species on Pt nanoclusters, including O, CO, CO_2, NO, and NO_2 (Figure 7). The adsorption energies of O, CO_2 and NO_2 display a maximum at Pt_2 followed by a minimum at around Pt_5, after which they gradually rise toward the level on the bulk Pt surface. The adsorption energy of CO, on the other hand, rises monotonically with cluster size, so cluster size may serve as a fairly reliable predictor of CO adsorption strength on Pt clusters. NO adsorption energy percolates on the smallest Pt_x before rising toward the bulk surface level. Overall, the adsorption of CO is substantially stronger on the Pt nanoclusters than on the bulk Pt surface. The adsorption of NO and NO_2 are also strongly enhanced, followed by the adsorption of CO_2. The effect of cluster size on the adsorption of the O atom is less pronounced.

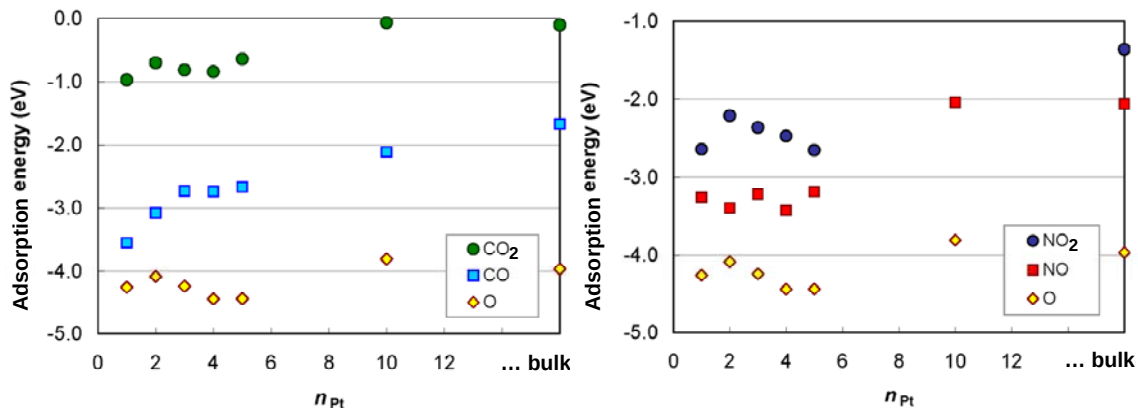

Figure 7: The adsorption energies of O, CO, CO_2, NO, and NO_2 on Pt_x nanoclusters plotted against the number of Pt atoms in the clusters.

That the adsorption of these species is enhanced to different extents compared to the bulk Pt surface means that the energy profiles of CO and NO oxidation on the clusters also differ from their bulk-surface counterparts (Figure 8). For instance, CO oxidation on the bulk Pt surface is exothermic every step along the reaction path, but because of the enhanced adsorption of CO, there is a minimum in energy when CO adsorbs on the clusters, which indicates that the ability of the Pt nanoclusters to catalyze CO oxidation may be strongly inhibited by CO itself. The same problem exists for NO oxidation. Here, in addition, both NO and NO_2 may poison the Pt nanoclusters. Furthermore, because of the smaller enthalpy of the overall reaction ($NO + ½O_2 \rightarrow NO_2$), the somewhat more strongly bound O atoms could make the Pt nanoclusters insufficiently oxidizing for NO oxidation.

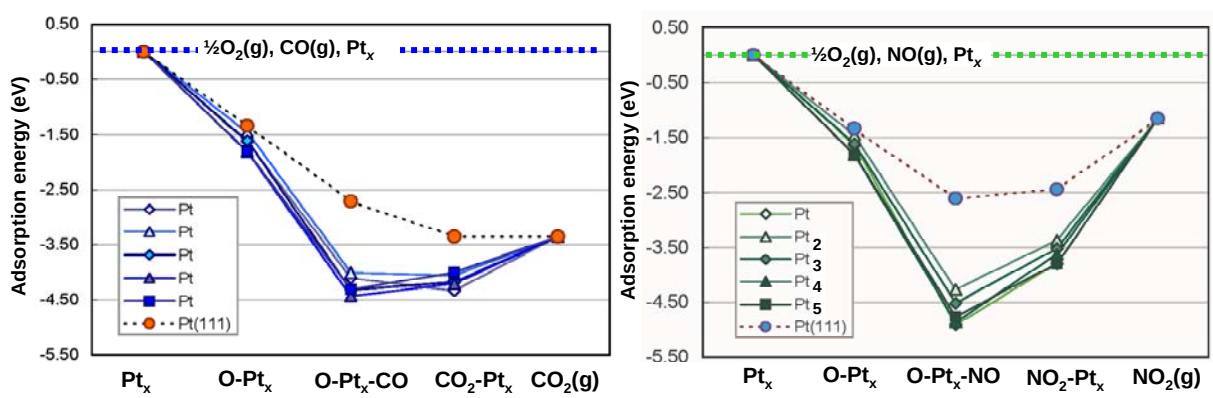

Figure 8: The reaction energy profiles for $CO + ½O_2 \rightarrow CO_2$ and $NO + ½O_2 \rightarrow NO_2$ on Pt_x (x = 1-5). The profiles on the bulk Pt surface [represented by the Pt(111) facet] are included for comparison.

Figure 9 shows the effect of cluster oxidation on the adsorption of O and CO. We find that the adsorption energies on Pt_xO_x are weaker than those on the pure Pt_x but stronger than those on Pt_xO_{2x}. Thus it appears that the more heavily oxidized the cluster is, the weaker the adsorption of O and CO becomes. The oxidation of Pt nanoclusters weakens the adsorption of NO as well.

We speculate that the energetics of CO and NO oxidation may be more favorable on the oxidized clusters than on the pure Pt clusters because of the weakened adsorption of the reactants.

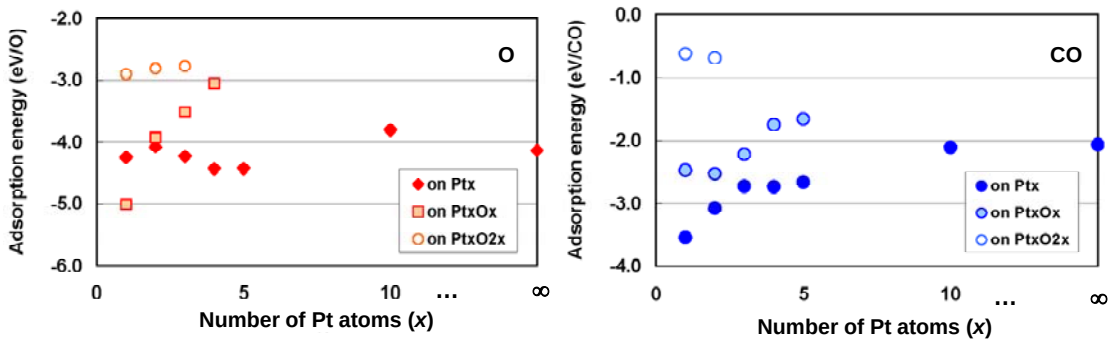

Figure 9: The adsorption energies of O and CO on Pt (Pt_x) and Pt oxide (Pt_xO_x and Pt_xO_{2x}) clusters, plotted against the number of Pt atoms in the clusters.

These results are interesting since the experimental results show that 10-20 atom Pt clusters rapidly increase in size in the presence of CO at relatively low temperatures. We are carrying out experiments to understand this result.

Next Steps: We plan to carry out the following tasks:

- We plan to complete CO oxidation studies of already synthesized Pt and Re clusters on alumina to determine the metal species involved in CO oxidation. The results will be compared with the results from theoretical calculation. If consistent, we will proceed with the evaluation of the catalysts for NO_x and hydrocarbon oxidation.

- We will synthesize Pt clusters on sol-gel and molecular sieve alumina and. This will create a matrix of samples with varying Pt particles size and oxidation on alumina substrate with increasing surface area and pore structure. We will carry out CO, NOx and HC oxidation on these samples to study the effect of morphological changes in substrates leading to changes in metal substrate interactions.

- We will continue to study the thermochemistry of CO and NO oxidation on Pt and Pt oxide clusters. We will also begin to investigate the properties of Pt and Pt oxide clusters on oxide supports (include alumina) and to extend our thermodynamic model to include support effects. These investigations will help us gain a better understanding of the structural and catalytic properties of the supported Pt clusters and by comparing these results to our earlier work on Pt and Pt clusters, we will be able to gain an understanding of the effect of the support on these important properties.

Barriers: The transfer of HD-2000 electron microscope to CNMS has delayed microstructural analysis of samples. We have submitted a proposal and we expect to be able to use this instrument again beginning July 2006.

Publications/Presentations

1. C.K. Narula, M. Moses, L.F. Allard, Society of Automotive Engineers Meeting, 2006, (Abstract Accepted)

2. Y. Xu (speaker), W. A. Shelton, and W. F. Schneider, "Platinum nanoclusters for oxidation catalysis: Thermodynamics, reactivity, and size dependence," 231st ACS National Meeting, Atlanta, GA, 3/2006.

3. Y. Xu, W. A. Shelton, and W. F. Schneider, "Effect of particle size on the oxidizability of platinum clusters," in press, *Journal of Physical Chemistry A*.

Advanced Cast Austenitic Stainless Steels for High Temperature Components

P. J. Maziasz, John P. Shingledecker, and N. D. Evans
Oak Ridge National Laboratory

M. J Pollard
Caterpillar, Inc.

Objective/Scope

This is the 2nd ORNL CRADA project with Caterpillar, which is focused on commercialization of the new CF8C-Plus cast austenitic stainless steel, which was developed during the first ORNL/CAT CRADA. CF8C-Plus stainless steel is a cost-effective material upgrade for much more performance, durability and temperature capability relative to current heavy-duty diesel engine exhaust components made from SiMo ductile cast iron. In FY 2005, this project completed the initial properties data base needed for alternate materials selection, and component design or redesign, including fatigue, thermal fatigue, and creep, and studies of aged materials. Longer term creep-testing and fatigue studies at much lower frequencies are underway, together with new tests directly related to specific component applications, like turbocharger housings. This CRADA (Cooperative Research and Development Agreement) project (ORNL02-0658) was extended beyond the initial 3-year term last year, and will be completed in July, 2007. Requests for more detailed information on this project should be made directly to Caterpillar, Inc.

Highlights

Caterpillar, Inc.
CF8C-Plus stainless steel diesel exhaust components are being made by one of Caterpillar's suppliers, and are being evaluated and tested.

Fatigue testing of the large CF8C-Plus cast gas-turbine housing component was completed at 650°C.

ORNL
New commercial heats of CF8C-Plus Cu/W show a significant creep-rupture strength advantage at 750°C and above.

Longer-term, lower stress creep tests of sand-cast CF8C-Plus stainless steel at 750°C began previously, and continued this quarter.

Technical Progress, 1st Quarter, FY 2006

Background

Current cast iron heavy diesel engine exhaust manifolds and turbocharger housings are being pushed beyond their temperature capabilities as normal duty cycles approach or exceed 750°C; the rapid and severe thermal cycling contributes to increased failures. The new cast CF8C-Plus austenitic stainless steel is now being commercialized and evaluated for this and many other

high-temperature applications. Caterpillar, Inc. and ORNL are completing the systematic and thorough properties data base required by designers to optimize component design, and are characterizing the properties of trial or prototype commercially cast stainless steel components.

Approach

Multiple commercial heats of CF8C-Plus have been cast by several commercial foundries, including static sand and centrifugal casting methods. Now, both large and small prototype CF8C-Plus components are being cast. In July 2004, a large turbine housing for an industrial gas-turbine was cast by MetalTek, International, Inc. from an 8000 lb heat of the new CF8C-Plus stainless steel. In 2005, three foundries obtained trial-licenses for CF8C-Plus steel, including MetalTek and Stainless Foundry & Engineering. By the end of 2005, over 31,000 lb of CF8C-Plus components have been cast, including exhaust manifolds, and some new, thin-walled piping. In 2005, new commercial heats of CF8C-Plus Cu/W were made, and found to have more tensile strength and more creep resistance than CF8C-Plus at 750°C and above. The outstanding castability and freedom from post-cast heat-treatments are distinct advantages for CF8C-Plus and CF8C-Plus Cu/W steels for advanced diesel components, and many other applications.

Technical Progress – Caterpillar, Inc.

The large industrial gas-turbine housing cast of CF8C-Plus stainless steel by MetalTek (6,700 lb), sectioned and inspected previously, and found to be free of defects.

Mechanical properties specimens have been made from this cast turbine housing, and mechanical testing continued this quarter. Fatigue testing at 650°C of CF8C-Plus steel component specimens was completed this quarter.

The prototyping effort for new cast austenitic stainless steel diesel exhaust components continued this quarter.

Technical Progress - ORNL

In 2005, a new commercial heat of modified CF8C-Plus steel with further additions of Cu and W, was made for ORNL by MetalTek. The initial tensile testing of as-cast material found that the Cu and W additions significantly boosted the YS relative to CF8C and CF8C-Plus at 600-850°C, particularly above 750°C. Tensile testing and preliminary fatigue testing (very high cycling frequency) of as-cast material are complete. Aging continued at ORNL this quarter on these steels, and creep, and slower cycle-rate fatigue and creep-fatigue studies began last quarter. Longer-term creep-rupture testing at 750°C at lower stresses that are more relevant to the low-stress exhaust component applications of CF8C-Plus steel began last quarter and continue this quarter, with the test going beyond 7000 h.

Communications/Visits/Travel

Detailed team communications between ORNL and Caterpillar occur regularly. The new 3-year CRADA began on July 21, 2002, when the previous CRADA ended and is scheduled to end on July 21, 2005. The two-year ORNL/Caterpillar CRADA extension was done last year until July 21, 2007.

Status of Milestones (ORNL for DOE)

FY2006 (1) Complete properties measurements of new CF8C-Plus Cu/W heats, including static and centrifugally cast materials, at 700-850°C **(02/06). Completed**. (2) Expand commercialization opportunities and complete licensing of CF8C-Plus to commercial foundries and other end-users **(08/06).** Some efforts continue, but reductions in FY 2006 funding have seriously curtailed this effort.

Publications/Presentations/Awards -

Publications

J.P. Shingledecker, P.J. Maziasz, N.D. Evans, M.L. Santella, and M.J. Pollard, "CF8C-Plus: A New High Temperature Austenitic Casting Alloy for Advanced Power Systems," in *Energy Materials*, published by Institute of Materials, Metals and Mining, W.S. Maney & Sons, Ltd., **1** (2006) 25-32.

Presentations

An invited seminar was given by J.P. Shingledecker on "Mechanical Behavior, Microstructure, and Applications for CF8C-Plus," was given Materials Science and Engineering Department at North Carolina State University, Raleigh, NC on Nov. 15, 2005.

Friction and Wear Reduction in Diesel Engine Valve Trains

Peter Blau and Jun Qu
Oak Ridge National Laboratory

Objective/Scope

The objective of this effort is to enable the selection and use of improved materials, surface treatments, and lubricating strategies for value train components in energy-efficient diesel engines. Depending on engine design and operating conditions, between 5 and 20% of the friction losses in an internal combustion engine are attributable to the rubbing between valve train components. Wear and consequent leaks around valve seats can reduce cylinder pressure and engine efficiency. Contacting surfaces in the valve train include the valve heads, seats, tappets, guides, and stems. This effort is designed to address key rubbing interfaces within the valve train where there are opportunities to employ advanced materials and surface treatments to reduce friction and save energy.

A two-pronged, interdisciplinary approach is planned to address both materials and lubrication-related aspects. The first task concerns the design and construction of a laboratory testing apparatus to simulate the thermal, chemical, and mechanical contact environment characteristic of valves and valve seats. A second task involves improving the performance of the valve stems as they oscillate within the valve guides. The latter takes into consideration not only the selection of stem and guide materials, but also the characteristics of thin lubricant films and the micromechanics of the moving surfaces. Therefore, this project embodies surface science and tribology to solve practical engineering challenges.

Technical Highlights

Design and Use of a High-Temperature, Controlled Environment, Valve Material Testing System. Work continues on the design of a controlled-environment, repetitive-impact system for studying the durability of candidate value materials, identifying their primary modes of surface damage, and providing guidance for the selection of new bulk materials, coatings, and surface treatments for valves in engines that burn a variety of fuels.

The first design drawings have been prepared and the first set of mechanical parts has been ordered. Initial construction has focused on the oscillating drive that opens and closes the simulated valve-seat contact. The next subassembly to be built is the testing chamber, its heating system, and its gas supply. In designing the testing chamber, the intent is to be capable of testing actual diesel engine valves as well as much simpler test coupons. The latter will permit screening studies of candidate valve materials and surface treatments, and to avoid the need to produce full-scale valves for testing purposes.

A major diesel engine manufacturer has provided several sets of exhaust valves (six varieties). These will be used both to ensure that our design is correct and to provide specimens of current valve materials for the first round of benchmark testing once the apparatus has been constructed.

A literature review of valve materials and their characteristic surface damage modes continues. By understanding the mechanisms of valve seat degradation that occurs in fired engines, it will

be possible to validate the operating characteristics of the new testing system and to ensure its relevance for material and surface treatment selection.

Model Boundary Lubrication Experiments. Two sets of experiments were conducted to help provide insights into the operation of valve guides under oscillating motion. One involved the design of a parallel plate apparatus to study break-away (starting) friction, and the other set involved use of an existing pin-on-flat reciprocating tester to measure the boundary friction coefficients when sliding occurs in several types of oils.

The break-away friction apparatus was designed study simple, 'model' systems. It slowly increases the pulling force (15 mN/s) until movement is observed. Variables include initial surface roughness, presence of contaminating particles, state of lubrication, and operating friction mechanism (see Fig. 1). Five different frictional processes were embodied in these experiments: (1) dry friction of smooth, hard, non-interpenetrating surfaces in which ambient, adsorbed moisture may have played a role in lubrication (e.g., glass on glass); (2) dry friction with minor abrasion (e.g., SiC abrasive surfaces on flat glass); (3) dry friction of rough, inter-penetrating hard asperities (SiC abrasive paper rubbing on itself); (4) friction in the presence of hard, loose particles; and (5) lubricated, inter-penetrating hard asperities (mineral oil lubricated SiC paper). Studies were also conducted on two stacked, parallel interfaces to simulate multi-layers of material that can occur in practical sliding systems. In recognition of the latter capability, the apparatus was named the multiple-plate tribometer (MPT).

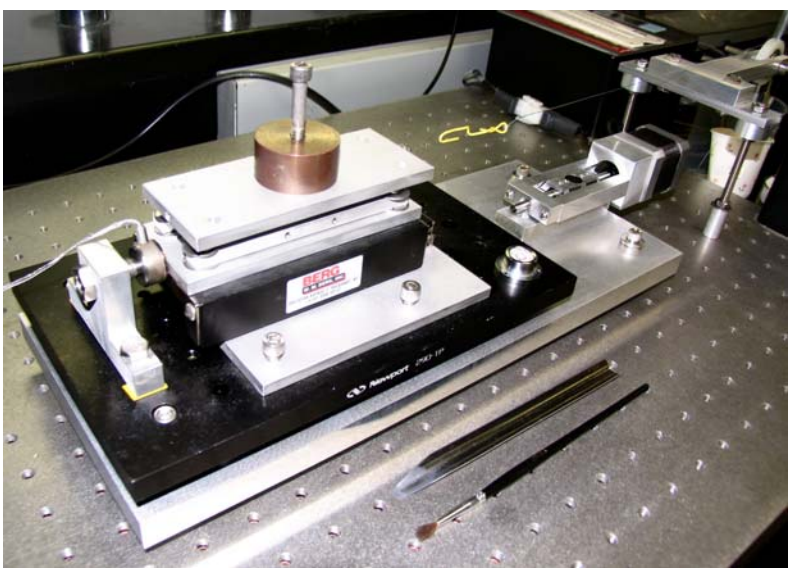

Figure 1. MPT showing the anti-vibration table, low-friction bearing stage, load cell (at the left), the upper plate containing a brass loading weight, and a nylon low-friction pulley (upper right corner) over which the loading filament passes.

As shown in Figure 2, the lowest break-away friction was observed for loose dry sand between the surfaces. The rounded particles rolled easily to reduce friction more than any of the other cases, including lubrication with mineral oil. High capillary forces between the lubricated plates and the need to shear the viscous fluid layer produced break-away friction levels higher than would be expected for typical boundary lubrication conditions ($\mu_{kinetic}$ ~ 0.08-0.12).

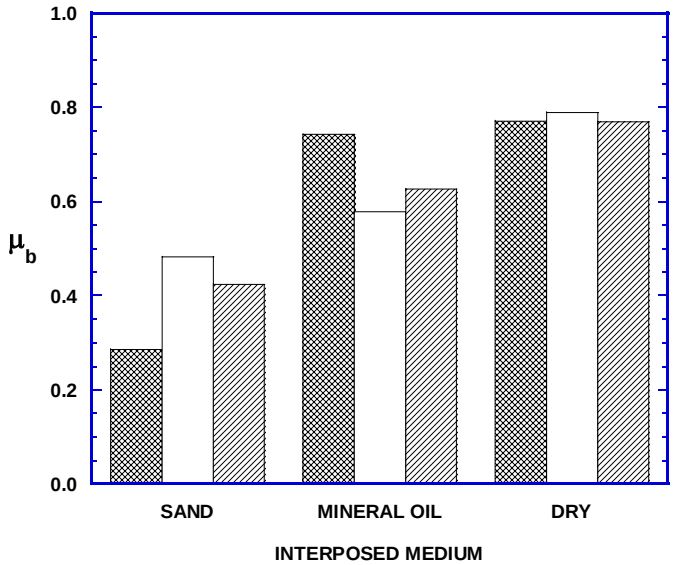

Figure 2. Break-away friction coefficients for sand, mineral oil, and dry sliding in the interface between abrasive-covered surfaces.

In reciprocating tests, the average kinetic friction coefficients were highly repeatable, and provided values typical of boundary lubrication (see Table 1). Analysis was performed of the stroke-by-stroke details for each test. Peaks at the turnaround points suggested film break-down, and slight dips in friction at the center of the strokes hinted at a transition to mixed lubrication when the sliding speed was at a maximum. Formulated diesel oils, both fresh and used, had similar friction coefficients and were about 15% lower than those for pure mineral oil.

Table 1. Friction Coefficients for Reciprocating Sliding Experiments.
(average of two tests, 1.51 N, 13.3 mm/s, 6.7 mm stroke, 440°C steel on flat glass)

Lubricant	μ_{ave}
Mineral oil	0.081
15W40 diesel oil	0.069
M11-EGR test oil	0.066

A more detailed discussion of these experiments, the apparatus, the materials, the procedures, and the results may be found in the project milestone report, dated March 2006.

Future Plans

1) Continue the literature review of valve degradation modes.

2) Continue the design and construction of an elevated temperature, repetitive-impact testing system for exhaust and intake valve materials.

Travel

P. Blau and J. Truhan (U. of Tennessee – Knoxville) traveled to Columbus, Indiana, to give invited presentations at Cummins Engine Company's 2006 Conference on Advanced Mechanics, Materials, and Reliability Engineering (AMMRE), in Columbus, Indiana. On March 2, Blau gave an extended overview of ORNL's friction and wear capabilities related to diesel technology, and on the following morning, Truhan presented a tutorial on friction and wear concepts related to diesel engines, including comments on the changing landscape of lubricant requirements as emissions and fuel efficiency continue to drive the technology. The visit concluded with a tour of the light-duty diesel engine plant where Dodge Ram engines are built.

Status of Milestones

1) Complete low-speed friction experiments that will serve as the basis for modeling the boundary-lubrication characteristics of valve stems and guides. **(03/06)**

2) Construct a valve seat simulator and establish baseline material performance data under high-temperature, engine-like conditions. **(09/06)***

* An unanticipated reduction in the FY 2006 funding for this project could delay completion of this milestone. The completion date will be updated to reflect this if and when necessary.

Publications and Presentations

1) P. J. Blau and J. Qu (2006) Starting and Steady-State Friction in Dry, Abrasive, and Boundary-Lubricated Contacts, Milestone report, Oak Ridge National Laboratory, March 31, 14 pp.

2) P. J. Blau (2006) "Oak Ridge National Laboratory Capabilities in Tribology Related to Heavy Vehicles," presented at Cummins Engine Company, Columbus, Indiana, March 2.

3) J. J. Truhan (2006) "Fundamentals of Engine Tribology," presented at Cummins Engine Company, Columbus, Indiana, March 3.

Advanced Machining and Sensor Concepts

Albert Shih
University of Michigan

Objective/Scope

The objective of this research is to investigate new technologies for cost-effective machining of Ti alloys. Metallurgical studies, including scanning electron microscopy (SEM), X-ray diffraction (XRD), electron microprobe, and nanoindentation tests were conducted on the machined surface and chips of the high throughput drillling of Ti-6Al-4V. The influence of process parameters on the change of microstructure, crystal phase, chemical composition, and mechanical properties were studied.

Technical Highlights

SEM and XRD analysis revealed that high throughput drilling of Ti-6Al-4V decreased the size of crystallite and changed the original texture. In dry drilling, the transformation of BCC β pahse into HCP α phase was identified in the subsurface layer 10-15 μm wide adjecent to the drilled hole surface of Ti-6Al-4V. This transformation was proved to be diffusionless, i.e., without chemical composition change. High hardness was found in this layer by nanoindentation test. No obvious $\beta \rightarrow \alpha$ phase transformation occurred with the supply of cutting fluid. The high hardness layer were also narrower than that of dry drilling. The saw-tooth feature in drilling chip only formed at the outmost region of the drill cutting edge, mainly due to the variable cutting speed along the cutting edge. Narrrow shear bands could be observed in the cross-sections of chips with distinct saw teeth, but no significant change of mechanical properties along the chips was found in nanoindentation tests.

1. Experimental Design and Setup

Metallurgical studies, including SEM, XRD, electron microprobe, and nanoindentation tests were conducted on the hole surface, subsurface adjacent to the hole surface, and drilling chips of the high throughput drillling of Ti-6Al-4V, which has two crystal structures: the hexagonal closed-pack (hcp) α phase, and body centered cubic (bcc) β phase [1,2]. The high throughput drilling tests has been reported in 2005 and the 1st quarter of 2006.

1.1. Experiment design

Four drilling experiments using 4 mm diameter WC-Co spiral point drills as listed in Table 1 were investigated. All drilling tests had the same 0.75 mm/s feed rate and 156 mm^3/s material removal rate.

Table 1. Experimental conditions for high throughput drilling tests.

Exp.	I	II	III	IV
Cutting speed (m/min)	183	183	91	61
Feed (mm/rev)	0.051	0.051	0.102	0.152
Cutting fluid	No	Yes	Yes	Yes

1.2. Experimental setup

After drilling, each specimen was cut in half axially along each drilled hole. One of the sectioned specimens was metallographically mounted in epoxy potting and then polished with fine diamond compound for nanoindentation testing and chemical composition analysis. After nanoindentation, the specimens were etched with a solution containing 6 ml HNO_3 and 3 ml HF in 100 ml H_2O to distinguish the α and β phase structure of Ti-6Al-4V in the SEM. The other sectioned specimen was used for XRD. An original Ti-6Al-4V bulk material was also polished and etched to extract the initial α–β phase information in SEM and XRD testing. The chips were cleaned by acetone, metallographically mounted in epoxy, and sectioned and polished for nanoindentation testing and SEM work.

The polished and etched hole and chip cross sections were examined by a Hitachi S-4700 SEM machine to identify the changes in the microstructure. The phase transformation of α–β phase was examined by a PANalytical XPERT-PRO MPD X-ray diffractometer with Cu tube (generator setting: 40 mA, 45 kV) and proportional detector with parallel beam optics, incident parabolic multilayer mirror and diffraction-side 0.09° radial divergence limiting slits. The chemical composition, especially the Al as α stabilizer and V as β stabilizer was investigated by a JEOL 8200 electron microprobe. The nanoindentation tests were conducted on the subsurface adjacent to the hole surface by using a Hysitron triboindenter™. For each indent, the applied load was 2 mN. A MTS Nano-indenter™ II was used for the nanoindentation of drilling chips. For each indent, the displacement of the indenter was about 150 nm.

2. Metallurgical Analysis of Hole Surface and Subsurface Layer

The microstructure of subsurface layer adjacent to the hole surface was observed by SEM. The change of α/β phase ratio within the drilled hole surface was analyzed quantitatively by XRD. The chemical composition was investigated by electron microprobe. The mechanical properties were examined by nanoindentation.

2.1. Microstructural observations

Fig. 1 shows the SEM micrographs of the hole cross-sections of Exps. I and II, which have the same drilling peripheral cutting speed and feed per revoluation. In Exp. I (dry drilling), the hole surface is rough with many debris welded on the hole surface and 10-15 μm thick subsurface layer. In this layer, there is a gradation of distinct grain boundaries between α and β phases to indiscernable ones from the bulk toward the hole surface. The high magnification micograph of the subsurface layer shows some tiny acicular or elongated grains. This phenomenon is likely due to two factors: one is the phase transformtion from β to α as a result of high temperature and the other is the decrease of grain size due to large plastic deformation.

In Exp. II, the β structure is obseravable at regions very close to the hole surface, suggesting that the extent of the $\beta \rightarrow \alpha$ phase transformation is significantly reduced due to the cutting fluid cooling effect. The subsurface layer is about only 3 μm. As shown in the high magnification micograph, the grain structure within the subsurface layer is elongated parallel with the hole edge, indicating the severe plastic deformation. The micrographs of Exps. III and IV showed similar features and dimensions of the features as those in Exp. II.

2.2. Quantitative XRD analysis of the β→α phase transformation

X-ray diffraction analysis results of as-polished bulk material and drilled hole surface of Exp. I are shown in Fig. 2. The X-ray diffraction pattern of the as-polished bulk material shows the bcc β phase has a (110) preferred orientation/texture. The hcp α phase is also textured on the (100) and (002) planes. In Exp. I (dry drilling), compared to the pattern of as-polished bulk material, the α peaks are clearly broader due to the decreased size of crystallite and likely rms strains (i.e. nanostrains) [3], resulting from the severe plastic deformation in the subsurface layer. Drilling process also changes the original texture and makes the α crystallites in the material more randomly distributed. The peaks corresponding to α (100) and (200) planes are weakened relative to the (101) planes. All peaks corresponding to β phase disappear.

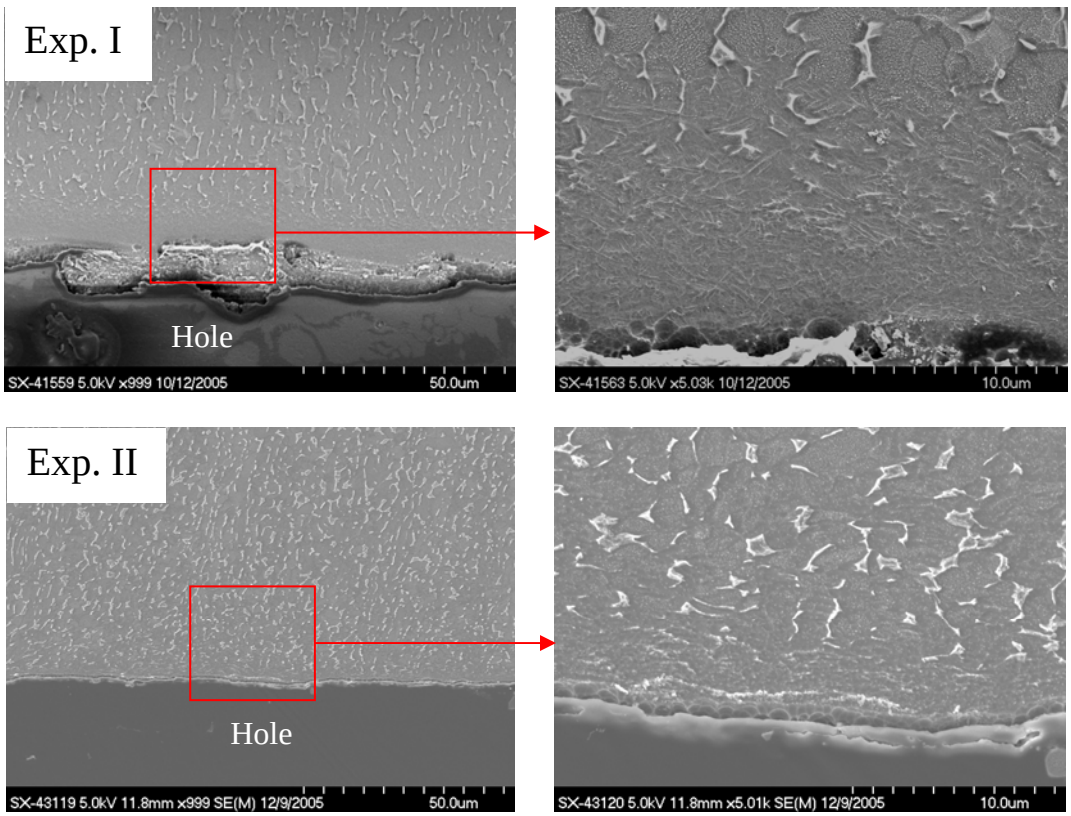

Fig. 1. SEM micrographs of the polished and etched cross-sections with drilled holes.

Quantitative analysis by Rietveld method shows 7.3% β in the bulk material. In Exp. I, the β is reduced to 0%. The X-ray penetration depth is estimated to vary from 4 to 12 μm at 30 to 90° 2θ, respectively, assuming 95% of the total diffraction intensity. According to the micrographs in Fig. 1, small amount of β grains still exists in the subsurface layer very close to the hole edge. This is slightly different with the XRD observation. There are two possible causes for the disappearance of β peaks. The main cause is the transformation of a large portion of the β to α phase. The other cause is that the residual β peaks are submerged by broadened neighboring α peaks and become indiscernible. The amount of β phase increases to 13.6, 7.8, and 11.4% for Exps. II-IV, respectively, with the introduction of cutting fluid. These values are slightly higher

than the 7.3% β phase in the bulk material and indicates that only a small amount, if any, of the β phase transformed to α on the hole surface during drilling due to the better cooling with cutting fluid.

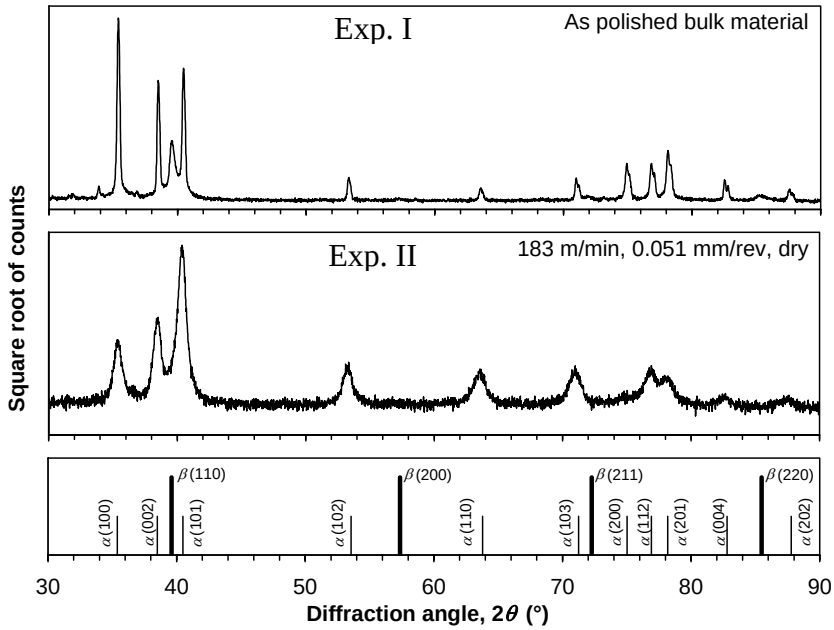

Fig. 2. X-ray diffraction patterns of the as-polished bulk material and hole surface of Exp. I (intensity shown in square root of counts to distinguish the weak peaks from background).

2.3. Chemical composition analysis

The Al and V contents were measured at seven points randomly chosen within the region less than 10 μm from the hole surface and seven points in the region far from the hole surface (bulk material). Table 2 summarizes the average and standard deviation of the Al and V contents from Exps. I and II. No statistical significant change of Al and V composition can be observed between the regions close to and away from the hole surface. Results in Table 2 support the hypothesis that the β phase decomposition under dry drilling condition is a diffusionless transformation in crystal structure and microstructure, i.e., the transformation without chemical composition change. The α to β transformation is more likely due to high temperature.

Table 2. Comparison of Al and V content in the chemical analysis of cross-sectional subsurface layer (within 10 μm from the hole surface) in Exps I and II with bulk material.

	Exp. I		Exp. II		Bulk	
	Avg	Std	Avg	Std	Avg	Std
Al (%)	6.7	0.6	6.5	0.2	6.7	0.3
V (%)	4.1	0.1	4.1	0.5	4.0	0.8

2.4. Nanoindentation hardness

Fig. 3 compares the nanoindentation hardness vs. distance from the hole surface in Exps. I-IV. The layer of high hardness exists in all conditions, but the extent and the depth of high hardness layer are different from one condtion to another. The highest hardness exists under the dry drilling condition with 183 m/min cutting speed and 0.051 mm/rev feed (Exp. I). At the reigon

less than 5 μm from the hole surface, the hardness is over 9 GPa, which is about twice the hardness measured away from the hole surface. The high hardness layer is about 15-20 μm wide. The existence of this hardened layer is the result of severe plastic deformation outweighing the thermal softening effect, as shown in the SEM micrograph, Fig. 1. The phase transformation from β to α as stated in Sec. 2.2 due to high temperature may also contributes to the formation of this layer [5,6] . Beyond this layer, the hardness is stablized around 4.1-5 GPa.

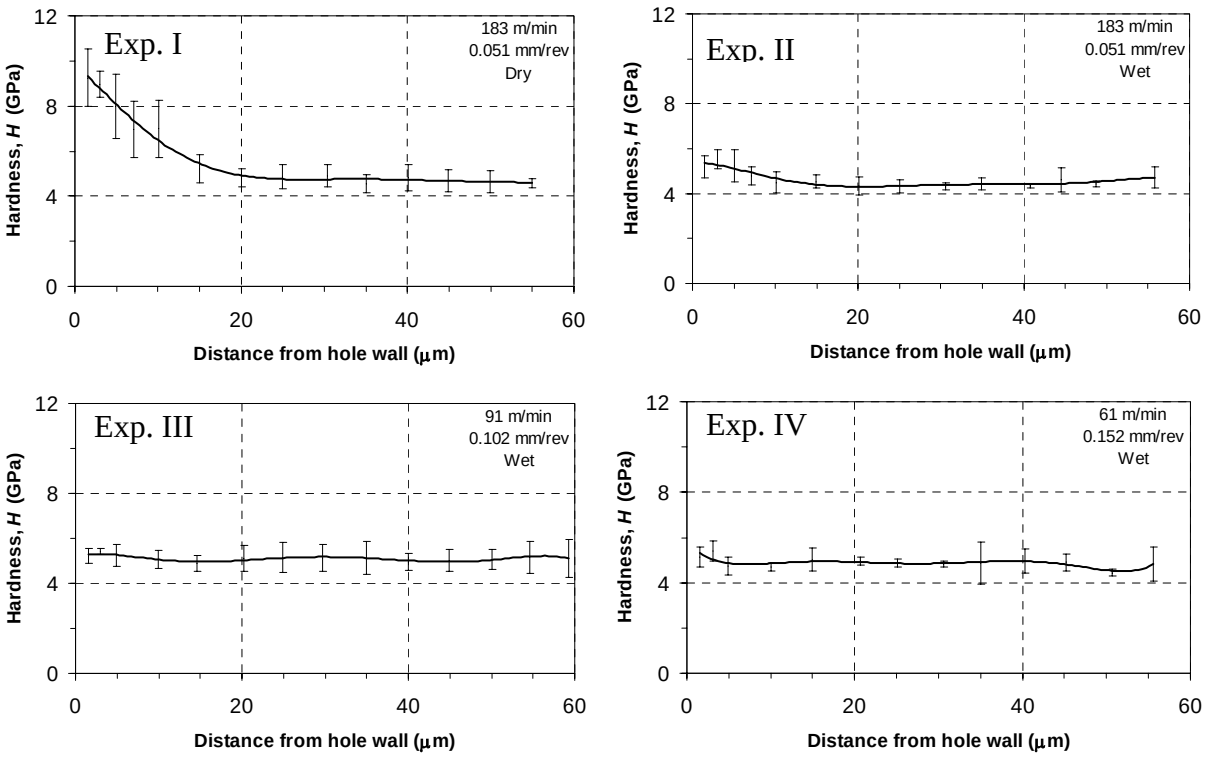

Fig. 3. Nanoindentation profile of hole subsurface hardness.

When the cutting fluid is supplied at the same cutting speed and feed (Exp. II), the peak hardness is 5-5.5 GPa in the subsurface layer close to the hole edge, which is just slightly higher than the hardness of bulk material. The thickness of hardened layer is reduced to between 5-15 μm. The introduction of the cutting fluid produces less plastic deformation relative to dry drilling because the fluid lubricates the tool-chip interface. The workpiece temperature is also reduced by the cooling effect of the liquid in additoin to reduced friction. With the supply of cutting fluid and same feed rate, the cutting speed and feed do not change the hardenss profile significantly. For Exps. III and IV, the peak hardnesses are both in the range of 5-5.5 GPa. The thickness of machining affected layer is around 5μm in both conditions, which is smaller than that of Exp. II. The decrease of layer thickness is possibly the result of smaller plastic deformation and a lower strain hardening effect at lower cutting speed.

3. Drilling Chips

According to the results of Sec. 2, the significant difference exists between dry drilling and drilling with supply of cutting fluid. With the supply of cutting fluid, the different cutting speeds

and feeds in the selected range do not influence the product quality metallurgically. As a result, only results of Exps. I and II, are presented for drilling chips.

3.1. Chip Morphology

As reported in the 1st quarter 0f 2006, the same chip morphology, a continuous chip with spiral cone followed by folded long ribbon chip, can be seen in all Ti drilling tests in this study. Different from turning, the saw tooth is not a common feature throughout the chip free surface in drilling. As labeled as point 1 in Fig. 4(a) and magnified in Fig. 4(b), saw teeth are obvious at the outmost edge of the chip which is generated at the outmost point of the drill cutting edge. This region is less than 50 μm from the chip edge. It is generated at a very small part of cutting edge whose total length is nearly 2mm. For the rest of chips, this feature becomes indiscernible and degrades to lamellae on the free surface of chip [7], as labeled as point 2 in Fig. 4(a) and magnified in Fig. 4(c).

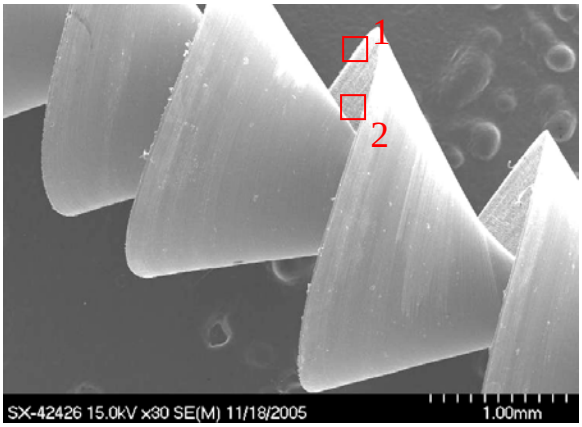

(a)

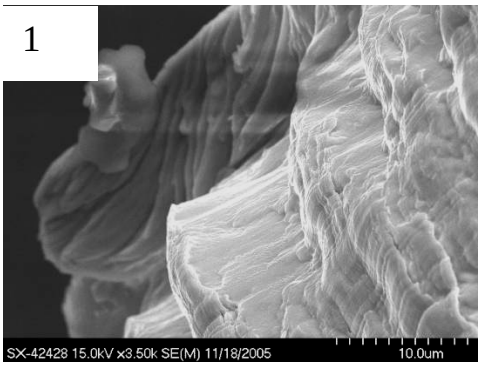

(b)

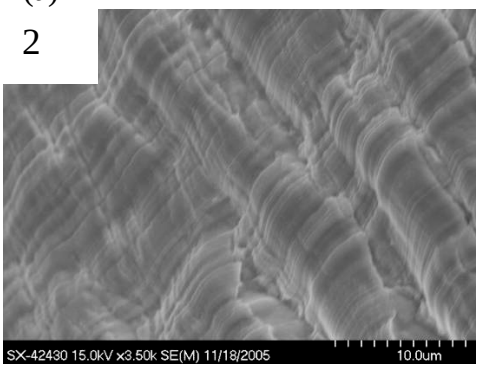

(c)

Fig. 4. SEM micrographs of chip morphology at 183 m/min cutting speed and 0.051 mm/rev feed in dry drilling (Exp. I): (a) spiral cone type chip, (b) outer edge of the chip and (c) inner side of the chip.

3.2. Microstructural observations

The SEM micrographs of chip cross-sections of Exp. I are shown in Fig. 5. Both saw teeth and small lamellae can be observed, depending on the locations where cross-sections were taken. Even in dry drilling condition, the light β phase can be observed, as well as in the condition with cutting fluid supply. It means the temperature does not reach the β transus temperature across

the entire primary shear zone during the drilling process. In chips, shear bands are observed to initiate from the valley of saw-tooth chips, as in Fig. 10 (c). The grain structures are elongated along the both sides of shear bands, clearly identifying the severe plastic shear deformation.

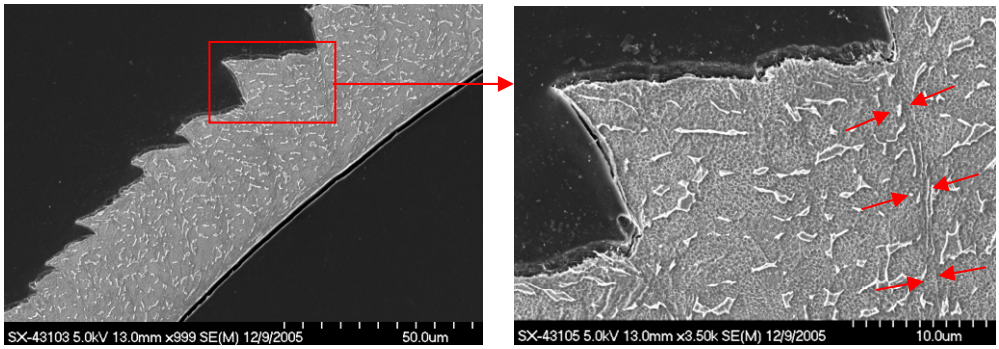

Fig. 5. SEM micrographs of chip cross-section in Exp. I.

3.3. Nanoindentation hardness

In the chip formation process at the outmost part of drill cutting edge, high temperature and strain are concentrated in the narrow bands dividing the chips into segments. High temperature tends to soften the material and possibly change the crystal structure, while high strain is expected to increase the hardness. The influence of these competing factors on the mechanical properties was examined by comparing the hardness of shear bands with that of other regions in nanoindentation tests. Fig. 6 shows an example of indents on a chip sample. The spacing between each indent is 3-6 μm. No significant difference of hardness can be found between the indents on the shear bands and those on the bulk of chips. Over 140 and 60 indents were made in a similar configuration on saw-tooth chip cross-sections under dry and wet conditions, respectively. The experimental results conclude that the formation of saw tooth feature and shear bands does not change the mechanical properties of chips severely.

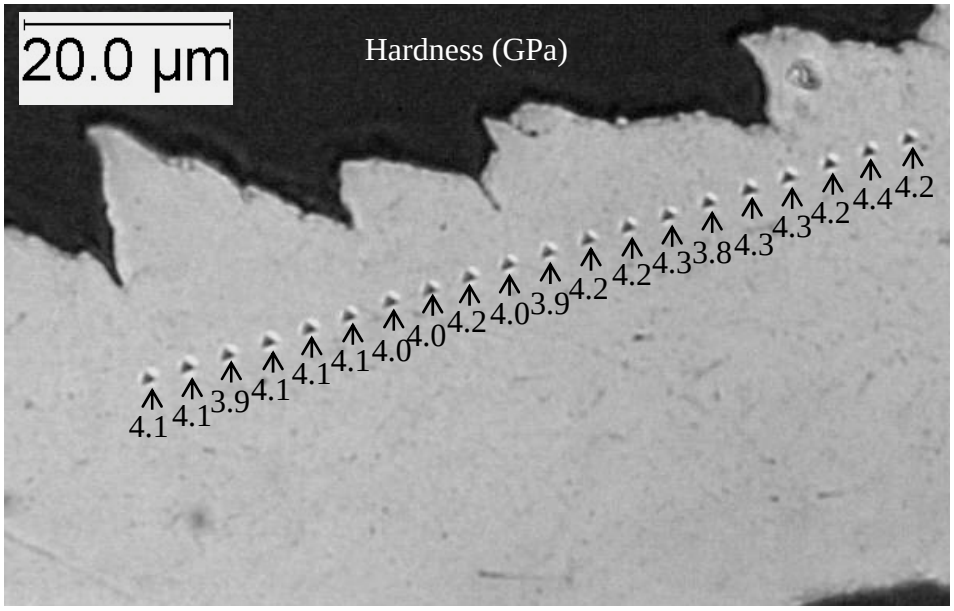

Fig. 6. Nanoindentation on the chip cross-section.

Future Work

The research will continue in the 3D finite element modeling of Ti drilling with the collaboration of Third Wave Systems and expanded to the manufacturing of HCCI diesel fuel systems. The temperature measurement using the inverse heat transfer method will be attempted for high throughput drilling with the supply of cutting fluid. As the next step, the research will be expanded to the field of high-throughput milling of Ti. Daniel Johnson, a student who is expecting to start in this project, has received and accepted an offer from Caterpillar to work at Caterpillar Technical Center during the summer to transition the project to HCCI materials and manufacturing.

Status of Milestones

Milestone 1: Experimental study of Ti drilling.

Status: Extensive tests of Ti drilling have been conducted and reported. The 183 m/min cutting speed and 156 mm^3/s material removal rate have been achieved in drilling Ti-6Al-4V using 4 mm diameter WC-Co spiral point drill. The high throughput drilling of Ti alloy is proved technically feasible.

Milestone 2: 3D finite element modeling of titanium drilling process.

Status: This work is continuing. A new version of Third Wave drilling has been released and is testing at University of Michigan.

Milestone 3: Investigation of TiC-based cutting tool material.

Status: Exploratory tests of two TiC-Ni_3Al cermets with 5% and 9% matrix material have both failed. The performance of the tool inserts with surface and cutting edge professionally prepared has been tested without obvious advantages over the current WC-Co tools. The brittleness of the TiC-Ni_3Al is identified as the main direction to improve for its future application as tool material.

Milestone 4: Measure of Ti drilling temperature.

Status: The inverse heat transfer method was developed to analyze the tool temperature in Ti drilling. High drill temperature was observed in drilling Ti, particularly at high cutting speed.

Milestone 5: Metallurgical analysis of machined surface and chips

Status: SEM, XRD, electron microprobe, and nanoindentation tests were conducted on the machined Ti-6Al-4V surface and chips after the high throughput drillling.

Communications/Visit/Travel

- Albert Shih visited ORNL in December 2005.
- Albert Shih and Dr. Marion (Bill) Grant of Caterpillar visited Caterpillar's Laredo fuel systems plant in Dec. 2005.
- Albert Shih and Daniel Johnson visited Caterpillar in March 2006 to discuss the HCCI manufacturing.

Publications

R. Li and A. J. Shih, "Finite Element Modeling of 3D Turning of Titanium," *International Journal of Advanced Manufacturing Technology* (in print).

R. Li, P. Hegde, A.J. Shih, 2006, "High Throughput Drilling of Titanium Alloys," *International Journal of Machine Tools and Manufacture* (in print).

R. Li, A.J. Shih, 2004, "Finite Element Modeling of 3D Turning of Titanium," 2004 ASME International Mechanical Engineering Congress & Exposition, November 13-19, 2004, Anaheim CA.

R. Li, A.J. Shih, 2006, "High Throughput Machining of Titanium Alloys," 2006 International Conference on Frontiers of Design and Manufacturing, Guangzhou, China, June 19-22, 2006 (accepted).

T.D. Marusich, S. Usui, R. Aphale, N. Saini, R. Li, and A.J. Shih, 2006, "Three-Dimensional Finite Element Modeling of Drilling Processes," 2006 ASME International Conference on Manufacturing Science and Engineering, October 8-11, 2006, Ypsilanti, Michigan (submitted in 2006).

References

[1] G. Lütjering, J.C. Williams, 2003, Titanium, Springer, Berlin Heidelberg.

[2] M. J. Donachie, Jr., 1988, Titanium: A Technical Guide, ASM Internal, OH.

[3] B.D. Cullity, 1978, Elements of X-Ray Diffraction, Addison-Wesley, Reading, Massachusetts.

[4] R.A. Young, 1995, Rietveld Method, Oxford University Press, New York.

[5] A.R. Machado, J. Wallbank, 1990, "Machining of Titanium and Its Alloys-A Review," Proceedings of Institution of Mechanical Engineers, Part B: Management and Engineering Manufacture, 204(1), 53-60.

[6] J. Cantero, M. Tardío, J. Canteli, M. Marcos, M. Miguélez, 2005, "Dry Drilling of Alloy Ti-6Al-4V", International Journal of Machine Tool s and Manufacture, 45(11), 1246-1255.

[7] J. Barry, G. Byrne, D. Lennon, 2001, "Observations on Chip Formation and Acoustic Emission in Machining Ti-6Al-4V Alloy," International Journal of Machine Tools and Manufacture, 41(7), 1055-1070.

Synergistic Process-Enhanced Grinding of Advanced Engine Materials

R. H. Chand
Oak Ridge National Laboratory

Objective/Scope

The objective of this effort is to understand, develop, and apply synergistic process-enhanced grinding (SPEG) to improve the efficiency of grinding advanced materials while ensuring surface quality. The three tasks involved in meeting this objective comprise a systematic approach: Evaluate current technology, develop new technology, and acquire an understanding of the fundamental principles that underlie that technology.

Task 1: Conduct a comprehensive investigation of the current state of the art in SPEG methods, especially as related to the preparation of advanced materials like ceramics and composites being considered for diesel engine components. Experience gained from leading the DOE, Cost-Effective Ceramic Machining project in the 1990's will be used to expedite completion of this task. This study will include identification of both U.S. and non-U.S. developments, including where the leading research efforts and applications of technology are being implemented.

Task 2: Modify one or more existing machine tools at ORNL to conduct instrumented, SPEG experiments on ceramics, cermets, and/or metal matrix composites that are candidates for diesel engine components. Correlations between process parameters and the quality of the resulting surfaces, assessed by metrology and microscopy, will be performed. The selection of the SPEG technique to be developed will be based on the information acquired during the accomplishment of Task 1. Modification of the grinding equipment will be initiated during FY 2006 and continue into FY 2007 when initial trials will be conducted on selected materials.

Task 3: Develop and use a high-speed, instrumented scratch testing system to study the microstructural response of advanced materials like ceramics and composites to the high deformation rates they experience during grinding. This activity will be based on ORNL's extensive experience in developing ASTM scratch hardness testing standards and in conducting dynamic hardness tests. The apparatus to be developed will have the capability of applying heat or coolants to the surface while scratching occurs. The response of advanced materials to high strain rate, single or multiple-point scratches should provide a deeper understanding the SPEG process. The completion of the instrument and an initial series of experiments are planned for the end of FY 2006.

Progress to date

Task 1: Dr. Claus Daniel, Eugene P. Wigner Fellow, analyzed, with the help of ISI Web of Knowledge by The Thomson Corporation, 2,000 most recent publications in the area of laser assisted machining, treatment, or structuring.

His findings, to date, are summarized below:

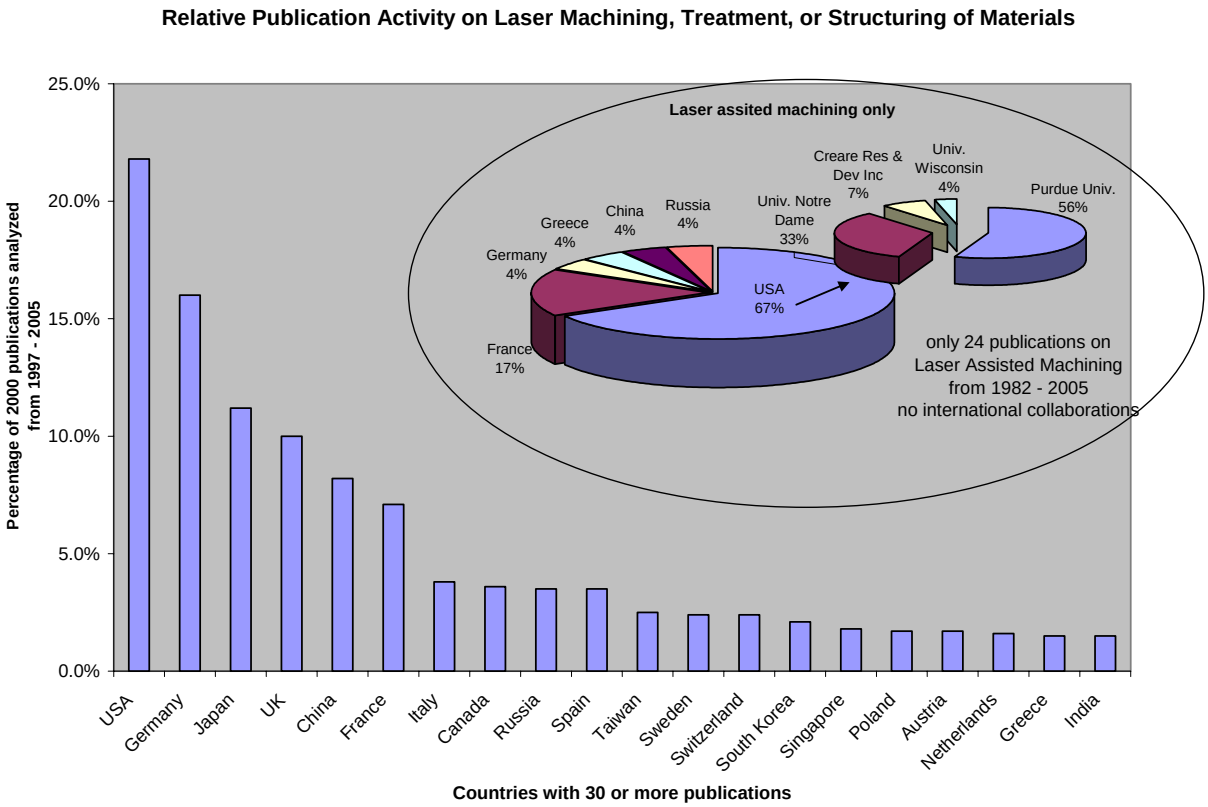

In analyzing the literature and trend, Dr. Daniel is of the opinion that

1. Materials' processing with lasers is continuing to expand.
2. Laser as a tool is making conventional manufacturing more accurate and cost-effective.
3. Laser technology is also opening up new manufacturing technologies that go beyond conventional methodologies.
4. Laser technology can be arranged in four categories, as depicted in the following diagram:

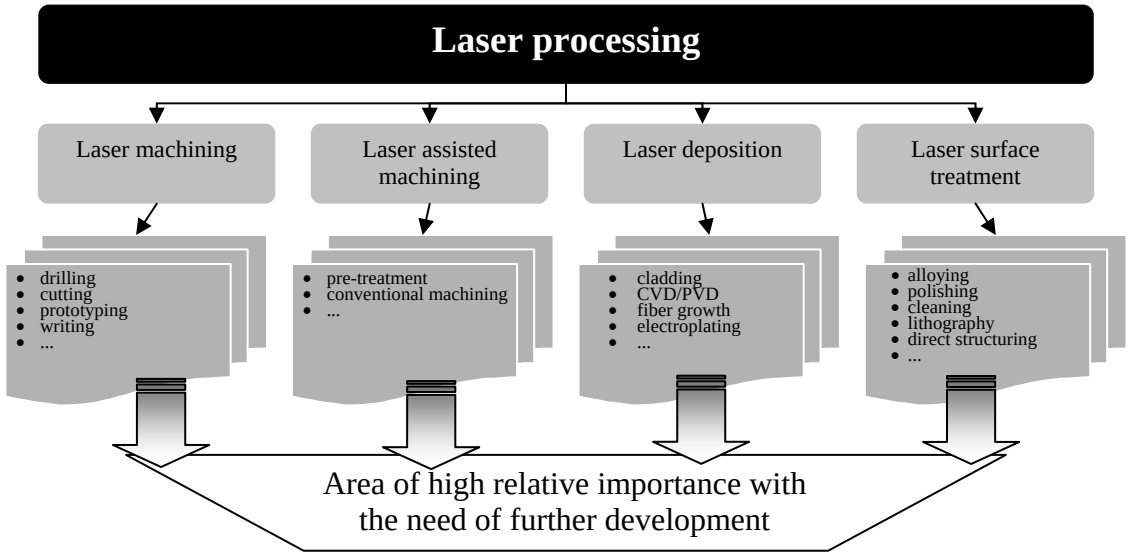

Task 2: Work is underway on:

21. Laser healing of surface cracks in silicon nitride roller-follower for diesel engine application.
2.2 Design of a system utilizing force controlled hone for machining the ID of a silicon nitride roller follower.
2.3 In-process laser dressing of a Superabrasive wheel.

Task 3: Two activities are being conducted under this task.

3.1 Jun Qu has developed a grinding model for Superabrasive grinding

$$MRR = C\left(\frac{\alpha \cdot l^{1/2} \cdot E}{K_c^{1/2} \cdot H^{19/12-\lambda/3}}\right) \cdot \left(\frac{\gamma^{1/12+2\lambda/3} \cdot l_s^{1/4+2\lambda}}{d_s^{1/24+\lambda/3} \cdot f_v^{1/18+4\lambda/9}}\right) \cdot \left(\frac{v_s}{w^{1/12+2\lambda/3} \cdot a^{1/24+\lambda/3}}\right) \cdot P_n^{13/12+2\lambda/3}$$

Work material properties — Wheel specs and dressing condition — Grinding parameters

Where MRR (mm^3/s): Material removal rate
P_n: Normal grinding force
C: Material-independent constant
α, λ: Material-dependent constants
l: Grain size of work material
E: Elastic modulus of work material
K_c: Fracture toughness of work material
H: Hardness of work material

γ: dressing factor
l_s: Particle size of grinding wheel abrasive grits
d_s: Grinding wheel diameter
f_v: Volume fraction of the abrasive of grinding wheel (diamond concentration)
v_s: Surface speed of grinding wheel
w: Grinding width
a: Depth of cut

Further work on this model and experimental verification is being planned.

3.2 A diamond wheel consisting of a in-line diamond grits of known size and spacing has been designed for conducting a high speed scratch test. The test is being designed now and the wheel configuration is shown below:

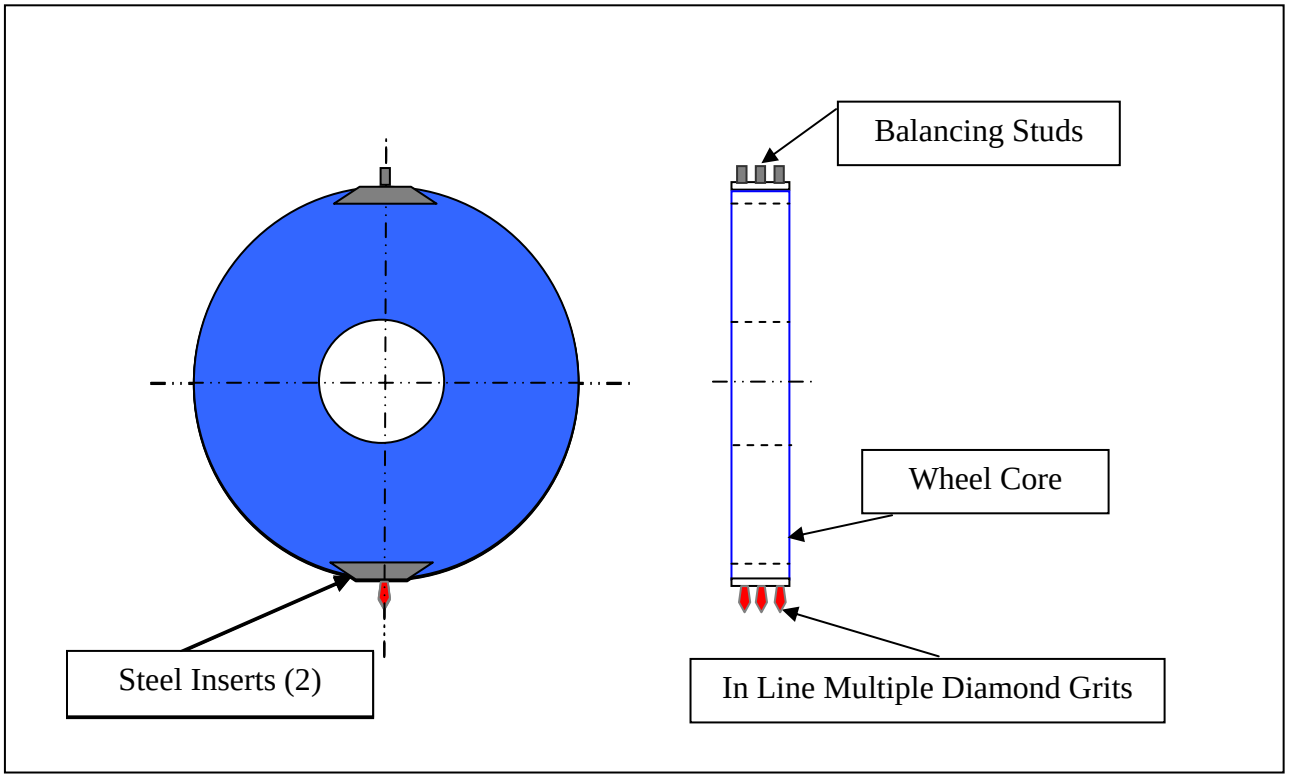

Future Plans

Task 1: Further analysis of techniques is being conducted to define relative importance of each area. Some of the techniques are state-of-the-art in manufacturing technologies; others still have barriers that need to be overcome. Our focus will continue on fields of high importance that need further development.
Task 2: Continue with work already underway. Test low surface speed machining methodology.
Task 3: Establish the high speed scratch test matrix. Build the new test wheel.

Travel

None this quarter.

FY 2006 Milestones

1) Complete survey of non-traditional machining processes that combine synergistic effects to enhance materials removal. **(06/06)**

2) Complete construction of a high strain-rate scratch testing system to enable basic grinding studies under environmentally-controlled conditions. (**09/06**)

Presentations and Publications

None this quarter.

NDE Development for Ceramic Valves for Diesel Engines

J. G. Sun and J. S. Tretheway*

Argonne National Laboratory
***Caterpillar, Inc.**

Objective/Scope

Emission reduction in diesel engines designated to burn fuels from several sources has lead to the need to assess ceramic valves to reduce corrosion and emission. The objective of this work is to evaluate several nondestructive evaluation (NDE) methods to detect defect/damage in structural ceramic valves for diesel engines. One primary NDE method to be addressed is elastic optical scattering. The end target is to demonstrate that NDE data can be correlated to material damage as well as used to predict material microstructural and mechanical properties. There are two tasks to be carried out: (1) Characterize subsurface defects and machining damage in flexure-bar specimens of NT551 and SN235 silicon nitrides (Si_3N_4) to be used as valve materials. Laser-scattering studies will be conducted at various wavelengths using a He-Ne laser and a tunable-wavelength solid-state laser to optimize detection sensitivity. NDE studies will be coupled with examination of surface/subsurface microstructure and fracture surface to determine defect/damage depth and fracture origin. NDE data will also be correlated with mechanical properties. (2) Assess and evaluate surface and subsurface damage in Si_3N_4 and TiAl valves to be tested in a bench rig and in an engine. All valves will be examined at ANL prior to test, during periodic scheduled shut downs, and at the end of the planned test runs.

Technical Highlights

Work during this period (January-March 2006) focused on analysis of laser-scattering NDE data for TiAl intermetallic natural-gas valves that were tested in a cyclic-impact rig for 20 hours, and on development of a cross-polarization confocal microscopy setup to examine 3D subsurface microstructure in a NT551 Si_3N_4 specimen.

1. Laser-Scatter NDE Evaluation of Rig-Tested TiAl Valves

During this period we acquired and analyzed laser-scattering NDE data for 5 oxidation-treated TiAl valves that were proof tested in a cyclic-impact rig at Caterpillar for 20 hours. Table 1 lists the test parameters for these valves. Figure 1 is a photograph of TiAl valve #9. It is apparent that the oxidation treatment caused chemical reaction in the Ti-alloy rod surface. These valves will be used by Caterpillar in an engine duration test.

Table 1. List of rig-test and NDE-scan parameters for TiAl engine valves.

No.	Valve type	Valve #	Rig test duration (h)	NDE scan
1	TiAl exhaust	5	20	head
2	TiAl exhaust	6	20	head
3	TiAl exhaust	7	20	head
4	TiAl exhaust	8	20	head
5	TiAl exhaust	9	20	head

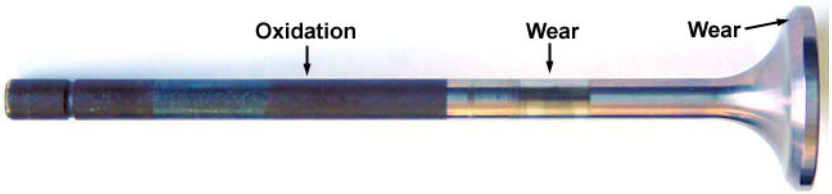

Fig. 1. Photograph of TiAl valve #9 after 20-h rig test.

From visual inspection it was noticed that all TiAl valves have become non-eccentric by ~0.5 mm off axis, likely due to the high-temperature oxidation treatment. Some wear was observed on the TiAl rod and impact surfaces as indicated in Fig. 1. When mounted on the rotation stage for NDE scans, the valves exhibited considerable wobbling, causing some difficulty in focusing the laser beam on the surface. Figure 2 shows the laser-scatter image of the valve-head surface of TiAl valve #9 after 20-h rig test, which displays a slightly higher laser-scatter intensity in the "wear scar" region than in the surrounding region of the impact surface. The wear scar is detected in all TiAl valves; another example is shown in Fig. 3 for TiAl valve #6. The higher laser-scatter intensity indicates some surface damage on the wear-scarred regions. Figure 4 shows photomicrographs of wear-scarred surfaces in TiAl valve #9; it is seen that scarred surface becomes rougher with some surface marks. It would be interesting to continuously monitor the progress of these wears with additional accumulated impact times. Nevertheless, these wears are minor compared with those observed on non-oxidation treated TiAl valve surfaces which showed considerable lost of surface materials (see Figs. 6 and 7 in our Oct-Dec 2005 quarterly report). Therefore, oxidation of the TiAl surface has significantly improved its wear resistance.

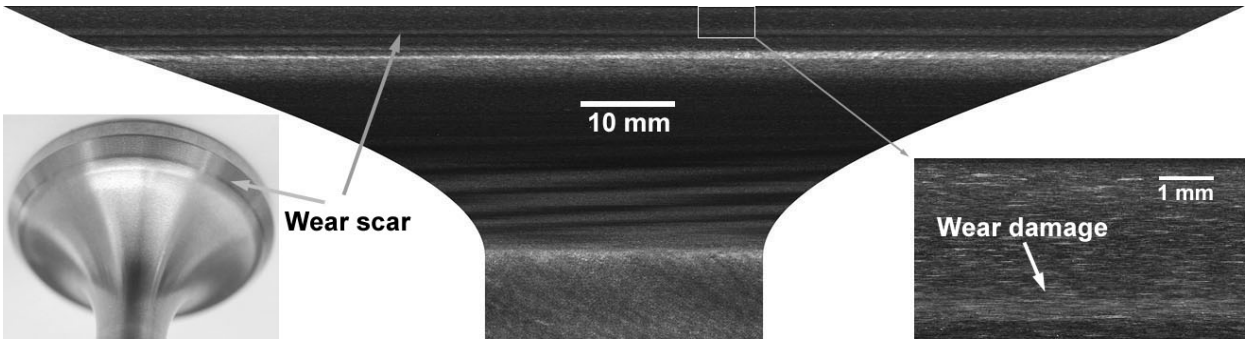

Fig. 2. Laser-scatter scan image of head surface of TiAl valve #9 after 20-h rig test.

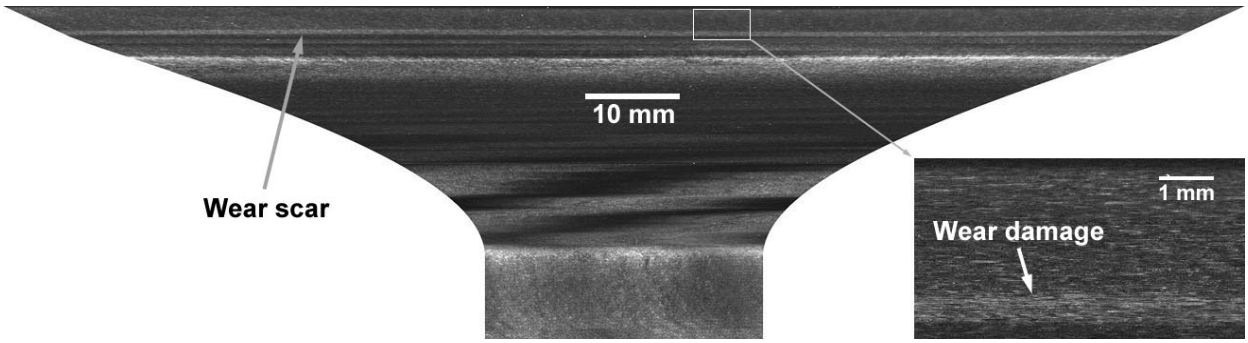

Fig. 3. Laser-scatter scan image of head surface of TiAl valve #6 after 20-h rig test.

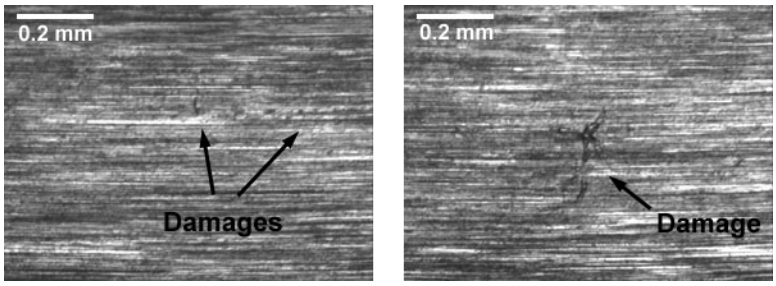

Fig. 4. Detailed photomicrograph of contact surface of TiAl valve #9 after 20-h rig test.

Caterpillar has indicated that engine test for Si_3N_4 and TiAl valves will be started in the next period. NDE inspection of these valves will be conducted during the periodic engine stops. Available results will be presented in the next period.

2. Development of a Cross-Polarization Confocal System for Measurement of 3D Subsurface Microstructure in Silicon Nitride Ceramics

Measurement of detailed 3D subsurface microstructure is critical in determining material properties. However, the laser-scatter method used for subsurface damage detection for ceramic valves can only image the 2D microstructure in the subsurface without the depth resolution. To resolve depth and improve spatial resolution, a cross-polarization confocal microscopy technology was developed at Argonne. A schematic diagram of the system is shown in Fig. 5. This setup is similar to a conventional confocal setup, except the use of a polarized laser and a polarizing beam splitter (PBS) necessary for cross-polarization backscatter detection. During a typical test, the sample is scanned in the x-y-z directions in a raster fashion, and the resulting 3D scattering data can be viewed as lateral or cross-sectional images showing the subsurface microstructure of the sample. Preliminary tests indicated that, with a moderate 40X objective lens at an optical wavelength of 633 nm, the system has an axial (depth) resolution of ~2 µm and a lateral resolution of ~0.6 µm, which are significantly higher than other available optical methods used for direct subsurface structure measurement.

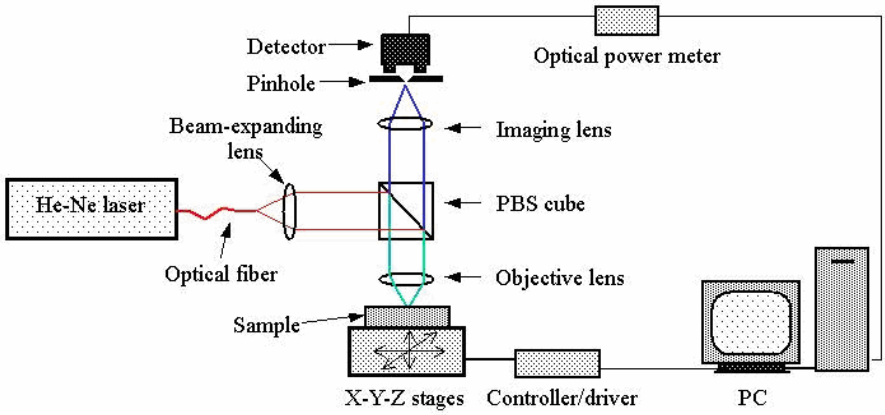

Fig. 5. Illustration of cross-polarization confocal microscopy system.

A NT551 silicon nitride specimen with known subsurface damage was tested using the confocal system. The damage is subsurface C cracks induced by indentations with different loading forces. Figure 6 shows a lateral scan image of a damaged region with two C cracks generated by 2800 and 3000N loads. Strong laser scattering intensity is observed from both C cracks as well as from many individual material defects likely porosity spots. In order to examine the crack angle and depth of the C cracks, two cross-sectional scans, marked as lines A and B in Fig. 6, were performed. The scan results are shown in Fig. 7, which provides clear visualization of the direction and depth of the C-crack extensions in the subsurface. It is evident that the C-cracks exhibit complex damage patterns that may be the results of interaction with the material's subsurface microstructure. However, the results in Fig. 7 also indicate that the detection depth is only about 40 micron for the NT551 material when using a laser wavelength of 633 nm. The depth of optical penetration can be increased using longer laser wavelengths. Work will be continued to utilize an infrared 850nm wavelength to improve the detection depth.

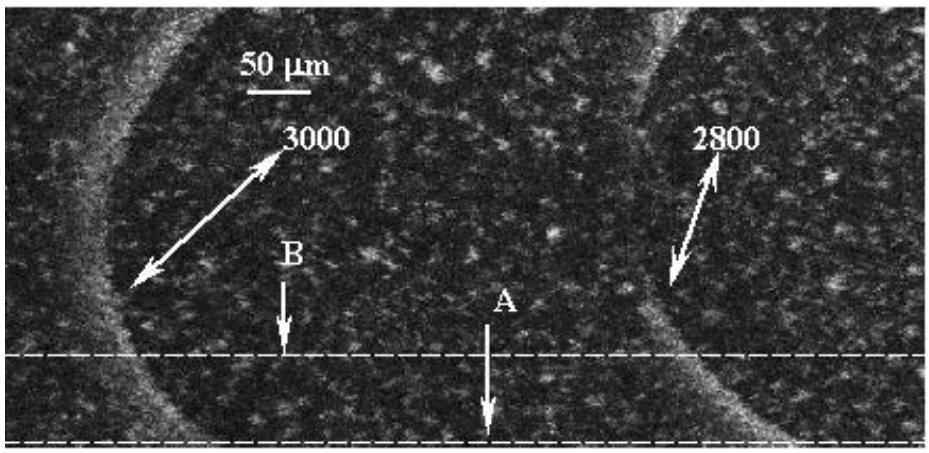

Fig. 6. Lateral confocal-scan image of a NT551 silicon nitride specimen with two C cracks.

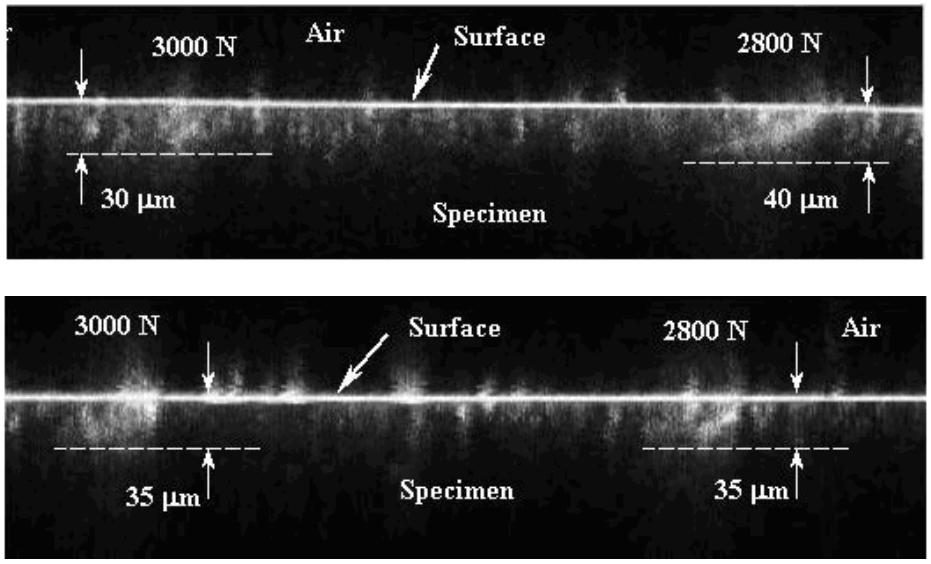

Fig. 7. Cross-sectional confocal-scan images along lines A (top) and B (bottom) as indicated in Fig. 5.

Status of Milestones
Current ANL milestones are on schedule.

Communications/Visits/Travel
J. G. Sun attended the 30th International Cocoa Beach Conference and Exposition on Advanced Ceramics & Composites, Cocoa Beach, FL, Jan. 22-27, 2006 and presented a paper entitled "Nondestructive Evaluation of Machining Damage in Silicon-Nitride Ceramic Valves," and an invited talk on "Optical NDE Methods for Characterization of Subsurface Microstructure in Silicon Nitride Ceramics."

Problems Encountered
None this period.

Publications
J. M. Zhang, J. G. Sun, M. J. Andrews, A. Ramesh, J. S. Trethewey, and D. M. Longanbach, "Characterization of Subsurface Defects in Ceramic Rods by Laser Scattering and Fractography," in *Review of Quantitative Nondestructive Evaluation*, Vol. 25, eds. D.O. Thompson and D.E. Chimenti, pp. 1209-1216, 2006.

Life Prediction of Diesel Engine Components

H. T. Lin, T. P. Kirkland, Hong Wang, A. A. Wereszczak
Oak Ridge National Laboratory

Jeremy Trethewey and Nan Yang
Caterpillar Inc.

Objective/Scope

The valid prediction of mechanical reliability and service life is a prerequisite for the successful implementation of structural ceramics and advanced intermetallic alloys as internal combustion engine components. There are three primary goals of this research project which contribute toward that implementation: the generation of mechanical engineering data from ambient to high temperatures of candidate structural ceramics and intermetallic alloys; the microstructural characterization of failure phenomena in these ceramics and alloys and components fabricated from them; and the application and verification of probabilistic life prediction methods using diesel engine components as test cases. For all three stages, results are provided to both the material suppliers and component end-users.

The systematic study of candidate structural ceramics (primarily silicon nitride) for internal combustion engine components is undertaken as a function of temperature (< 1200°C), environment, time, and machining conditions. Properties such as strength and fatigue will be characterized via flexure and rotary bend testing.

The second goal of the program is to characterize the evolution and role of damage mechanisms, and changes in microstructure linked to the ceramic's mechanical performance, at representative engine component service conditions. These will be examined using several analytical techniques including optical and scanning electron microscopy. Specifically, several microstructural aspects of failure will be characterized:

(1) strength-limiting flaw-type identification;
(2) edge, surface, and volume effects on strength and fatigue size-scaling
(3) changes in failure mechanism as a function of temperature;
(4) the nature of slow crack growth; and
(5) what role residual stresses may have in these processes.

Lastly, numerical probabilistic models (i.e., life prediction codes) will be used in conjunction with the generated strength and fatigue data to predict the failure probability and reliability of complex-shaped components subjected to mechanical loading, such as a silicon nitride diesel engine valve. The predicted results will then be compared to actual component performance measured experimentally or from field service data. As a consequence of these efforts, the data generated in this program will not only provide a critically needed base for component utilization in internal combustion engines, but will also facilitate the maturation of candidate ceramic materials and a design algorithm for ceramic components subjected to mechanical loading in general.

Technical Highlights

TiAl intermetallic alloys

Studies of long-term creep behavior of TiAl alloys manufactured by Daido and Howmet were continued during this reporting period. Two types of TiAl cylindrical creep specimens different in final densification process (i.e., one is HIP and the other one is Non-HIP) manufactured by Daido, Tokyo, Japan, were received from end user. The test conditions specified are relevant to the temperature and stress profile encountered by TiAl turbo wheel under the application environments. The database generated will then be used for verification of probabilistic life prediction of turbo wheel under engine operation conditions. Figure 1 and 2 show the creep strain versus time curves of Daido HIP TiAl material tested at 650°C/240 MPa and 750°C/240 MPa, respectively after the completion of the creep test. Note that the pre-mature fracture of specimen tested at 650°C/240 MPa arises from the unexpected power failure caused by thunderstorm. The estimated steady-state creep rate for test at 650°C/240 MPa and 750°C/240 MPa is ~ 1.29×10^{-9} 1/s and 2.90×10^{-8} 1/s, respectively. Results showed that an increase of 100°C in test temperature leads to at least 20-times increase in creep deformation rate under the same applied stress level. Figure 3 and 4 show the preliminary creep curves for specimens tested at 650°C/390 MPa and 700°C/390 MPa, respectively. The cause for one at 650°C/390 MPa exhibiting abnormally erratic creep strain history was presently not clear. However, the cyclic erratic-type creep curve observed for 700°C/390 MPa test is probably due to the fluctuation in environment temperature that consequently causes the dimension change in contact extensometer fixture and thus measured displacement. Note that the creep curve at 700°C/390 MPa seems still at the primary (or transient) stage. Creep rates obtained as a function of applied stress level and test temperature would allow one to understand the creep controlling mechanisms as well as the activation energy. Tensile creep specimens of TiAl manufactured by Howmet were also received during this reporting period and will be tested under the similar creep test matrix to Daido TiAl materials.

TiAl alloys are also considered for exhaust valve application. In general these exhaust valves are always subject to the high-speed reciprocal movement during services. The responses of TiAl materials in the corresponded application condition need to be properly addressed before they can be successfully implemented in the engine system. This approach is employed because of its advantages over the traditional sliding scratch technique in characterizing the materials removal mechanisms. Thus, studies of dynamic scratch test using a single-grit pendulum (rotational) scratch technique (Fig. 5) were initiated in order to provide insight into the dynamic abrasion of TiAl alloys in sliding contact. TiAl alloys evaluated include Daido HIP and non-HIP TiAl, and Howmet TiAl material, which exhibit differences in grain domain and lamellar size, and thus could lead to difference in mechanical and wear response.

Silicon nitride and TiAl exhaust valves

Preparation of the Caterpillar G3406 nature gas engine for testing both the silicon nitride and TiAl exhaust valve has been completed during this reporting period. The engine was also proof-tested with metallic valves currently employed in the engine. The first 100-h engine test with both silicon nitride and TiAl valves will be initiated under specified engine conditions.

Status of Milestones
Milestone: "Complete mechanical testing and analysis of prototype silicon nitride and TiAl valves after natural gas engine field test." On schedule.

Communications / Visitors / Travel
Monthly meeting with Jeremy Trethewey at Caterpillar, and Michael Kass and Tim Theiss at NTRC on the updated status of engine preparation for the testing of Si_3N_4 and TiAl exhaust valves.

Communications with Jeremy Trethewey and Nan Yang at Caterpillar on the update of tensile creep tests for TiAl materials.

Communications with Jeremy Trethewey and Nan Yang at Caterpillar on the update of machining of biaxial discs from airfoils of TiAl turbo wheel for mechanical strength evaluation.

Problems Encountered
None.

Publications
None

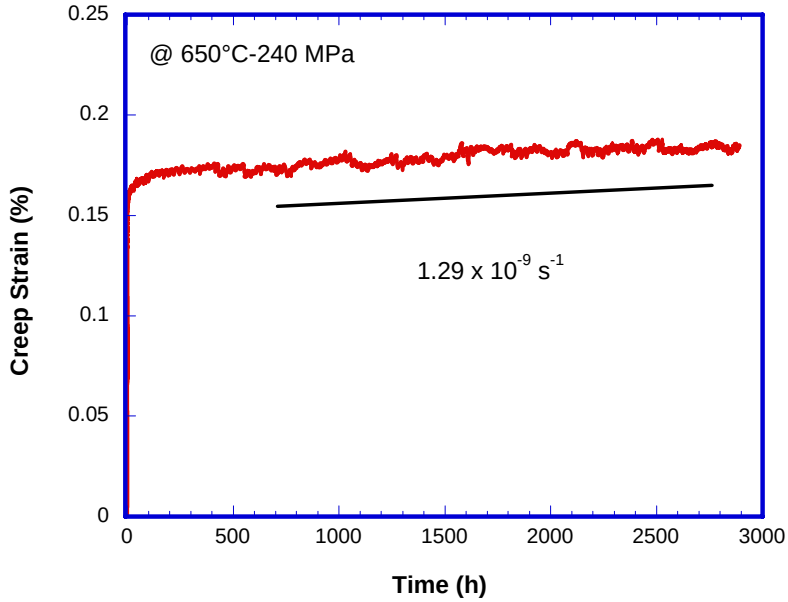

Figure 1. Creep strain versus time curve of Daido HIP TiAl material tested at 650°C and 240 MPa in air.

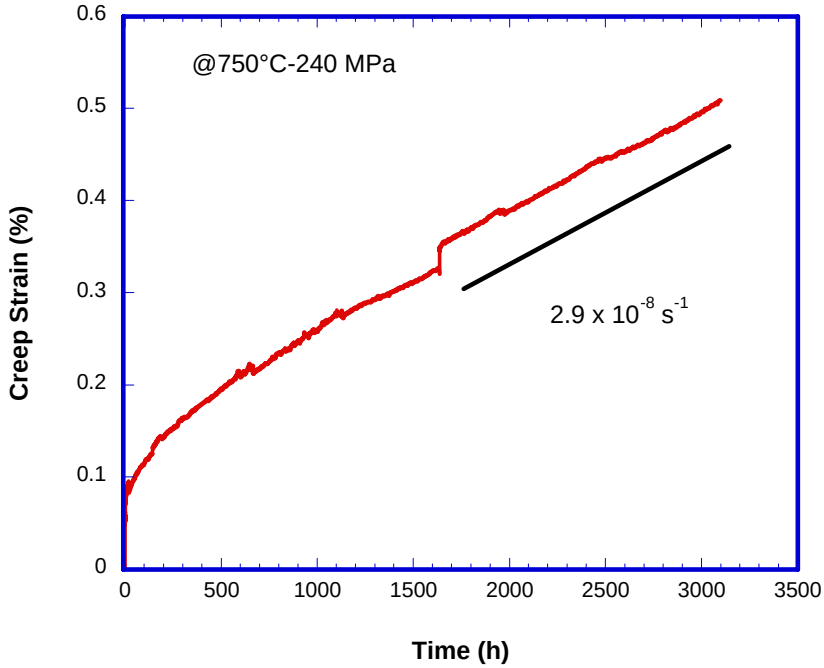

Figure 2. Creep strain versus time curve of Daido HIP TiAl material tested at 750°C and 240 MPa in air.

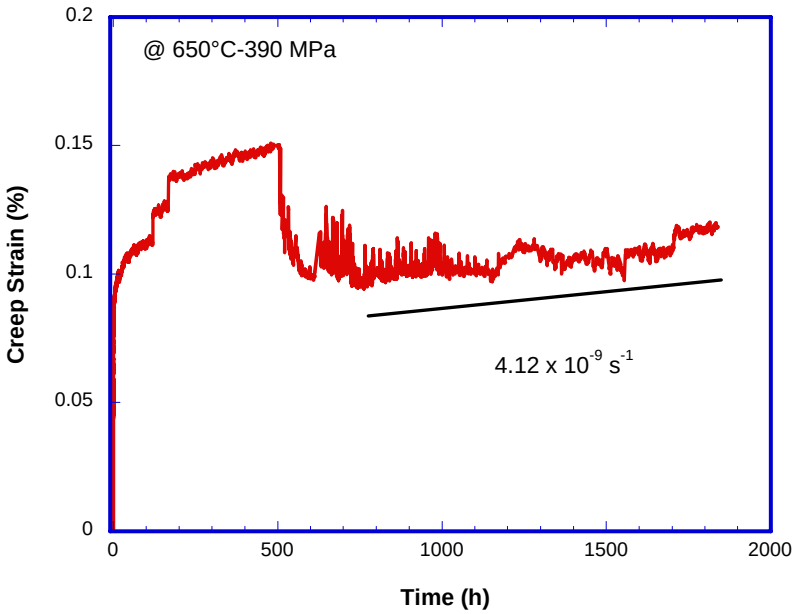

Figure 3. Creep strain versus time curve of Daido HIP TiAl material tested at 650°C and 390 MPa in air.

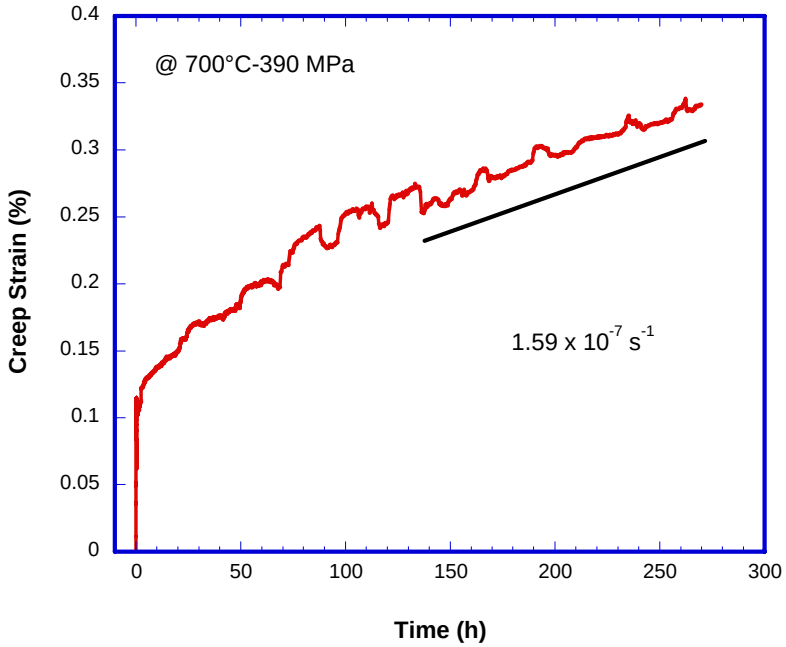

Figure 4. Creep strain versus time curve of Daido HIP TiAl material tested at 700°C and 390 MPa in air.

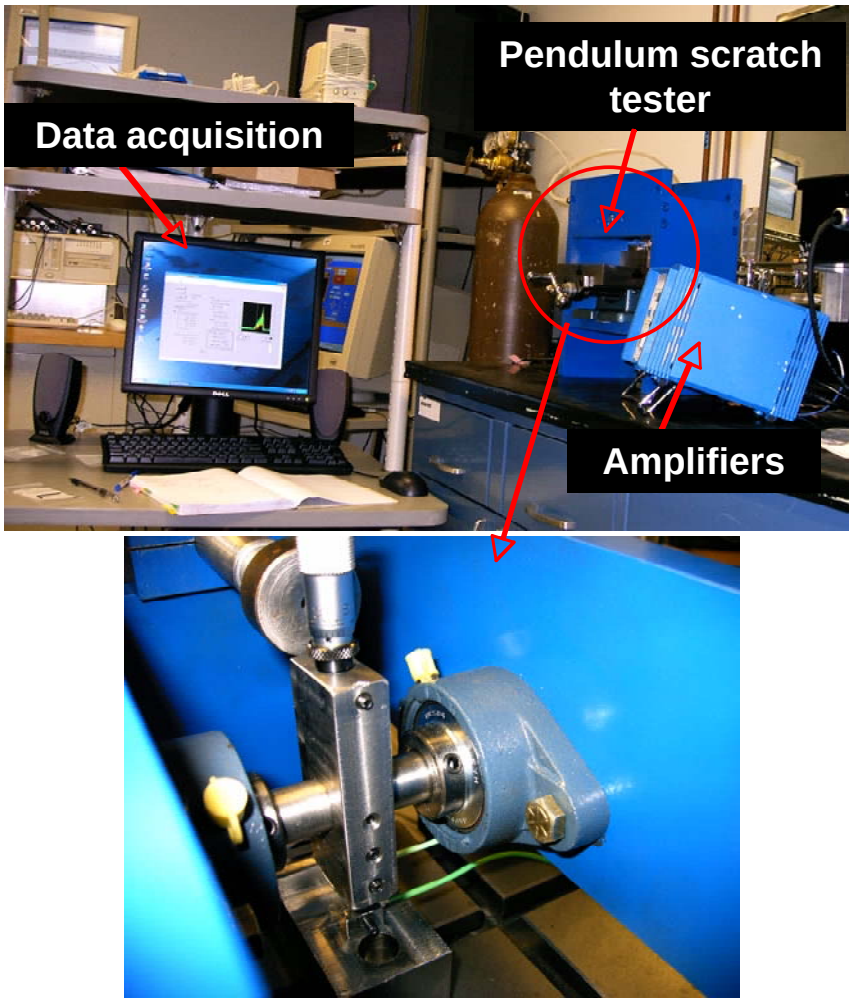

Figure 5. Photos show the setup of dynamic (rotational) scratch test system.

Lightweight Valve Train Materials

Jeremy S. Trethewey
Caterpillar Inc.

Introduction

Valve train components in heavy-duty engines operate under high stresses and temperatures, and in severe corrosive environments. In contrast, the valve train components in the light-duty engine market require cost-effective reliable materials that are wear resistant and lightweight in order to achieve high power density. For both engine classes, better valve train materials need to be identified to meet market demand for high reliability and improved performance, while providing the consumer lower operating costs.

Advanced ceramics and emerging intermetallic materials are highly corrosion and oxidation resistant, and possess high strength and hardness at elevated temperatures. These properties are expected to allow higher engine operating temperatures, lower wear, and enhanced reliability. In addition, the lighter weight of these materials (about 1/3 of production alloys) will lead to lower reciprocating valve train mass that could improve fuel efficiency. This research and development program is an in-depth investigation of the potential for use of these materials in heavy-duty engine environments.

The overall valve train effort will provide the materials, design, manufacturing, and economic information necessary to bring these new materials and technologies to commercial realization. With this information, component designs will be optimized using computer-based lifetime prediction models, and validated in rig bench tests and short-and long-term engine tests.

Program Overview

Information presented in this report is based on previous proprietary research conducted under Cooperative Agreement DE-FC05-97OR22579.

Ceramic Materials

Silicon nitride materials have been targeted for valve train materials in automotive and diesel industries since the early 1980's. Some silicon nitride material grades have reached a mature level of materials processing, capable of being implemented into production. Commercial realizations have been reported in both automotive and diesel valve trains, with large-scale production underway. The silicon nitride valve train components in production are used in high rolling contact stress applications and have exhibited superior wear resistance and longevity.

Intermetallic Materials

Titanium aluminide based intermetallics retain their strength at elevated temperature and are highly corrosion-resistant. They are lightweight and possess high fracture toughness. These alloys are actively being investigated for several aerospace and automotive applications.

Summary

Engine testing of Titanium Aluminide, Silicon Nitride and production valves

A primary goal of this study is to evaluate the performance and durability of γ-TiAl and Si_3N_4 valves in a heavy-duty engine environment. A Caterpillar G3406 natural gas genset has been identified as the preliminary test engine. To date, significant progress has been made towards the goal of testing "advanced valve" hardware on this engine. Previous quarterly reports have documented the design changes that have required modifications to valve train peripheral components (Apr-Jun 2005) and pre-engine test valve characterization efforts (Oct-Dec 2005). In this quarter an array of "advanced valves" were successfully installed on the G3406 genset. A 1000-hour durability test is scheduled to be conducted over the next quarter.

Caterpillar and NTRC (National Transportation Research Center) personnel oversaw the installation of 4 TiAl and 10 Si_3N_4 valves at Stowers Industrial Power, the East Tennessee Regional Caterpillar dealership. During the installation process, it was requested that the mechanic handle the valves with the same degree of care in which he would handle a standard steel valve. Figure 1 shows the valves as they are being installed. It is more realistic to require that the new material is sufficiently robust to survive the current standard installation procedure than to modify the procedure to conform to the limitations of the new material. The fact that all 14 of the "advanced valves" survived installation is an indication of the handling robustness of the materials. Figure 2 shows the valve array immediately after installation. It is worth noting that all of the custom-designed peripheral valve train components (seat inserts, guides, keeper locks, and bridges) were successfully integrated in the "advanced valve" head re-build.

In addition to valve train hardware, instrumentation specific to this engine test was also installed. Calibrated Kistler 6125B pressure pick-ups have been installed in each of the six cylinders. Pressure traces from these transducers will enable evaluation of the valve material's effect on the combustion performance (i.e., heat release rate). Also, a fuel consumption meter was installed to estimate the valves' aggregate effect on fuel efficiency. Finally, as a safety precaution, a fuel line shut-off valve was installed upstream of the genset intake and was calibrated to trigger if abnormal engine vibration occurs.

Development of a valve life prediction tool using CARES/life

As discussed in previous reports (FY2005 Annual Report), Jadaan Engineering & Consulting has been developing a probabilistic lifetime prediction model for TiAl and Si_3N_4 valves as they experience engine-like thermo-mechanical loads. Progress in this quarter expands upon the establishment of a three-dimensional FEA model for a Si_3N_4 valve (Oct-Dec 2005) by incorporating TiAl material properties. Also, a sensitivity study using the Probabilistic Design System (PDS) function in ANSYS was performed. Below are three significant conclusions that may be drawn from this set of analyses:

- **Si_3N_4 Valve Performance:** Life prediction estimations for Si_3N_4 valves can be construed as a cautious "vote of confidence" in the material's reliability. For example, after 15,000 hours, a valve will have a probability of failure of $8x10^{-11}$. Assuming an engine will contain 12 Si_3N_4 valves, 1 out of one billion *engines* would experience a catastrophic valve failure. However, doubling the stress field, an exceedingly conservative approach,

would increase the probability of failure to $2x10^{-4}$ (1 out of 450 engines would experience a catastrophic valve failure).

- **TiAl Valve Performance:** Results for TiAl valves were inconclusive. Two factors suggest that the TiAl valve predictions are of questionable accuracy. First, there was insufficient data to develop reliable statistical material characteristics. Second, the maximum stress, shown in Figure 3, is atypical of valve behavior. This may be an artifact of the insufficient material properties and/or boundary conditions. Caterpillar will review the FEA model for discontinuities. However, if this analysis is an accurate representation of the TiAl/Ti-6-4 stress field, this atypical stress "hot spot" may suggest that a re-design may be required to mitigate the valve's maximum stresses. In other words, it is likely that TiAl may not be regarded as a "drop in" replacement for either the "current steel" ***or*** "advanced Si_3N_4" valve design.

- **PDS Results:** The sensitivity study examined the importance of six variables (valve face pressure, Weibull modulus, scale parameter, Young's modulus, coefficient of thermal expansion and thermal conductivity) on the probability of failure and maximum stress of TiAl and Si_3N_4 valves. Figure 4 summarizes these results. Young's modulus, valve face pressure, and coefficient of thermal expansion are found to be the critical variables for defining the maximum stress found in the valve. However, Weibull modulus, Young's modulus, and the scale parameter are the three strongest influences on the valve's ultimate probability of failure. Of course, the accuracy of the PDS analysis is only as good as the accuracy of the FEA model (discussed above). With this in mind, the PDS analysis suggests that controlling the latter set of variables would have the largest impact on improving the valves' durability.

Future Work

The installation of the "advanced valves" in the Caterpillar G3406 engine marks a significant milestone in this project. Over the past several quarters, the TiAl and Si_3N_4 valves have progressed through the design, synthesis and characterization stages. In early next quarter the three-phase engine test will begin. In the first phase, the valves will accumulate 100 hours of engine time. After this initial break-in phase, the valves will be removed from the cylinder head and evaluated at ORNL (profilometry, SEM) and ANL (laser scatter NDE). The valves will then be reinstalled and, after an additional 400 hours of accumulated engine time, they will be removed again for a second round of characterization. After a final 500 hours of engine time (1000 total hours) the valves will be removed and characterized. The valves will then be subjected to fast fracture mechanical tests to evaluate their retained strength. Although the acquired strength data will be insufficient for rigorous statistical analysis, they may reveal a trend in material degradation. This retained strength data will be compared to the life predictions as derived from the CARES/life lifetime prediction tool.

Presentations & Relevant Travel

"Reliability of high temperature lightweight valve train components in a total probabilistic design environment," O. Jadaan, J.S. Trethewey, 30th International Conference & Exposition on Advanced Ceramics & Composites, Cocoa Beach, FL, Jan 22-27, 2006.

"Nondestructive evaluation of machining damage in silicon-nitride ceramic valves," J.G. Sun, J.M Zhang, J.S. Trethewey, 30th International Conference & Exposition on Advanced Ceramics & Composites, Cocoa Beach, FL, Jan 22-27, 2006.

Jeremy Trethewey visited the National Transportation Research Center at Oak Ridge National Laboratory to meet with NTRC & ORNL staff and provide guidance during installation of Si_3N_4 and TiAl valves on Caterpillar G3406 engine, Mar 6-8, 2006.

Dr. Osama Jadaan (University of Wisconsin – Platteville) visited the Caterpillar Technical Center to discuss the progress of the life prediction analysis, Mar 23, 2006.

Figure 1: Si_3N_4 valve under compression from an installation tool.

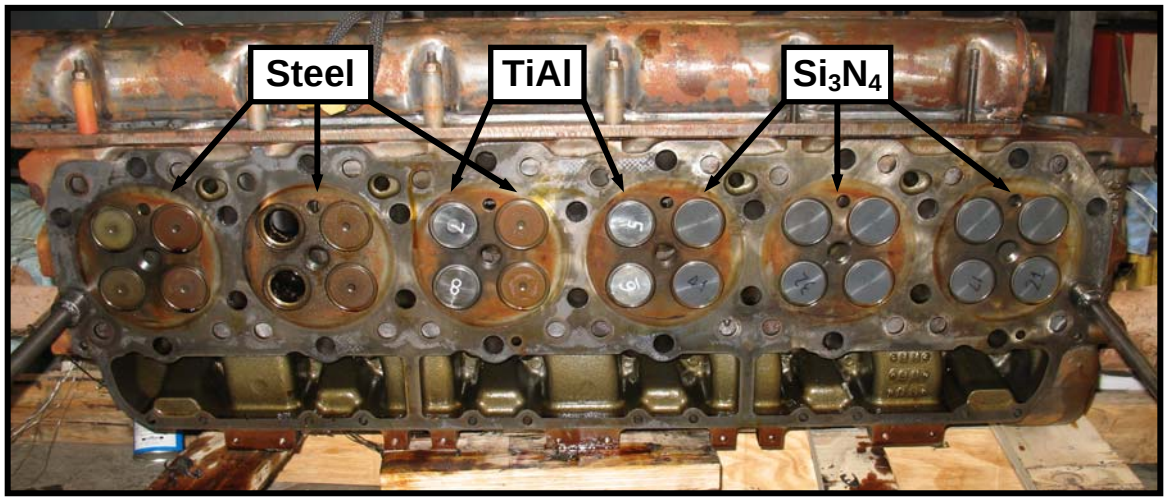

Figure 2: Caterpillar G3406 cylinder head after “advanced valve” installation. From left to right there are 10 production steel valves (2 temporarily removed), 4 TiAl exhaust valves and 10 Si_3N_4 valves.

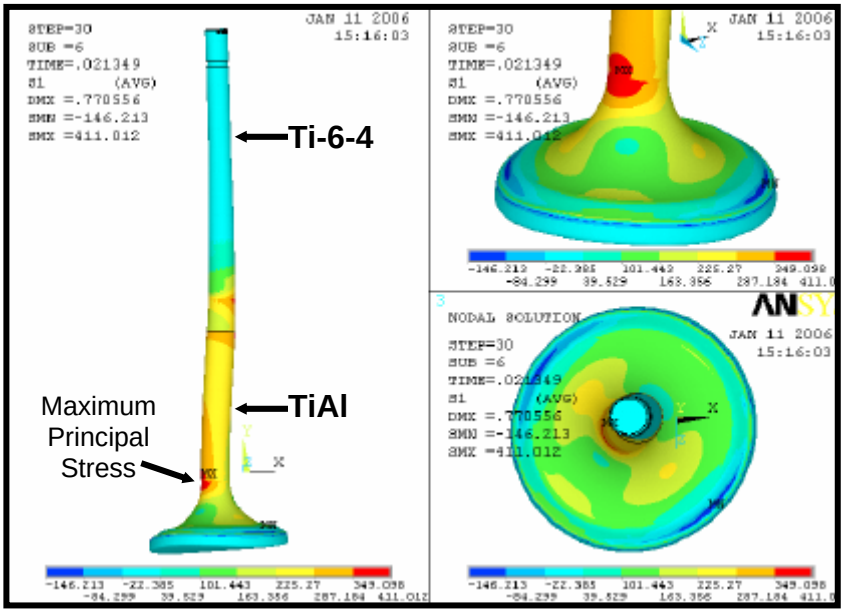

Figure 3: Principal stress field of TiAl/Ti-6-4 valve near peak cylinder pressure. The location of the maximum stress value (431 MPa) is not at the center of the fillet radius, which may indicate that the valve design is not optimized for the TiAl's material properties.

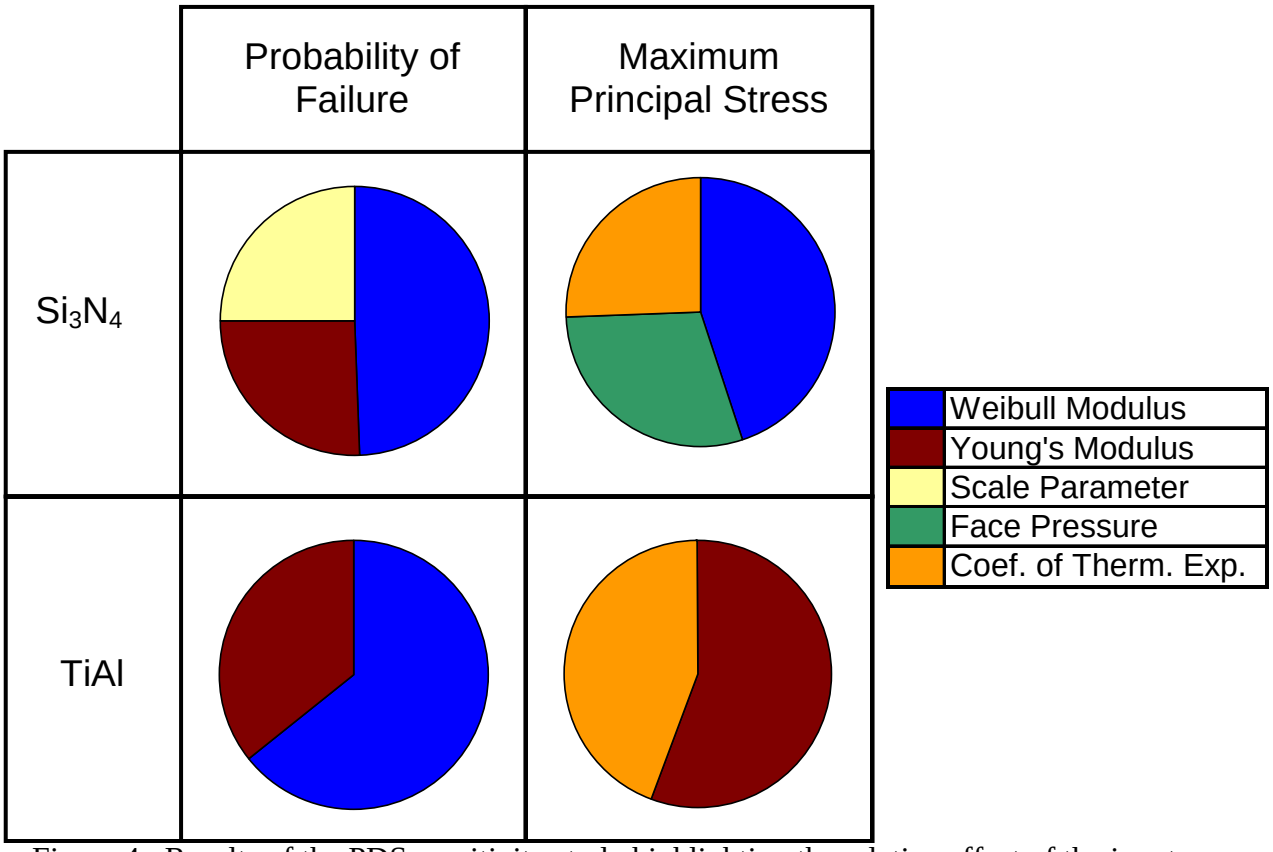

Figure 4: Results of the PDS sensitivity study highlighting the relative effect of the input variables on the probability of failure and maximum principal stress for Si_3N_4 and TiAl valves.

An Integrated Surface Modification of Engineering Materials for Heavy Vehicle Applications

Stephen Hsu, Huan Zhang, Yanan Liang, Charles Ying, Jing Yang, and Wen Li
National Institute of Standards and Technology

Objectives

- Develop design guidelines for surface texturing features that can reduce friction and enhanced durability for heavy duty diesel engine components.
- Develop cost-effective fabrication techniques for textural features
- Develop appropriate thin films and coatings to achieve synergistic and complementary relationship with texturing to enhance performance.
- Discover and develop surface chemistry for texture protection and improve friction reduction
- Develop theory and models to predict friction reduction in textured surfaces.

Approach

- Determine the effect of size, shape, pitch, and patterns of surface textural features on friction under 1) high speed, low load regime; 2) high load, high speed regime; 3) high load, low speed regime.
- Develop cost effective fabrication technologies for creating surface textural features on various surfaces including metals, ceramics, and coatings.
- Develop test methodology to measure the effects of the textures on friction
- Conduct research to develop an integrated system approach to combine the best practices in thin films, coating, and surface chemistry for performances unrealizable by individual approach alone.
- Concurrently, organize an international cooperative research program under the auspice of the International Energy Agency (IEA) to pool resources and share this energy conservation technology worldwide.

Accomplishments in this quarter

- We initiate a combined approach of theoretical modeling with experimental design for the high load, low speed contact conditions. We found that number of dimples per unit area and the depth of the dimple to be more important as the contact severity was increased.
- The IEA IA-AMT Executive Committee was successfully convened in Porto on Oct. 11, 2005 with delegates from China, UK, Australia, Finland, Japan, Belgium, Portugal, and the US. Germany and China have agreed to join the AMT technical activities.
- The next IEA IA-AMT Executive Committee is being scheduled for May 7, 2006 in Calgary, Canada. Reports on strategic planning and management report on this activity have been submitted to IEA headquarters as requested.

Introduction

Frictional losses are inherent in most practical mechanical systems. The ability to control friction offers many opportunities to achieve energy conservation. Over the years, materials, lubricants, and surface modifications have been used to reduce friction in automotive and diesel engines. However, in recent years, progress in friction reduction technology has slowed because much obvious inefficiency has been eliminated. A new avenue is needed.

Designing surfaces specifically for friction and durability control has emerged as the last frontier in surface engineering. Recently, laser ablated dimples on surfaces have shown friction reduction properties and have been demonstrated successfully in conformal contacts such as seals where the speed is high and the load is low. The friction reduction mechanism in this regime appears to depend on the size, patterns, and density of dimples in the contact.

The objective of this project, therefore, is to develop an application specific engineered surface (combining surface textures, thin films, surface chemistry) tailored for the optimum friction reduction and durability.

Such technology is aimed at energy transmission components, cylinder liner ring contacts, cam and lifters, and overhead bearing components. To ensure that the durability criteria are met, the texture patterns have to be protected by thin films/coatings and appropriate lubricating chemistry over a broad range of operating conditions. The final outcome of the project will be a general design principle and guidelines for various engine components under a wide range of operating conditions. To achieve maximum energy conservation, this technology should be implemented worldwide through international cooperation such as the International Energy Agency Implementing Agreement on Advanced Materials for Transportation (IEA IA-AMT). Therefore, a concomitant international cooperative research under the auspice of the International Energy Agency is being conducted to pool resources from various countries to accelerate this technology development. Towards this end, UK, China, Australia, Finland, Sweden, Israel, and Japan have agreed to participate under the IEA annex IV on surface technology.

Approach

Previously, experiments were conducted to examine various surface textures on steel surfaces using photolithography and chemical etching. Using the same area coverage (% of area occupied by the surface textural features), surface features such as grooves, triangles, ellipses; circles were compared under high speed low load conditions similar to the seals operating conditions. Results suggested that: 1) surface texture size and shape had significant influence on friction; 2) orientation of the surface features with respect to the sliding direction changed the friction; 3) the primary effect of surface textures is to accelerate the transition into hydrodynamic lubrication regime. The fundamental friction reduction mechanisms in this regime, based on our work, are: a) cavitation induced pressure lift; b) back flow within the dimple; c) additional hydrodynamic lift due to the geometric shape of the dimples. There may be additional mechanisms that we have not discovered yet. Since this regime has the lowest friction, it is important to understand the mechanisms so that when conditions are appropriate, lowest friction can be designed into the components.

From energy conservation point of view, most parasitic losses in engines take place under high load and medium to low speed conditions. Therefore, we need to extend the surface texturing concept to more severe contact conditions. However, when we ran the same surface texture patterns under boundary lubrication conditions, friction increased. A collaborative effort with Northwestern University using a sophisticated elastohydrodynamic friction model confirmed our experimental observations. Basically, under boundary lubricated conditions (high load low speed), the edge stresses around the dimple increase frictional losses as if the surface is much rougher. So there is a trade-off in this regime.

Technical Highlight

In the previous quarters, we developed a new surface textural feature with an inclined plane at the bottom of the feature to artificially generate a hydrodynamic wedge effect under plastic deformation loading; we called this elasto-plastic lubrication model. Experiments conducted demonstrated significant friction reductions for steel on steel contacts.

L/D ratio and size effects

One of the critical issues in fabricating the new surface features was the effect of the slope at the bottom of the feature. In bearing applications, this typically was called the L/D ratio (bearing length over radius of the bearing) to estimate the lift force. We borrowed this concept and applied to our design in terms of the length over the depth of the slope fabricated at the bottom of the surface features. Another important factor was the size of the surface feature over the contact area. In boundary lubrication conditions, since the edges of the surface features served as rough spots increasing the friction, therefore, the optimum number of the features might be much smaller than the high speed low load regime. So we decided to conduct a series of experiments to investigate this effect.

We fabricate several surface features by varying the L/D ratio and the size of the surface features. Results showed that the classical wedge orientation has the highest friction reduction capacity, reducing the average friction coefficient of the untextured (UNT) from 0.09 to about 0.05, a 44% decrease in a 52100 bearing steel on 52100 bearing steel contact.

In this quarter, we varied the size of dimple, area coverage, and depth to seek the optimum combination of parameters to effect friction reduction under increasingly severe contact conditions. A series of samples were prepared to using the high-load tribotester to precisely fabricate these surface dimple features for testing. Based on the theoretical analysis results performed last quarter, we decided to determine the relationship between depth of the feature and load, and the effect of area density under high load conditions.

Area density and depth of dimple effects on friction

Etsion suggests that there is an optimum of number of dimples in the contact under high speed low load conditions based on hydrodynamic theory and the results have been supported by his experimental finding under conformal surface contacts. However, as the load begins to increase, edge stresses and deformation induced frictional resistance become more significant and our analysis last quarter confirmed this hypothesis. In order to consistently design surface features effective at increasingly higher contact pressures, it is important to under the effects of density and depth of the dimples under high contact sliding conditions.

We designed our experiments by fabricating dimples with approximately the same L/D ratios and systematically decreased the size of the dimples, thereby increased the area density. The dimpled surfaces were then subjected to friction testing in a modified ball on three plates contact geometry in a four ball wear tester. Loads of 5 kg, 10, 20, 30 kg were used (corresponding to apparent contact pressures of 86MPa, 168MPa, 337MPa, and 470MPa respectively). Each experiment was conducted using a speed-step change from high speed to low speed (1.34 m/s to 0.19 m/s). Table 1 shows the details of the designed surface features.

Table 1. Surface feature dimensions and area densities

	Dimple length µm	L/d		Area ratio %		Dimple # / contact area	Shape
		Target	Actual	Target	Actual		
C1-200	9.81±0.32	8	9.85 ±0.78	7	6.41±0.34	426±30	
C2-400	14.91±0.41	8	9.95 ±1.30	7	6.77±0.35	206±15	
C4-800	22.31±0.62	8	9.22 ±0.78	7	7.14±0.33	106±8	
C2-400-2	14.72±0.34	8	9.62 ±0.87	3.5	3.42±0.14	106±8	

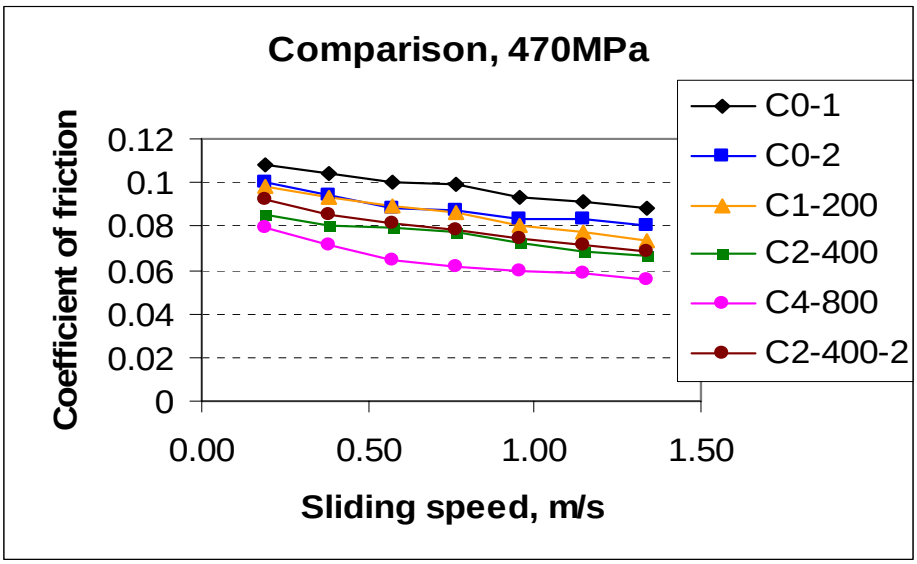

Figure 1. Frictional reduction achieved under 30kg load as compared to the baseline

Results are shown in Fig. 1. As can be seen, at 30 kg load (apparent contact pressure of 470 MPa, asperity contact stresses at 2-3 GPa, C4-800 has the lowest friction coefficient, about 40% reduction from the untextured surface, C0-1. The untextured surface has a coefficient of friction from 0.11 to 0.09 which are typical boundary lubrication frictional values. Yet as we introduce the dimples, the friction values decrease to 0.06 which is typical of hydrodynamic lubrication. Worn surface topography shows wear and deformation as a result of the contact severity under this condition. As the contact severity increases, the number of dimples required for friction control decreases, as predicted by our model analysis last quarter for increasing the edges stresses (the surface effectively becomes rougher). In this experimental design, larger sizes appear to be beneficial under high loading condition. This needs to be confirmed next quarter.

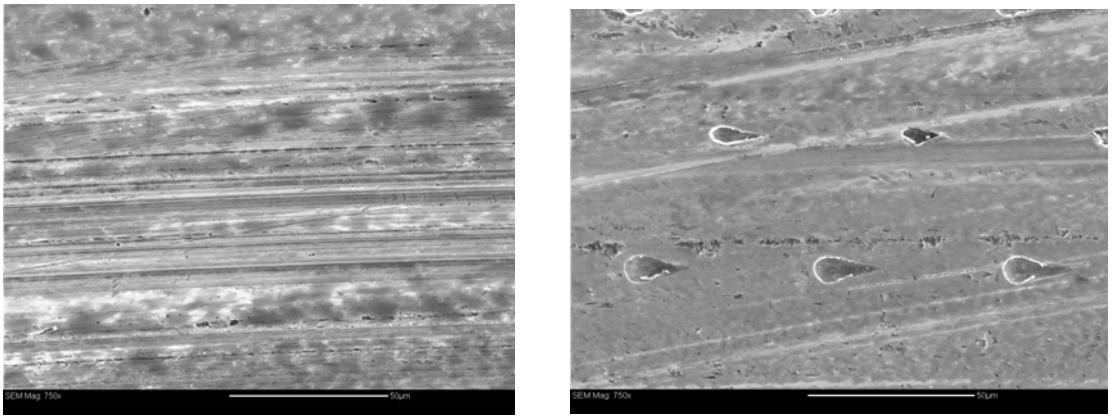

Fig. 2. Comparison of surface damage between untextured surface vs. textured surface for C4-800 case

Figure 2 shows the surface damage for the untextured surface as compared to the C4-800 textured case. As it can be seen, the untextured surface under identical conditions suffers severe deformation and wear while the textured surface shows very little wear and deformation. This result is remarkable for such high load conditions.

Publications/Presentations

Presentations:

S. M. Hsu, "An integrated surface modification technology: project review," DOE project review, Oak Ridge National Laboratory, Oak Ridge, Tennessee, Sept. 13-15, 2005.

S. M. Hsu, "Integrated Surface Modification Technology: a progress report," COST 532 symposium on surface textures, Porto, Portugal, Oct. 12, 2005.

Publications:

"Surface Texturing: Comparison of Various Geometric Shapes on Friction under High Speed Low Load Conditions," Wang, X., Hsu, S.M., published in the proceeding of the International Tribology Conference, Kobe, Japan, May 29-June 2, 2005

"Surface Texturing: A New Design Principle for Friction Reduction Under Boundary Lubrication Conditions," Wang, X., Hsu, S.M., published in the Proceedings of the International Tribology Conference, Kobe, Japan, May 29-June 2, 2005.

Collaborations:

A team from the Manufacturing Engineering Research Center, University of Strathclyde, Scotland, UK, visited us to discuss collaborations on surface texturing. The team consisted of Prof. Raj Balendra, the center director, Mr. Bob Smith, managing director, Pascoe Company and several other researchers. They have developed a rapid micro-machine capable of hundreds of operations to fabricate surface textures per minutes. We discussed the potential collaboration with them and the next step would be for me to visit them to see their operation first hand.

Mechanical Property Test Development

George Quinn
NIST

Objective/Scope

This task is to develop mechanical test method standards in support of the Propulsion Systems Materials Program. Test method development should meet the needs of the DOE engine community but should also consider the general USA structural ceramics community as well as foreign laboratories and companies. Draft recommendations for practices or procedures shall be developed based upon the needs identified above and circulated within the DOE engine community for review and modification. Round robins will be conducted as necessary. Procedures will be standardized by ASTM and/or ISO.

Technical Highlights.

1. General

The first draft of a Guide to Practice for Fractography was completed and was under review from October 2005 through March 2006. It is now being revised. It is book length and was reviewed by eight persons which accounts for the long time for the review. Intensive work continued on prestandardization testing of solid rods.

2. Fractography

The draft NIST "Guide to Best Practice" for fractographic analysis was reviewed by eight reviewers including Steve Freiman, Roy Rice, Grady White, Jeffrey Swab, Timothy Foecke, Lewis Ives. Portions were reviewed by Jack Mecholsky and Jonathan Salem. This document is over 500 pages long and has 677 figures that illustrate key fractographic markings in ceramics and brittle materials. It is very practical and is meant to help users solve problems. It will complement the ASTM standard C 1322, Standard Practice for Fractography and Characterization of Fracture Origins in Advanced Ceramics. The annex on how to measure fracture mirror sizes is being rewritten in light of some of the comments received. The new guidelines are the first step towards a possible ASTM standard. The Guidelines are being reviewed by a few selected expert fractographers. A paper on this topic will be presented at the July 2006 Fractography conference, at which time Mr. Quinn will solicit feedback and criticisms form the assembled world experts. If a consensus can be reached, then the guidelines will be written in ASTM standard format and submitted to ASTM Committee C-28 for review.

One notion that we had about measuring fracture mirrors had to do with the use of stereo photo pairs. Interpreting photos of fracture mirrors can be problematic. The guidelines strongly recommended that photos not be used unless there is no alternative. One exception may be with stereo pictures which can be viewed through a special viewer. These might give a better rendition of the fracture surface than a single photo alone. Stereo paired photos were made of Y-ZTP zirconia fracture surfaces and interpreted. The stereo pictures were somewhat better than a single photo, but still could not match the view in a microscope or a high resolution computer monitor.

3. Flexural Strength Testing of Cylindrical Ceramic Specimens

Intensive work continued on this subtask this quarter. **Figure 1** shows our dedicated fixture for testing round specimens. We have done many tests on rods of various materials and sizes and shapes as shown in **Figure 2.** **Figure 3** shows some faulty experiments that occurred when the span to thickness ratio was too small.

In the last quarterly period, we obtained some surprising results when we tested a number of alpha silicon carbide rods left over from the ceramic machining consortium program. **Figure 4** shows the outcomes. We broke 30 test pieces in the fixture with cradles and 30 in the fixture without cradles. Both sets produced nearly identical results. We tested 10 more in ordinary 20 x 40 mm fixtures for rectangular bend bars and also 10 small diameter as-fired rods for comparison. Fractography confirmed that surface voids were the fracture origins in nearly all these as-fired rods as shown in **Figure 5.**

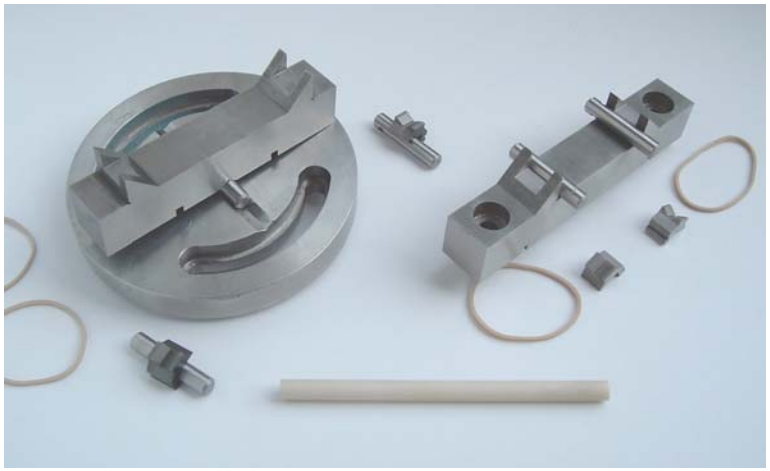

Figure 1. 40 x 80 mm span flexural bend fixtures. Four cradles apply load to the specimen and minimize contact stresses.

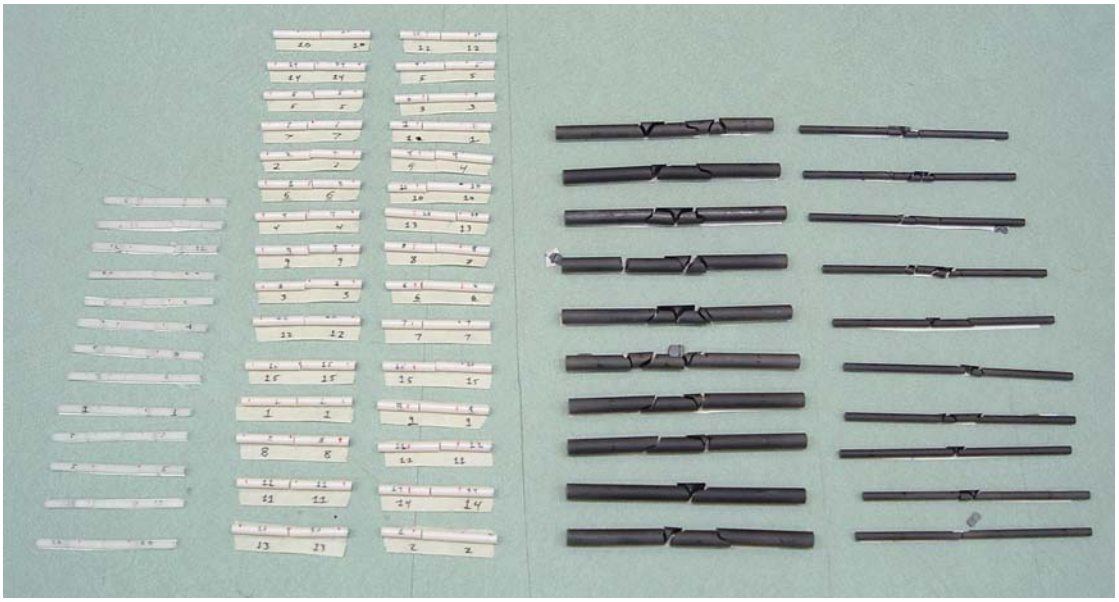

Figure 2. Broken rods.

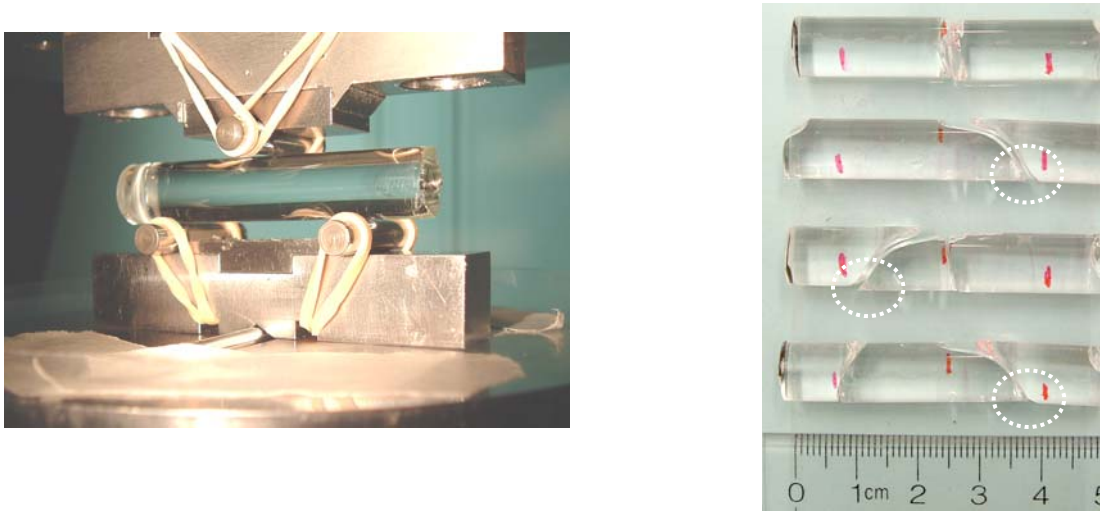

Figure 3 Broken glass rods. The first on the right was a legitimate break, but the other three were invalid. They broke from the outer loading points due to contact cracks as shown in the last quarterly report

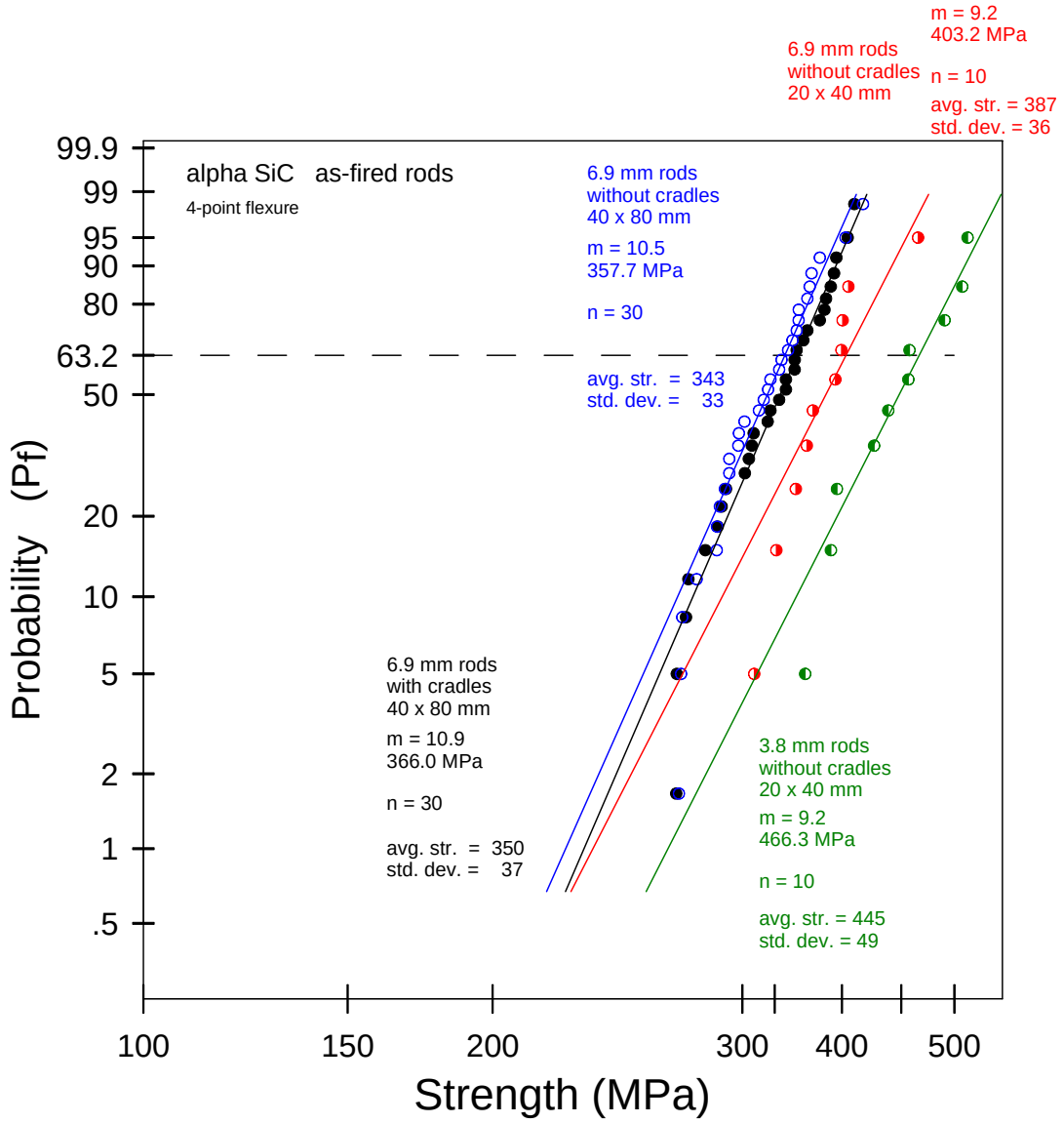

Figure 4. Weibull strength distribution of as-fired Hexaloy silicon carbide 6.9 mm rods of two different diameters. The rods tested on the 40 x 80 mm fixtures had comparable strengths whether or not cradles were used. The other two sets are stronger due to Weibull scaling effects. One set was tested on smaller fixtures (20 x 40 mm) and the other set featured smaller diameter (3.8 mm) rod specimens. The differences are for the most part accounted for by Weibull size scaling.

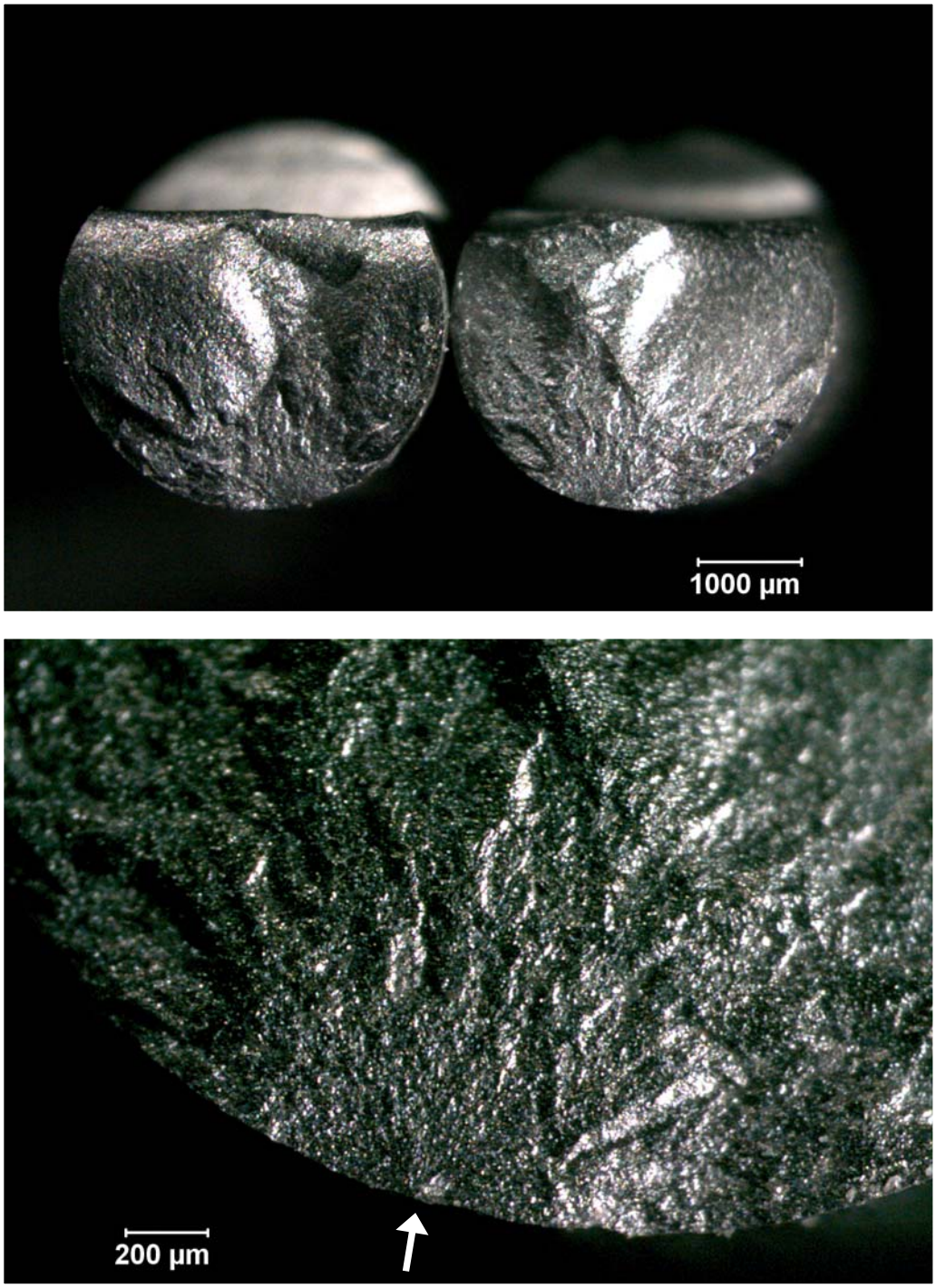

Figure 5. The alpha SiC rods broke from surface voids associated with the as-fired surface.

During this quarter we also experimented with a strain-gauged steel rod to check the stress distribution in a specimen tested in the bend fixtures with and without cradles. We first duplicated some results with this rod from a few years ago during the NIST Ceramic Machining Consortium program. It was used at that time to verify the new bend fixtures were satisfactory. We intended to use it again now to deliberately check errors from misalignments. We experienced a setback when the steel rod, which was a common 303 grade stainless steel, was loaded past its yield point without our noticing it. This material has a low yield stress (30×10^6 psi or 206 MPa). We used it initially to verify the fixtures worked well at modest loads, but it was overloaded when we used it at the loads that were appropriate for test ceramic specimens. When yielding occurs in a beam in bending, the yielding is confined to a small region at the outer most portion of the rod. It therefore does not generate a pronounced change in the load-deflection or load–strain curves. Our stress strain data for the rod showed a very small amount of nonlinearity which increased with loading. Initially we thought that this was problem with the fixtures, but we noticed the slight permanent set when the rod was extracted. It was tiny, but real.

A new tool steel rod was obtained and electric discharge machining used to apply a tiny flat to the rod. The flat is needed to provide a good surface for several tiny strain gages. We have measured the size of the flat and computed the moment of inertia and the section modulus for the new rod and are just about to start using it to continue our fixture evaluation work.

The universal testing machine (an Instron model 122 bench top model) experienced a major fault with the crosshead drive control. A replacement was ordered and the entire unit was swapped out with minimal down time.

As this report was written, it was unclear whether this task will continue much further due to program funding shortfalls. This may be the last progress report. Nevertheless, we will continue the strain gage work on the steel rod to explore fixture errors both with and without cradles. A Baratta-Quinn-Matthews style error analysis will be written this summer. A draft standard will be written in the fall, and the project will be put to bed. A review paper on rod flexural testing will be written.

4. Fracture Toughness

A review paper on the Vickers indentation cracks length method was prepared for the Cocoa Beach meeting. The goal of the paper was to alert users to the drawbacks and inaccuracies of this method. Dr. Edgar Lara-Curzio of ORNL invited Mr. Quinn to make this presentation.

The paper was well received and the author was encouraged to write a more comprehensive treatment as review article in a major journal. That work is underway.

5. Other

A draft final report by engineers at KRISS in Seoul, Korea, was reviewed by Mr. Quinn. This report was on the results of a VAMAS TWA 3 international round robin to measure the effects of environment on flexural strength.

Status of Milestones

412149 Prepare ballot-ready first ASTM draft of cylindrical rod flexure strength test Overdue, New schedule - May 2006

412151 Prepare review paper on flexural testing of cylindrical rods. Overdue, New schedule - Fall 2006

Communications/Visits/Travel

Mr. Quinn presented the two papers listed below at the American Ceramic Society conference in Cocoa Beach. Mr., Quinn met with Cummins engineers and discussed earlier results from testing split zirconia cylindrical specimens. A full report was prepared for Cummins on this work.

A large delegation of senior managers from Caterpillar came to visit NIST in February. The meeting was organized by the Manufacturing Engineering Laboratory of NIST. The Director of all of NIST also made an appearance and took special interest in this collaboration. Mr. Quinn presented a talk about materials standards, ceramics, and brittle materials and the occasional interactions that we have had with Caterpillar.

Mr. Quinn communicated with K. Breder at St. Gobain regarding the VAMAS draft final report on the effects of environment on measured flexural strength.

Mr. Quinn also helped write a draft manuscript on changes to the microstructure in hot pressed silicon nitride that occurred during ultra long stress rupture tests conducted when he was at Watertown Arsenal in the 1980s. The new paper was prepared by Dr. Joachim Kleebe of TU Darmstadt and Dr. W. Braue of DLR in Köln with Mr. Quinn. Mr. Quinn had turned over remnants of two bend test specimens of NC 132 which had fractured after 2 years in flexural stets rupture testing in air. These are to the best of our knowledge the longest failure times ever observed for a structural ceramic tested in stress rupture or creep. The two specimens were tested under identical conditions and had nearly identical outcome. At the end of the tests, the microstructure was radically altered as reveled by TEM. That is the subject of the paper.

Mr. Quinn attended the ASTM Committee C-28 Advanced Ceramics meeting in January at Cocoa Beach.

Mr. Quinn reviewed a paper on some interesting work in progress at Corning on using flexural testing to measure the strength of ceramic diesel particulate fixture substrates. A special meeting was held after the ASTM session between Corning engineers (DeMartineo, Helfinstine, and Webb), and Mr. Quinn, S. Gonczy and G. Crosbie of Ford.

The author wishes to thank the consistent support from the US Department of Energy and the Oak Ridge National Laboratory over the course of many years. Much was accomplished to develop a national and international standards infrastructure that will facilitate the introduction of novel materials to advanced engines.

Publications and Presentations

1. G. D. Quinn, "Segmented Cylinder Flexural Strength Test," accepted by Ceramic Eng. and Sci. Proc., Jan 2006, Proceedings of the Cocoa Beach January 2006 Conference.

2. G. D. Quinn, "Fracture Toughness of the Vickers Indentation Crack Length Method; A Critical Review," accepted by Ceramic Eng. and Sci. Proc., Jan. 2006 Proceedings of the Cocoa Beach January 2006 Conference.

3. H.-J. Kleebe, W. Braue, and G. D. Quinn, "Correlation Between Depletion of Grain Boundary Phase and Elastic Creep Deformation Upon Ultra-Long Flexure Stress Rupture Experiments of NC-132 Silicon Nitride," subm. to Communications of the American Ceramic Society, 2006

Coating Evaluation and Performance

M. J. Lance, A. A. Wereszczak, and K. E. Johanns
Ceramic Science and Technology (CerSAT)
Oak Ridge National Laboratory

Objective/Scope

Next generation thermal barrier, tribological, and environmental barrier coatings will enable enhanced diesel engine performance, higher operating efficiency, longer engine lifetimes, and lower emission of NO_x and particulates. Unfortunately techniques for assessing properties, particularly with respect to coating interface, are unproven. The sought attributes (thermal protection, improved wear resistance, and environmental barrier) of any of these coating applications can only be realized if their architecture is appropriately designed to withstand operating or service stress states. This project explores new, innovative, and promising test and characterization techniques that crosscut all these coating systems and whose results and interpretations will expedite their development and exploitation in the heavy vehicle sector.

Technical Highlights

Mechanical tests to measure adhesion or spallation resistance often revolve around a tensile test method where a pull rod is glued to the coating and loaded in tension until spallation is produced. The validity of the test is often dependent on the tester's ability to identify a suitable adhesive and to choose a specimen where end effects do not affect the results. Because polymeric adhesives are often used for room temperature tests, the ability to conduct tests at elevated temperatures is often inhibited.

Most thermal, environmental, and tribological coating materials have lower strains-to-failure (ε_f) than the substrate material they are bonded to. In recognition of this, a ball-on-ring biaxial flexure test method (Fig. 1) is under development to quantify coating strain-to-failure. The technique also lends itself well to elevated temperature testing.

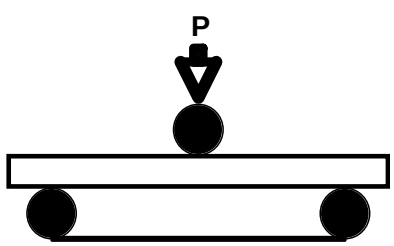

Figure 1. Side view and sectioned schematic of a ball-on-ring biaxial flexure configuration used to measure coating strain-to-failure.

A hard ball (e.g., WC or Si_3N_4) is contact-loaded on a specimen resting on a ring. Excessive deflection and induced plastic deformation of the specimen is actually sought. The specimen is deflected until spallation occurs, and the spall pattern or size is then linkable to a strain-to-failure. If the coating side is oriented on top in Fig. 1, then a gradually changing radius of

curvature produces a tensile strain in the coating. Conversely, if the coating is oriented on the bottom in Fig. 1, then the coating is subjected to a tensile strain. Examples of tested coupons are shown in Fig. 2.

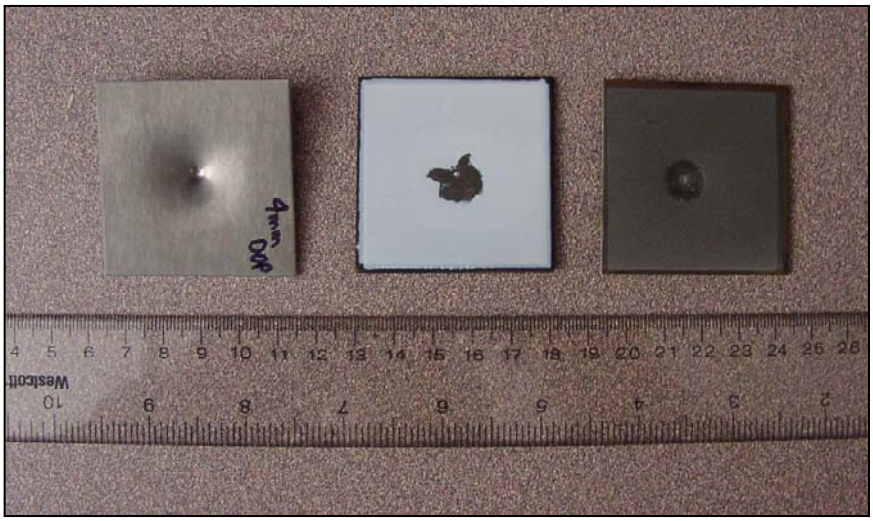

Figure 2. Ball-on-ring tested coupons. Uncoated 410SS (left) and coated specimens (middle and right).

The produced radius of curvature can be used to estimate strain using finite element analysis. For example, the induced strain in a 1.27 mm thick (0.050”) substrate resting on a 25 mm ring diameter loaded with a 6.35mm ball was analyzed. An axisymmetric model was used and the results are shown in Fig. 3. The radial displacements for a variety of peak depths of penetration show a gradually changing radius of curvature at radii beyond the ball’s contact radius. It is analogous to a “cam” profile. A corresponding strain profile (Fig. 4) for a maximum depth of penetration of 1.8 mm is then used to compare against the produced spall diameter measured experimentally. In one case, the estimated strain-to-failure was found to be ~ 2%.

The validity of the FEA results is being examined using optical fluorescence and an oxidized Aluchrome YHF alloy. Thin substrates of this alloy are being oxidized to produce an alumina scale. The oxidized alloy will then be subjected to ball-on-ring tests. The presence of the alumina scale on the plastically deformed alloy will enable optical fluorescence to be used to estimate strains and validate the FEA.

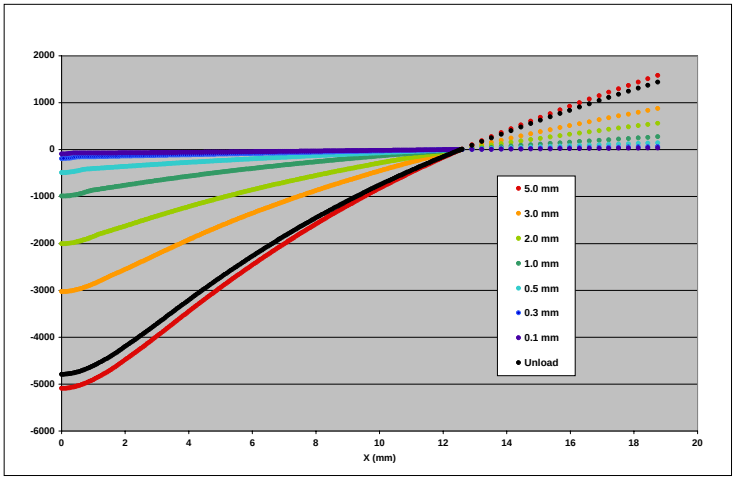

Figure 3. Deflection profiles of a 1.27 mm thick 410SS specimen subjected to ball-on-ring loading using a 6.35 mm diameter ball and a 25 mm ring diameter.

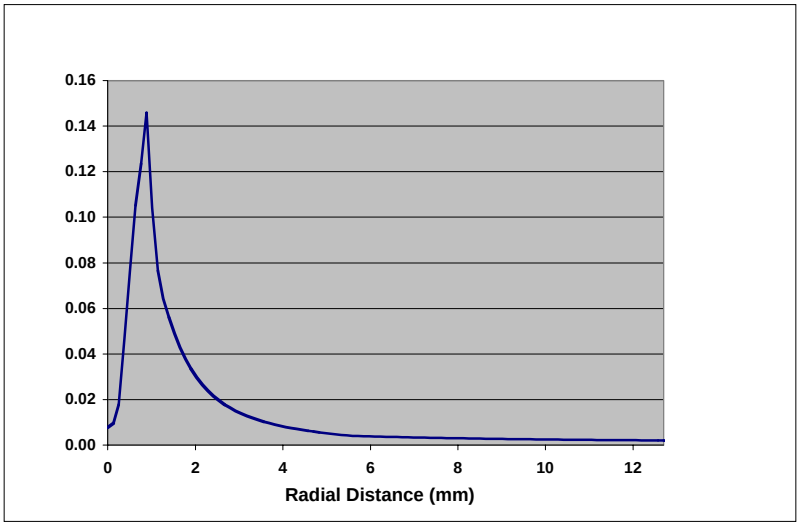

Figure 4. Strain as a function of radial distance when the maximum depth of penetration for the specimen was 1.8 mm, the specimen was 410SS with a thickness of 1.27 mm, the ball had a diameter of 6.35 mm and was WC, and the ring diameter was 25 mm. The experimentally measured spall diameter was ~ 5 mm, so using this profile, a strain-to-failure of ~2% was estimated.

Status of FY 2006 Milestones

Survey innovative test techniques that facilitate the coating performance and evaluation of thermal and tribological coatings. [09/06] *On schedule.*

Communications/Visits/Travel

None this quarter.

Publications
None.

References
None.

Mechanical Reliability of Thermoelectrics

A. A. Wereszczak, H. -T. Lin, and K. E. Johanns
Ceramic Science and Technology (CerSAT)
Oak Ridge National Laboratory

Objective/Scope

Potential next generation thermoelectric (TE) devices comprised of p- and n-type oxide ceramics enjoy strong interest for implementation in high temperature and oxidizing environments because their waste heat could be used to generate electricity. However, the intended TE function of these devices will only be enabled if the device is designed to overcome the thermomechanical limitations (i.e., brittleness) inherent to these oxides. Thermoelectric devices become more efficient with larger thermal gradients across them, and this is accomplished by large temperature differences (e.g., greater spatial size) across the TE's hot and cold junctions or the use of low thermal conductivity TE materials or both. A TE oxide with a combination of poor strength and low thermal conductivity can readily fail mechanically in the presence of a thermal gradient thereby preventing the desired thermoelectrical function.

This seemingly insurmountable problem can be overcome through the combined use of established probabilistic design methods developed for brittle structural components, good thermoelastic and thermomechanical databases of the candidate oxide material comprising the TE device, and iteratively applied component design sensitivity analysis. This project executes this process by interrogating prototypical TE devices (e.g., thin-film-based) and oxides.

There will be several outcomes from this work that will benefit TE oxide and device developers and end-users of these potentially high temperature TE devices:

- mechanical reliability of prototypical TE devices will be evaluated from a structural ceramic perspective and suggested redesigns will be identified,
- thermomechanical reliability of developmental TE oxides will be assessed, and
- minimum required thermomechanical properties of hypothetical TE oxides would be identified that produce desired reliability in a TE device.

Additionally, innovative and cost-effective methods to process high temperature capable TEs will be a part of this project's research portfolio.

Technical Highlights

The project initiated this quarter. Bismuth telluride TE devices were ordered from a commercial source and will be sectioned, polished, and imaged after they arrive early in Q3. Micromechanical testing will be performed to assess mechanical properties. The imaged internal architecture will then be inputted in our group's *μ-FEA*© software to enable what-if thermomechanical stress analysis. Professor Osama Jadaan (University of Wisconsin-Platteville) will fulfill a sabbatical at ORNL during parts of Q3 and Q4 and will assist in the FEA analysis and preliminary life prediction exams.

A cost-effective manufacturing method is under investigation for the production of high temperature oxide-based TEs.

Status of FY 2006 Milestones

Develop a general FEA model that can be used to assess and predict thermoelastic stress states in TE devices. **(09/06)** *On schedule.*

Communications/Visits/Travel

None.

Publications

None.

References

None.

Processing and Characterization of Structural and Functional Materials for Heavy Vehicle Applications

J. Sankar, Z. Xu and S. Yarmolenko
North Carolina A & T State University

Objective/Scope

Preparation and characterization of protonic conductive electrolyte thin films by flame-assisted chemical vapor deposition.

Task

Study the effects of the processing parameters, such as substrate temperature and metal concentration on the morphology and growth rate of the films.

Technical Highlights

Solid oxide fuel cells (SOFCs) have been the great interest to researchers and industry for energy solution because their overall advantages in efficiency, fuel flexibility, environmental issues, energy security and reliability compared to the other kinds of fuel cells. However, the cost is the major hurdle for SOFCs to be commercialized. The high costs of SOFCs arise mainly from the costs of the materials, including the cost of thin film processing of the electrolytes and the cost of the expensive ancillary materials to be used at that high temperature. Currently, the SOFCs usually use oxygen ion conductor yttria stabilized zirconia (YSZ) as an electrolyte material which needs to be operated at about 1000 °C. This high operating temperature, necessary to provide a reasonable conductivity, places high demands on interconnect materials. If the operating temperature could be reduced to 600-800 °C, where it can retain the ability of fuel reforming internally, the fuel cell could be constructed from cheaper materials. Moreover, other related problems such as thermal stresses, sealing, interconnections, and long start-up time will be greatly alleviated. The overall cost of the fuel cell will be reduced. However, at these lower temperatures, problems with fuel–electricity efficiency need special attention.

Thin film electrolyte techniques are very important for reducing the operating temperature of the present SOFCs [1-5]. A shorter path for oxygen ions that results from thin film will allow the YSZ electrolyte layer to have less ohmic resistance at reduced temperatures than thick films at about 1000°C**.** In addition to the thin film technologies, another way to reduce the SOFCs' operating temperature is to use electrolyte materials with high conductivities. Protonic conductors are among the most attractive ones, because they have lower activation energies than oxygen ion conductors. They may reduce the operating temperature to about 400-600°C; a temperature that still retains the fuel flexibility.

Proton conduction in doped perovskite oxides has been the subject of extensive investigation ever since Iwahara *et al*. demonstrated the utility of such materials in hydrogen sensors and other solid state ionic device. Recent reports have shown that Zr-substituted, Nd-doped barium cerate retains high conductivity in air up to compositions of 40% Zr on the Ce site [6]. These results suggest that solid solutions between $BaCeO_3$ and $BaZrO_3$ may combine the high proton conductivity of barium cerate with the good chemical stability of barium zirconate. Many protonic conducting ceramics of this type, which belong to simple perovskites, based on $SrCeO_3$,

$BaCeO_3$, $CaZrO_3$, or $SrZrO_3$ have been discovered. The chemical composition is written as $AB_{1-x}M_xO_{3-\delta}$, where M is some trivalent dopant like rare earth elements and δ is the oxygen deficiency per perovskite-type oxide unit cell. $SrCe_{0.95}Yb_{0.05}O_{3-\delta}$, $BaCe_{0.9}Nd_{0.1}O_{3-\delta}$ and $CaZr_{0.9}In_{0.1O}O_{3-\delta}$ are typical examples of this type of protonic conductor. A newer group of high-temperature protonic conductors belong to complex perovskites which can be expressed in the forms of $A_2(B'_{1+x}B''_{1-x})O_{6-\delta}$ or $A_3(B'_{1+x}B''_{2-x})O_{9-\delta}$. Experimental comparisons showed that the complex perovskites offer promising new materials for high-temperature protonic conductors [7].

In a previous paper, we have presented our development and optimization of a flame-assisted chemical vapor deposition system for thin film electrolyte processing [8]. We have succeeded in producing dense thin film YSZ coatings on both dense and porous substrates[9]. In this report, we are going to present the results of $SrCe_{0.95}Yb_{0.05}O_{3-\delta}$ thin films deposited on polished Si(100) substrates with the flame-assisted chemical vapor deposition technique. The morphology of the films was characterized with SEM and their phases were determined with XRD.

Sr-, Ce-, Y or Yb-2-EHs, (2-EH = 2-ethylhexanoate) were chosen to be the precursors and were dissolved in toluene. Substrate temperature and metal concentration are selected as the two processing parameters to study their effects on the deposited films. The experiment was designed in permutation of the two parameters at three levels as shown in Table 1.

Table 1. Experimental Design and Order

Experiment	Parameter A	Parameter B
1,2	0	0
3,4	0	1
5,6	0	2
7,8	1	0
9,10	1	1
11,12	1	2
13,14	2	0
15,16	2	1
17,18	2	2

Level of Parameter	0	1	2
A (Metal Concent. m)	2.0×10^{-3}	4.0×10^{-3}	6.0×10^{-3}
B (Substrate T, ^oC)	900	1050	1200
Experimental Order	6, 1, 3, 5, 2, 4, 12, 7, 9, 11, 8, 10, 18, 13, 15, 17, 14, 16		

Results and Discussion

Phase Determination

All the eighteen specimens were characterized with XRD at two thetas from 20 to 70 degrees. The spectra are shown in Figure 1. The major characteristic peaks of the designated perovskite material were obtained. There is a tendency that shows the specimens deposited at temperatures higher than 1000ºC present stronger intensity of the peaks. This means higher substrate temperatures outcome better crystallization and larger crystal sizes as well. Low substrate temperature such as 900ºC may produce small crystallites which results in lower peak intensities and wider peaks. This needs to be proved by further studies with TEM.

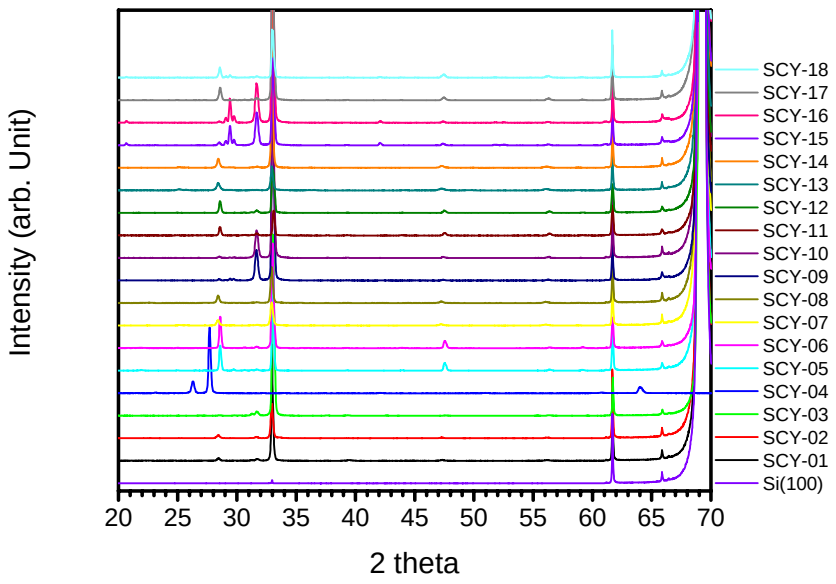

Figure 1. XRD spectra of the $SrCe_{0.95}Yb_{0.05}O_{3-\delta}$ thin films.

Surface Morphology

The surface morphologies of the specimens were observed with SEM. Figure 2 shows the typical results of the specimens deposited at all the conditions. The micrographs of the specimens deposited at 900ºC demonstrate the abnormally growth of the particles. When the metal concentration was high (6.0×10^{-3}) the particles are very large and the film was not dense. The smooth and dense films were obtained at all the substrate temperatures for the metal concentration of 4.0×10^{-3}. Higher substrate temperature of 1200ºC lead to larger particle sizes and more surface roughness as well.

Film Growth Rate

Film growth rate is usually related to the growth mechanisms in chemical vapor depositions. At low substrate temperature end, the growth is in surface reaction rate controlled regime. The

activation energy is relatively large and the growth rates are also relatively low. Increasing of temperature will steeply increase the growth rate. At high substrate temperature end, the film growth is controlled by gas-phase diffusion rate. The activation energy is relatively small and the growth rates are also relatively high. Increasing of temperature does increase the growth rates much. These rules also apply to our situation. However, a new growth rule called thermophoresis is also in effect in our experiments. This effect is caused by the temperature gradients between the flame and the substrate. Therefore, the film growth rates at the lowest substrate temperature in our experiment even beat those deposited at the highest substrate temperature in two of the three metal concentration cases as shown in Figure 3.

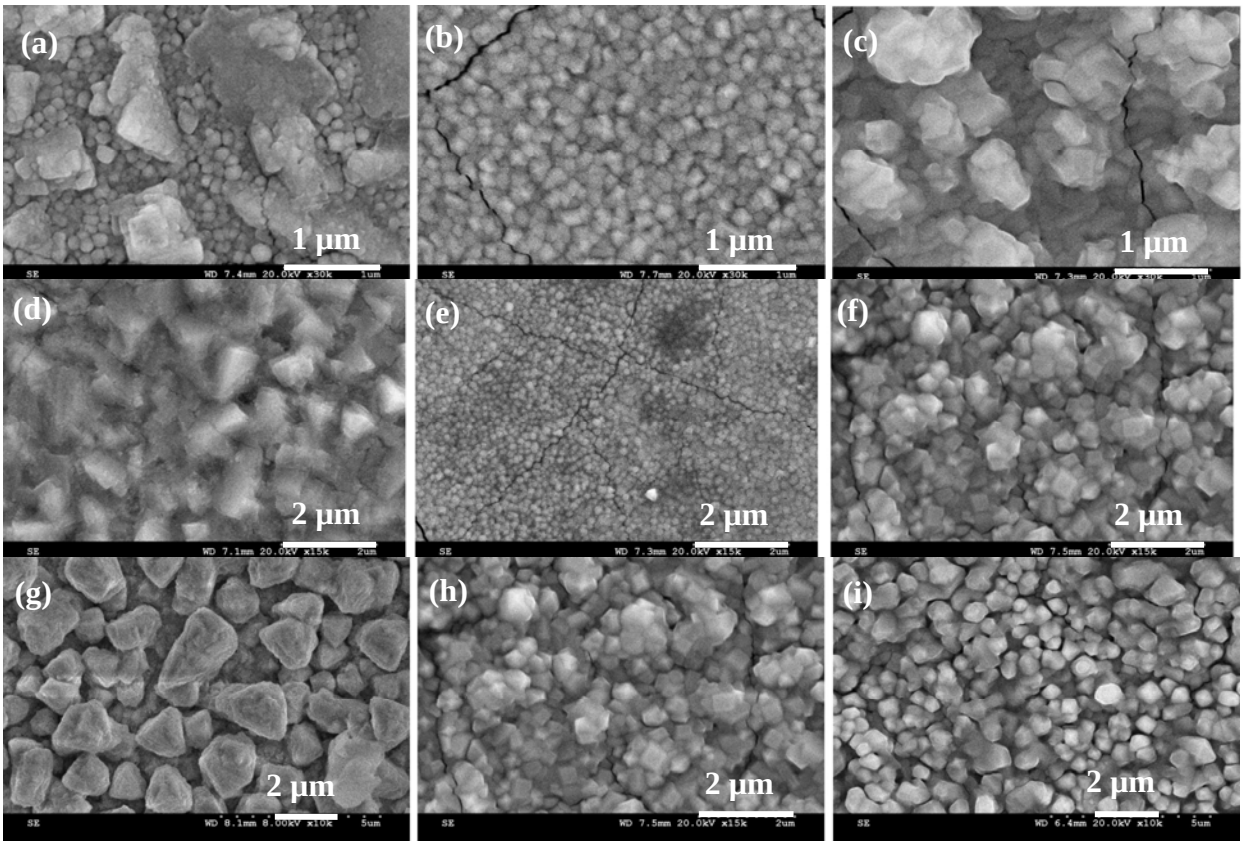

Figure 2. SEM micrographs of the $SrCe_{0.95}Yb_{0.05}O_{3-\delta}$ thin films deposited at metal concentration of $2.0x10^{-3}$ and substrate temperatures of (a) 900ºC, (b)1050 ºC and (c)1200 ºC; at metal concentration of $4.0x10^{-3}$ and substrate temperatures of (d) 900ºC, (e) 1050 ºC and (f) 1200 ºC; and at metal concentration of $6.0x10^{-3}$ and substrate temperatures of (g) 900ºC, (h)1050 ºC and (i)1200 ºC.

Conclusions

Flame-assisted chemical vapor deposition has been successfully used to process Sr-Cerate coatings. Film morphology and microstructure are dependent on the processing parameters, i.e., metal concentration and substrate temperature. Low temperature tends to have coatings with abnormally large particles. High temperature usually produces coatings with large grains and great surface roughness. Grain size and surface roughness also increase with increased metal

concentration in the precursor solution. Film thickness increases with increased metal concentration, but does not with increased substrate temperature.

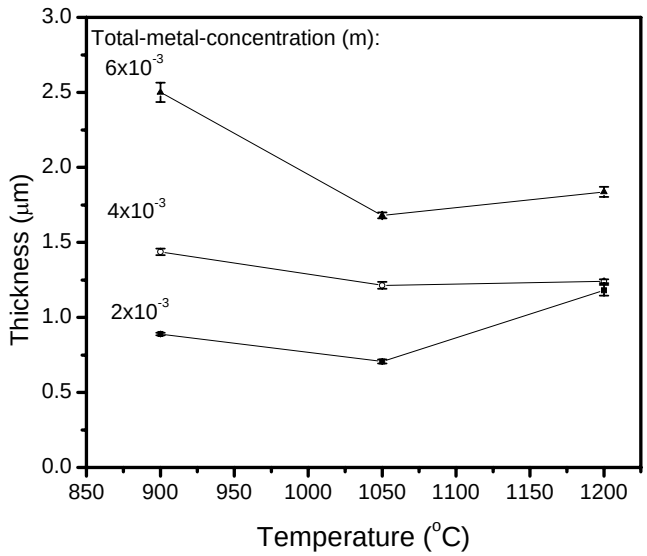

Figure 3. Measured film thickness from the specimens deposited in 20 min as functions of the substrate temperatures.

References

1. C. C. Chen, M. M. Nasrallah and H. U. Anderson, "Synthesis and characterization of YSZ thin film electrolytes," *Solid State Ionics*, 70/71(1994), pp.101-108.
2. K. Choy, W. Bai, S. Charojrochkul and B. C. H. Steele, "The development of intermediate-temperature solid oxide fuel cells for the next millennium," *J. Power Sources*, 71(1998), pp.361-369.
3. J. Will, A. Mitterdorfer, C. Kleinlogel, D. Perednis and L. J. Gauckler, "Fabrication of thin electrolytes for second-generation solid oxide fuel cells," *Solid State Ionics*, 131(2000), pp.79-96.
4. P. Bohac and L. Gauckler, **"**Chemical spray deposition of YSZ and GCO solid electrolyte films," *Solid State Ionics*, 119(1999), pp.317-321.
5. T. -L. Wen, D. Wang, M. Chen, H. Tu, Z. Lu, Z. Zhang, H. Nie and W. Huang, "Material research for planar SOFC stack," *Solid State Ionics*, 148(2002), pp.513-519.
6. S. Wienströer and H. -D. Wiemhöfer, "Investigation of the influence of zirconium substitution on the properties of neodymium-doped barium cerates," *Solid State Ionics*, 101-103(1997), pp.1113-1117.
7. A.S. Nowick, Yang Du, "High-temperature protonic conductors with perovskite-related structures," *Solid State Ionics*, 77(1995), pp.137-146.
8. Zhigang Xu, Jag Sankar, Sergey Yarmolenko, "YSZ Thin Film Coatings Using Combustion Chemical Vapor Deposition," *Surface and Coatings Technology* 177 –178 (2004) p.52–59.
9. Zhigang Xu, Corydon Hilton, Bobby Watkins, Sergey Yarmolenko, Jag Sankar, "Thin YSZ Electrolyte Film Depositions on Dense And Porous Substrates," paper IMECE2003-43330, 2003 ASME International Mechanical Engineering Congress and RD&D Expo.

Communications/Visitors/Travel
None

Problems Encountered
None

Powder Processing of Nanostructured Alloys Produced by Machining

S. Chandrasekar, K. P. Trumble, and W. D. Compton
Purdue University

Objective/Scope

The project seeks to create bulk nanostructured materials with enhanced mechanical properties for structural applications in the ground transportation sector. It builds on the discovery of a low-cost means of producing nanostructured materials in essentially any alloy via normal machining. Three routes are being pursued for realizing bulk nanostructured materials. *First*, comminution of the nanostructured chips will enable large scale production of nanocrystalline particulate, which can be converted into nanostructured bulk forms using powder processing methods. *Second*, the chips and particulates may be used as continuous or discontinuous reinforcements in metal or polymer matrices to create advanced composite bulk forms. *Third*, the possibility of directly making bulk materials in the form of wires, foils, plates and bars, by chip formation is being explored. These routes are all geared towards controlling deformation-temperature-time histories to realize microstructure refinement while minimizing thermal coarsening. The model material systems being investigated are Al alloys, titanium and steels.

Technical Highlights

Nanostructured Titanium and Functionally Graded Titanium Surfaces Realized

Interest in titanium and titanium alloys with Ultra-Fine Grained (UFG) microstructures is motivated by their attractiveness for use as high-temperature structural materials. UFG titanium has been produced by deforming titanium to large values of strain using ECAP at temperatures of ~ 400°C [1]. In some of these studies, the microstructure refinement was found to be insufficient to produce the desired properties, and an additional deformation process, such as cold rolling, was used to further refine the microstructure [1]. We have demonstrated the successful adaptation of chip formation by large strain machining, as an SPD process at ambient temperature, for making nanocrystalline titanium.

Severe Plastic Deformation (SPD) of titanium at ambient temperature was realized using large strain machining. The material that received the highest levels of strain, the chip, is seen to have a nanocrystalline structure with ~100 nm size grains (Figure 1). This microstructure is finer than that observed in Ti following Equal Channel Angular Pressing (ECAP) at elevated temperatures. The hardness and strength of the nanostructured titanium are substantially greater those of its microcrystalline counterpart. The machined surface of the workpiece is found to have a graded microstructure composed of ultra-fine grains at and near the surface and a preponderance of twins further into the sub-surface (Figure 2). The parameters of the large strain deformation field, namely strain rate and strain, are obtained using an adaptation of a Particle Image Velocimetry (PIV) technique (Figure 3). The microstructure characteristics are a consequence of the deformation field parameters (strain, strain rate) which activate both twinning and dislocation-mediated mechanisms of plastic flow [2].

Consolidation of Nanostructured Al alloy Particulate

High-Pressure Torsion (HPT) and warm extrusion processes are being explored for consolidation of nanostructured Al 3003 chip particulate created by machining. The preliminary results from

evaluation of consolidate are very promising in terms of retention of microstructure and hardness over large areas of the samples.

Problems Encountered

None

Status of Milestones

"Creation of Bulk Nanostructured Materials from Machining Chips and by Machining Chip Formation Processes", on schedule.

References

1. Y. T. Zhu, J. Y. Huang, J. Gubicza, T. Ungar, Y. M. Wang, E. Ma, and R. Z. Valiev, Nanostructures in Ti processed by severe plastic deformation. *Journal of Materials Research* 2003; 18(8): 1908-1917.
2. M. Ravi Shankar, B. C. Rao, S. Lee, S. Chandrasekar, A. H. King and W. D. Compton, "Severe Plastic Deformation of Titanium at Near-Ambient Temperature," *Acta Materialia*, accepted for publication.

Publications

1. M. Ravi Shankar, B. C. Rao, S. Lee, S. Chandrasekar, A. H. King and W. D. Compton, "Severe Plastic Deformation of Titanium at Near-Ambient Temperature," *Acta Materialia*, accepted for publication.

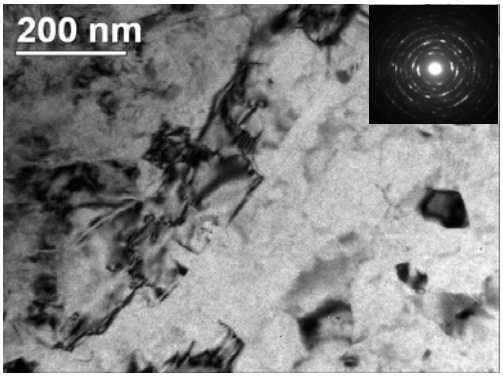

Figure 1: Nanocrystalline titanium

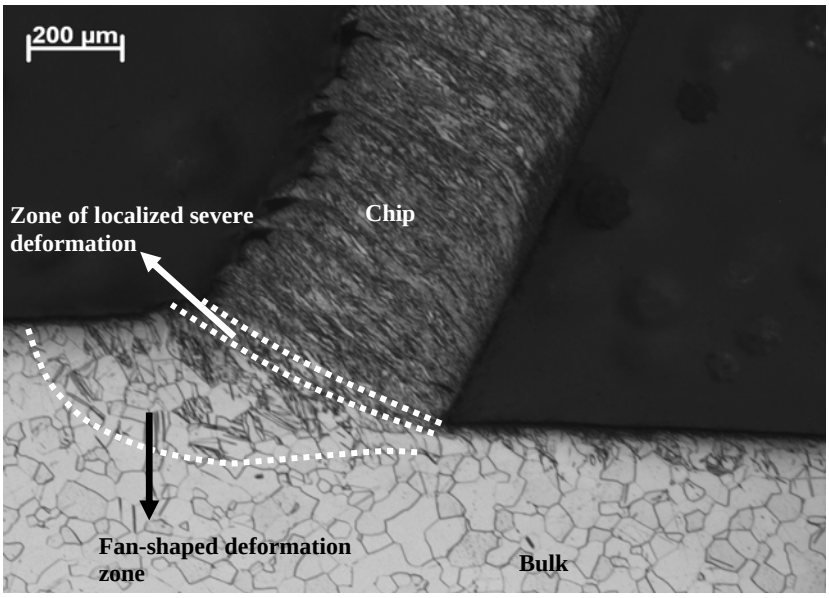

Figure 2: Graded microstructure in workpiece and deformation zone

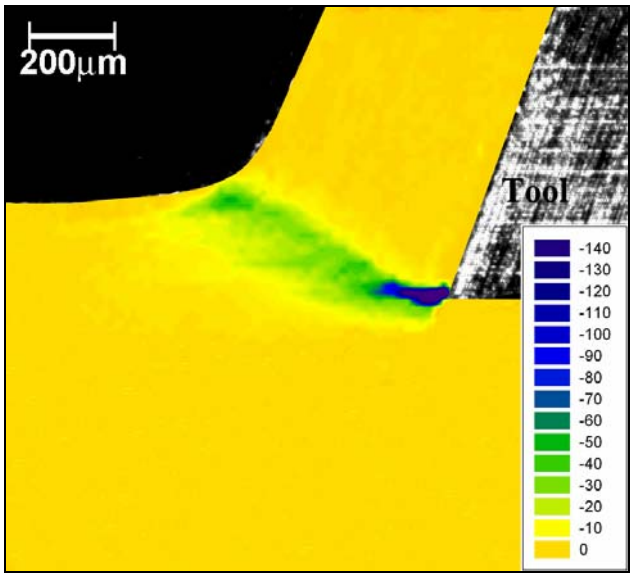

Figure 3: Shear Strain Rate Field (per sec)

Next Generation Ceramics for Heavy Vehicle Propulsion Applications

Paul F. Becher
Oak Ridge National Laboratory

Objective/Scope

In addition to lower specific weight, ceramics have a number of attractive properties for application as components in various heavy vehicle systems such as electrochemical properties needed to develop advanced sensors and wear resistance and low coefficients of friction to increase life in moving components. Significant new opportunities are beginning to evolve with the advent of nanocrystalline materials. Initial findings show that nanocrystalline ceramics have substantially improved electrochemical properties, which are being explored in sensors for combustion and emissions controls, and auxiliary power sources. Studies have also revealed that ceramics with grain sizes < 100 nanometers can exhibit very high hardness, which may translate to greater wear resistance either in the form of coatings or components (e.g., for valve train components) or to create low friction surfaces to enhance engine performance.

The goal being to develop the technology to form "green" (unfired) bodies of nanocrystalline particles to allow one to devise pressureless sintering profiles to produce dense monolithic bodies with grain sizes < 100 nm. This is aimed at finding approaches to produce sizeable monolithic bodies for subsequent evaluation. The second thrust focuses on the mechanical and wear behavior of nanocrystalline ceramics and the influence of external parameters (e.g., stressing rate, temperature, environment (e.g., air, vacuum), and electric fields (in collaboration with researchers at North Carolina State University) on the plastic deformation behavior.

Technical Highlight

Several dense sintered nanocrystalline zirconia disks received from Pennsylvania State University (PSU). Optical microscopy and scanning electron microscopy studies revealed that most disks contained 2 or more large cracks extending in from the edges of the disks and numerous small cracks. The small cracks are associated with the transformation to the monoclinic phase during cooling from the sintering temperatures. The large cracks appear to be generated during the pressing sequence prior to sintering. These finding were reported to the PSU researchers to allow them to modify the processing steps in order to prepare new samples free of cracks.

Status of Milestones

New project

Communications/Visits/Travel

Teleconference call (2/20/2006) with Richard Schorr of MetaMateria to establish collaborative effort. MetaMateria produces various nanocrystalline materials (powders, porous and dense bodies) including oxide ceramics and thermoelectric materials. Agreement reached that MetaMateria will supply samples and ORNL will conduct characterization studies.

Publications

None